E-ISSN: 2147-1959

MIRT

Molecular Imaging and Radionuclide Therapy

October 2023 Volume 32 Issue 3 www.tsnm.org

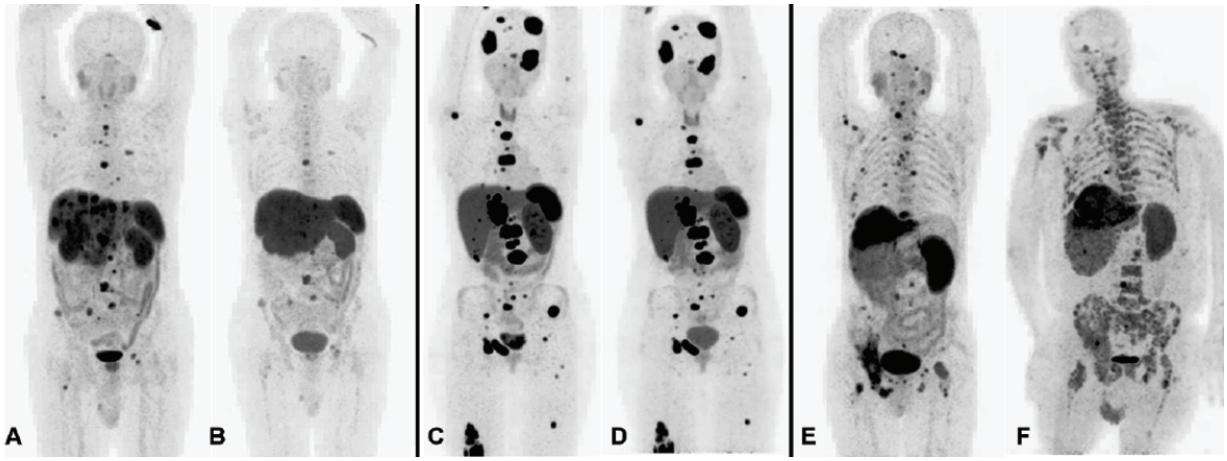

"Official Journal of the Turkish Society of Nuclear Medicine"

galenos yayınevi

TURKISH SOCIETY OF NUCLEAR MEDICINE 1975

MIRT

Molecular Imaging and Radionuclide Therapy

MIRT

Molecular Imaging and Radionuclide Therapy

Turkish Society of Nuclear Medicine
Cinnah Caddesi Pilot Sokak No: 10/12 Çankaya 06650 Ankara, Türkiye **Phone:** +90 312 441 00 45 **Fax:** +90 312 441 12 95 **Web:** www.tsnm.org **E-mail:** dernekmerkezi@tsnm.org
"Formerly Turkish Journal of Nuclear Medicine"

Reviewing the articles' conformity to the publishing standards of the Journal, typesetting, reviewing and editing the manuscripts and abstracts in English, creating links to source data, and publishing process are realized by Galenos.

Publisher Contact
Address: Molla Gürani Mah. Kaçamak Sk. No: 21/1 34093 İstanbul, Türkiye
Phone: +90 (530) 177 30 97 / +90 539 307 32 03
E-mail: info@galenos.com.tr/yayin@galenos.com.tr
Web: www.galenos.com.tr
Publisher Certificate Number: 14521

Online Publication Date: October 2023
ISSN: 2146-1414 **E-ISSN:** 2147-1959
International scientific journal published quarterly.

MIRT

Molecular Imaging and Radionuclide Therapy

ABOUT US

Molecular Imaging and Radionuclide Therapy (formerly Turkish Journal of Nuclear Medicine) is the official publication of Turkish Society of Nuclear Medicine.

Focus and Scope

Molecular Imaging and Radionuclide Therapy (Mol Imaging Radionucl Ther, MIRT) is a double-blind peer-review journal published in English language. It publishes original research articles, invited reviews, editorials, short communications, letters, consensus statements, guidelines and case reports with a literature review on the topic, in the field of molecular imaging, multimodality imaging, nuclear medicine, radionuclide therapy, radiopharmacy, medical physics, dosimetry and radiobiology. MIRT is published three times a year (February, June, October). Audience: Nuclear medicine physicians, medical physicists, radiopharmaceutical scientists, radiobiologists.

The editorial policies are based on the "Recommendations for the Conduct, Reporting, Editing, and Publication of Scholarly Work in Medical Journals (ICMJE Recommendations)" by the International Committee of Medical Journal Editors (2016, archived at http://www.icmje.org/) rules.

Molecular Imaging and Radionuclide Therapy is indexed in **Pubmed, Pubmed Central (PMC), Emerging Sources Citation Index (ESCI), TUBITAK-ULAKBIM, DOAJ, Scopus, Gale/Cengage Learning, EBSCO databases, Embase, ProQuest Health & Medical Complete, CINAHL, J-Gate, IdealOnline, Türkiye Atıf Dizini-Turkiye Citation Index, Turk Medline, Hinari, GOALI, ARDI, OARE** and **AGORA.**

Open Access Policy

This journal provides immediate open access to its content on the principle that making research freely available to the public supports a greater global exchange of knowledge.

Open Access Policy is based on rules of Budapest Open Access Initiative (BOAI) (http://www.budapestopenaccessinitiative.org/). By "open access" to [peer-reviewed research literature], we mean its free availability on the public internet, permitting any users to read, download, copy, distribute, print, search, or link to the full texts of these articles, crawl them for indexing, pass them as data to software, or use them for any other lawful purpose, without financial, legal, or technical barriers other than those inseparable from gaining access to the internet itself. The only constraint on reproduction and distribution, and the only role for copyright in this domain, should be to give authors control over the integrity of their work and the right to be properly acknowledged and cited.

Subscription Information

Manuscripts can only be submitted electronically through the Journal Agent website (http://www.journalagent.com/mirt/?plng=eng) after creating an account. This system allows online submission and review.

All published volumes in full text can be reached free of charge through the website http://mirt.tsnmjournals.org

Copyright Statement

Instructions for Authors

Instructions for authors are published in the journal and on the website http://mirt.tsnmjournals.org

Material Disclaimer

Scientific and legal responsibilities pertaining to the papers belong to the authors. Contents of the manuscripts and accuracy of references are also the author's responsibility. The Turkish Society of Nuclear Medicine, the Editor, the Editorial Board or the publisher do not accept any responsibility for opinions expressed in articles.

Financial expenses of the journal are covered by Turkish Society of Nuclear Medicine.

Correspondence Address

Editor in Chief Prof. Murat Fani Bozkurt, MD, FEBNM Hacettepe University, Medical School, Department of Nuclear Medicine, Ankara, Türkiye

E-mail: fanibozkurt@gmail.com

Web page: http://mirt.tsnmjournals.org/

Publisher Corresponding Address

Galenos Yayınevi Tic. Ltd. Şti.
Address: Molla Gürani Mah. Kaçamak Sk. No: 21/1 34093 Fındıkzade, İstanbul, Türkiye
Phone: +90 (530) 177 30 97 / +90 539 307 32 03
E-mail: info@galenos.com.tr

MIRT

Molecular Imaging and Radionuclide Therapy

INSTRUCTIONS TO AUTHORS

Molecular Imaging and Radionuclide Therapy (Mol Imaging Radionucl Ther, MIRT) publishes original research articles, short communications, invited reviews, editorials, case reports with a literature review on the topic, interesting images, consensus statements, guidelines, letters in the field of molecular imaging, multimodality imaging, nuclear medicine, radionuclide therapy, radiopharmacy, medical physics, dosimetry and radiobiology. MIRT is published by the Turkish Society of Nuclear Medicine three times a year (February, June, October).

Molecular Imaging and Radionuclide Therapy does not charge any article submission or processing fees.

GENERAL INFORMATION

MIRT commits to rigorous peer review, and stipulates freedom from commercial influence, and promotion of the highest ethical and scientific standards in published articles. Neither the Editor(s) nor the publisher guarantees, warrants or endorses any product or service advertised in this publication. All articles are subject to review by the editors and peer reviewers. If the article is accepted for publication, it may be subjected to editorial revisions to aid clarity and understanding without changing the data presented.

Manuscripts must be written in English and must meet the requirements of the journal. The journal is in compliance with the uniform requirements for manuscripts submitted to biomedical journals published by the International Committee of Medical Journal Editors (NEJM 1997; 336:309-315, updated 2016). Manuscripts that do not meet these requirements will be returned to the author for necessary revision before the review. Authors of manuscripts requiring modifications have a maximum of two months to resubmit the revised text. Manuscripts returned after this deadline will be treated as new submissions.

It is the authors' responsibility to prepare a manuscript that meets ethical criteria. The Journal adheres to the principles set forth in the Helsinki Declaration October 2013 (https://www.wma.net/policies-post/wma-declaration-of-helsinki-ethical-principles-for-medical-research-involving-human-subjects/) and holds that all reported research involving "Human beings" conducted in accordance with such principles.

Reports describing data obtained from research conducted in human participants must contain a statement in the MATERIALS AND METHODS section indicating approval by the ethical review board (including the approval number) and affirmation that INFORMED CONSENT was obtained from each participant.

All manuscripts reporting experiments using animals must include a statement in the MATERIALS AND METHODS section giving assurance that all animals have received humane care in compliance with the Guide for the Care and Use of Laboratory Animals (www.nap.edu) and indicating approval by the ethical review board.

If the study should have ethical approval, authors asked to provide ethical approval in order to proceed the review process. If they provide approval, review of the manuscript will continue.

In case report(s) and interesting image(s) a statement regarding the informed consent of the patients should be included in the manuscript and the identity of the patient(s) should be hidden.

Subjects must be identified only by number or letter, not by initials or names. Photographs of patients' faces should be included only if scientifically relevant. Authors must obtain written consent from the patient for use of such photographs. In cases of image media usage that potentially expose patients' identity requires obtaining permission for publication from the patients or their parents/guardians.

If the proposed publication concerns any commercial product, the author must include in the cover letter a statement indicating that the author(s) has (have) no financial or other interest with the product or explaining the nature of any relations (including consultancies) between the author(s) and editor the manufacturer or distributor of the product.

All submissions will be screened by Crossref Smilarity Check powered by "iThenticate". Manuscripts with an overall similarity index of greater than 25%, or duplication rate at or higher than 5% with a single source will be returned back to authors.

MANUSCRIPT CATEGORIES

1. Original Articles

2. Short Communications are short descriptions of focused studies with important, but very straightforward results.

3. Reviews address important topics in the field. Authors considering the submission of uninvited reviews should contact the editor in advance to determine if the topic that they propose is of current potential interest to the Journal. Reviews will be considered for publication only if they are written by authors who have at least three published manuscripts in the international peer reviewed journals and these studies should be cited in the review. Otherwise only invited reviews will be considered for peer review from qualified experts in the area.

4. Editorials are usually written by invitation of the editor by the editors on current topics or by the reviewers involved in the evaluation of a submitted manuscript and published concurrently with that manuscript.

5. Case Report and Literature Reviews are descriptions of a case or small number of cases revealing a previously undocumented disease process, a unique unreported manifestation or treatment of a known disease process, unique unreported complications of treatment regimens or novel and important insights into a condition's pathogenesis, presentation, and/or management. The journal's policy is to accept case reports only if it is accompanied by a review of the literature on the related topic. They should include an adequate number of images and figures.

6. Interesting Image

One of the regular parts of Molecular Imaging and Radionuclide Therapy is a section devoted to interesting images. Interesting image(s) should describe case(s) which are unique and include interesting findings adding insights into the interpretation of patient images, a condition's pathogenesis, presentation, and/or management.

7. Consensus Statements or Guidelines may be submitted by professional societies. All such submissions will be subjected to peer review, must be modifiable in response to criticisms, and will be published only if they meet the Journal's usual editorial standards.

8. Letters to the Editor may be submitted in response to work that has been published in the Journal. Letters should be short commentaries related to specific points of agreement or disagreement with the published work.

Note on Prior Publication

Articles are accepted for publication on the condition that they are original, are not under consideration by another journal, or have not been previously published. Direct quotations, tables, or illustrations that have appeared in

MIRT

Molecular Imaging and Radionuclide Therapy

INSTRUCTIONS TO AUTHORS

copyrighted material must be accompanied by written permission for their use from the copyright owner and authors. Materials previously published in whole or in part shall not be considered for publication. At the time of submission, authors must report that the manuscript has not been published elsewhere. Abstracts or posters displayed at scientific meetings need not be reported.

MANUSCRIPT SUBMISSION PROCEDURES

MIRT only accepts electronic manuscript submission at the web site http://www.journalagent.com/mirt/. After logging on to the website Click the 'online manuscript submission' icon. All corresponding authors should be provided with a password and a username after entering the information required. If you already have an account from a previous submission, enter your username and password to submit a new or revised manuscript. If you have forgotten your username and/or password, please send an e-mail to the editorial office for assistance. After logging on to the article submission system please read carefully the directions of the system to give all needed information and attach the manuscript, tables and figures and additional documents.

All Submissions Must Include:

1. Completed Copyright Assignment & Disclosure of Potential Conflict of Interest Form; This form should be downloaded from the website (provided in the author section), filled in thoroughly and uploaded to the website during the submission.
2. All manuscripts describing data obtained from research conducted in human participants must be accompanied with an approval document by the ethical review board.
3. All manuscripts reporting experiments using animals must include approval document by the animal ethical review board.
4. All submissions must include the authorship contribution form which is signed by all authors.

Authors must complete all online submission forms. If you are unable to successfully upload the files please contact the editorial office by e-mail.

MANUSCRIPT PREPARATION

General Format

The Journal requires that all submissions be submitted according to these guidelines:

- Text should be double spaced with 2.5 cm margins on both sides using 12-point type in Times Roman font.
- All tables and figures must be placed after the text and must be labeled.
- Each section (abstract, text, references, tables, figures) should start on a separate page.
- Manuscripts should be prepared as a word document (*.doc) or rich text format (*.rtf).
- Please make the tables using the table function in Word.
- Abbreviations should be defined in parenthesis where the word is first mentioned and used consistently thereafter.
- Results should be expressed in metric units. Statistical analysis should be done accurately and with precision. Please consult a statistician if necessary.
- Authors' names and institutions should not be included in the manuscript text and should be written only in the title page.

Title Page

The title page should be a separate form from the main text and should include the following:

- Full title (in English and in Turkish). Turkish title will be provided by the editorial office for the authors who are not Turkish speakers.
- Authors' names and institutions.
- Short title of not more than 40 characters for page headings.
- At least three and maximum eight keywords. (in English and in Turkish). Do not use abbreviations in the keywords. Turkish keywords will be provided by the editorial office for the authors who are not Turkish speakers. If you are not a native Turkish speaker, please reenter your English keywords to the area provided for the Turkish keywords. English keywords should be provided from http://www.nlm.nih.gov/mesh (Medical Subject Headings) while Turkish keywords should be provided from http://www.bilimterimleri.com.
- Word count (excluding abstract, figure legends and references).
- Corresponding author's e-mail and address, telephone and fax numbers.
- Name and address of person to whom reprint requests should be addressed.

Original Articles

Authors are required to state in their manuscripts that ethical approval from an appropriate committee and informed consents of the patients were obtained.

Original Articles should be submitted with a structured abstract of no more than 250 words. All information reported in the abstract must appear in the manuscript. The abstract should not include references. Please use complete sentences for all sections of the abstract. Structured abstract should include background, objective, methods, results and conclusions. Turkish abstract will be provided by the editorial office for the authors who are not Turkish speakers. If you are not a native Turkish speaker, please reenter your English abstract to the area provided for the Turkish abstract.

- Introduction
- Materials and Methods
- Results
- Discussion
- Study Limitations
- Conclusion

May be given for contributors who are not listed as authors, or for grant support of the research.

References should be cited in numerical order (in parentheses) in the text and listed in the same numerical order at the end of the manuscript on a separate page or pages. The author is responsible for the accuracy of references. Examples of the reference style are given below. Further examples will be found in the articles describing the Uniform Requirements for Manuscripts Submitted to Biomedical Journals (Ann Intern Med.1988; 208:258-265, Br Med J. 1988; 296:401-405). The titles of journals should be abbreviated according to the style used in the Index Medicus. Journal Articles and Abstracts: Surnames and initials of author's name, title of the article, journal name, date, volume number, and pages. All authors should be listed regardless of number. The citation of unpublished papers, observations or personal communications is not permitted. Citing an abstract is not recommended. Books: Surnames and initials of author's names, chapter title, editor's name, book title, edition, city, publisher, date and pages.

MIRT
Molecular Imaging and Radionuclide Therapy

INSTRUCTIONS TO AUTHORS

Sample References

Journal Article: Sayit E, Söylev M, Capa G, Durak I, Ada E, Yilmaz M. The role of technetium-99m-HMPAO-labeled WBC scintigraphy in the diagnosis of orbital cellulitis. Ann Nucl Med 2001;15:41-44.

Erselcan T, Hasbek Z, Tandogan I, Gumus C, Akkurt I. Modification of Diet in Renal Disease equation in the risk stratification of contrast induced acute kidney injury in hospital inpatients. Nefrologia 2009 doi: 10.3265/Nefrologia.2009.29.5.5449.en.full.

Article in a journal published ahead of print: Ludbrook J. Musculovenous pumps in the human lower limb. Am Heart J 2009;00:1-6. (accessed 20 February 2009).

Lang TF, Duryea J. Peripheral Bone Mineral Assessment of the Axial Skeleton: Technical Aspects. In: Orwoll ES, Bliziotes M (eds). Osteoporosis: Pathophsiology and Clinical Management. New Jersey, Humana Pres Inc, 2003;83-104.

Books: Greenspan A. Orthopaedic Radiology a Pratical Approach. 3th ed. Philadelphia, Lippincott Williams Wilkins 2000, 295-330.

Website: Smith JR. 'Choosing Your Reference Style', Online Referencing 2(3), http://orj.sagepub.com (200, accessed October 2008).

- Tables

Tables must be constructed as simply as possible. Each table must have a concise heading and should be submitted on a separate page. Tables must not simply duplicate the text or figures. Number all tables in the order of their citation in the text. Include a title for each table (a brief phrase, preferably no longer than 10 to 15 words). Include all tables in a single file following the manuscript.

– Figure Legends

Figure legends should be submitted on a separate page and should be clear and informative.

– Figures

Number all figures (graphs, charts, photographs, and illustrations) in the order of their citation in the text. At submission, the following file formats are acceptable: AI, EMF, EPS, JPG, PDF, PPT, PSD, TIF. Figures may be embedded at the end of the manuscript text file or loaded as separate files for submission. All images MUST be at or above intended display size, with the following image resolutions: Line Art 800 dpi, Combination (Line Art + Halftone) 600 dpi, Halftone 300 dpi. Image files also must be cropped as close to the actual image as possible.

Short Communications:

Short communications should be submitted with a structured abstract of no more than 200 words. These manuscripts should be no longer than 2000 words, and include no more than two figures and tables and 20 references. Other rules which the authors are required to prepare and submit their manuscripts are the same as described above for the original articles.

Invited Review Articles:

- Title page (see above)
- Abstract: Maximum 250 words; without structural divisions; in English and in Turkish . Turkish abstract will be provided by the editorial office for the authors who are not Turkish speakers. If you are not a native Turkish speaker, please reenter your English abstract to the area provided for the Turkish abstract.
- Text
- Conclusion
- Acknowledgements (if any)
- References

Editorial:

- Title page (see above)
- Abstract: Maximum 250 words; without structural divisions; in English and in Turkish. Turkish abstract will be provided by the editorial office for the authors who are not Turkish speakers. If you are not a native Turkish speaker, please re enter your English abstract to the area provided for the Turkish abstract.
- Text
- References

Case Report and Literature Review

- Title page (see above)
- Abstract: Approximately 100-150 words; without structural divisions; in English and in Turkish. Turkish abstract will be provided by the editorial office for the authors who are not Turkish speakers. If you are not a native Turkish speaker, please re-enter your English abstract to the area provided for the Turkish abstract.
- Introduction
- Case report
- Literature Review and Discussion
- References

Interesting Image:

No manuscript text is required. Interesting Image submissions must include the following:

Title Page: (see Original article section)

Abstract: Approximately 100-150 words; without structural divisions; in English and in Turkish. Turkish abstract will be provided by the editorial office for the authors who are not Turkish speakers. If you are not a native Turkish speaker, please re-enter your English abstract to the area provided for the Turkish abstract.

Image(s): The number of images is left to the discretion of the author. (See Original article section)

Figure Legend: Reference citations should appear in the legends, not in the abstract. Since there is no manuscript text, the legends for illustrations should be prepared in considerable detail but should be no more than 500 words total. The case should be presented and discussed in the Figure legend section.

References: Maximum eight references (see original article section).

Letters to the Editor:

- Title page (see above)
- Short comment to a published work, no longer than 500 words, no figures or tables.
- References no more than five.

Consensus Statements or Guidelines: These manuscripts should typically be no longer than 4000 words and include no more than six figures and tables and 120 references.

Proofs and Reprints

Proofs and a reprint orders are sent to the corresponding author. The author should designate by footnote on the title page of the manuscript the name and

MIRT
Molecular Imaging and Radionuclide Therapy

INSTRUCTIONS TO AUTHORS

address of the person to whom reprint requests should be directed. The manuscript when published will become the property of the journal.

Archiving

The editorial office will retain all manuscripts and related documentation (correspondence, reviews, etc.) for 12 months following the date of publication or rejection.

Submission Preparation Checklist

As part of the submission process, authors are required to check off their submission's compliance with all of the following items, and submissions may be returned to authors that do not adhere to these guidelines.

1. The submission has not been previously published, nor is it before another journal for consideration (or an explanation has been provided in Comments to the Editor).
2. The submission file is in Microsoft Word, RTF, or WordPerfect document file format. The text is double-spaced; uses a 12-point font; employs italics, rather than underlining (except with URL addresses); and the location for all illustrations, figures, and tables should be marked within the text at the appropriate points.
3. Where available, URLs for the references will be provided.
4. All authors should be listed in the references, regardless of the number.
5. The text adheres to the stylistic and bibliographic requirements outlined in the Author Guidelines, which is found in About the Journal.
6. English keywords should be provided from http://www.nlm.nih.gov/mesh(Medical Subject Headings), while Turkish keywords should be provided fromhttp://www.bilimterimleri.com
7. The title page should be a separate document from the main text and should be uploaded separately.
8. The "Affirmation of Originality and Assignment of Copyright/The Disclosure Form for Potential Conflicts of Interest Form" and Authorship Contribution Form should be downloaded from the website, filled thoroughly and uploaded during the submission of the manuscript.

TO AUTHORS

Copyright Notice

The author(s) hereby affirms that the manuscript submitted is original, that all statement asserted as facts are based on author(s) careful investigation and research for accuracy, that the manuscript does not, in whole or part, infringe any copyright, that it has not been published in total or in part and is not being submitted or considered for publication in total or in part elsewhere. Completed Copyright Assignment & Affirmation of Originality Form will be uploaded during submission. By signing this form;

1. Each author acknowledges that he/she participated in the work in a substantive way and is prepared to take public responsibility for the work.
2. Each author further affirms that he or she has read and understands the "Ethical Guidelines for Publication of Research".
3. The author(s), in consideration of the acceptance of the manuscript for publication, does hereby assign and transfer to the Molecular Imaging and Radionuclide Therapy all of the rights and interest in and the copyright of the work in its current form and in any form subsequently revised for publication and/or electronic dissemination.

Privacy Statement

The names and email addresses entered in this journal site will be used exclusively for the stated purposes of this journal and will not be made available for any other purpose or to any other party.

Peer Review Process

1. The manuscript is assigned to an editor, who reviews the manuscript and makes an initial decision based on manuscript quality and editorial priorities.
2. For those manuscripts sent for external peer review, the editor assigns at least two reviewers to the manuscript.
3. The reviewers review the manuscript.
4. The editor makes a final decision based on editorial priorities, manuscript quality, and reviewer recommendations.
5. The decision letter is sent to the author.

Contact Address

All correspondence should be directed to the Editorial Office:
Cinnah Caddesi Pilot Sokak No:10/12 06650 Çankaya / Ankara, Türkiye
Phone: +90 312 441 00 45
Fax: +90 312 441 12 97
E-mail: info@tsnmjournals.org

MIRT
Molecular Imaging and Radionuclide Therapy

CONTENTS

Editorial

Original Articles

Interesting Images

MIRT
Molecular Imaging and Radionuclide Therapy

CONTENTS

Editorial
Mol Imaging Radionucl Ther 2023;32:191-194 DOI:10.4274/mirt.galenos.2023.38233

Celebrating the 50th Anniversary of Nuclear Medicine in Türkiye Along with the 100th Anniversary of Turkish Republic

Türkiye'de Nükleer Tıbbın 50. Yılını, Türkiye Cumhuriyetinin 100. Yıldönümü ile Birlikte Kutluyoruz

Murat Fani Bozkurt

Hacettepe University Faculty of Medicine, Department of Nuclear Medicine, Ankara, Türkiye

Keywords: Nuclear medicine, Türkiye, Turkish Republic, anniversary

Anahtar kelimeler: Nükleer tıp, Türkiye, Türkiye Cumhuriyeti, yıldönümü

October 2023 is definitely a very special and unique time for Turkish nuclear medicine professionals, as both the 100th anniversary of the foundation of Turkish Republic will be proudly celebrated with great honour and excitement on the 29th of October and the 50th anniversary of nuclear medicine as an independent medical branch and residency program in Türkiye will be celebrated as well; on the best occasion to host such a special birthday party at the nuclear medicine week in October.

Looking back to history of nuclear medicine in Türkiye, such an honour to state that nuclear medicine had been recognised as an individual medical branch and moreover an independent residency program officially years before many countries in different parts of the world. In the year 1973, nuclear medicine had been officially recognised as a separate and independent medical branch of internal medicine and an individual residency program by Ministry of Health of Republic of Türkiye (Figure 1). This recognition gave rise to a rapid development of nuclear medicine practice, which at the first time avaliable in major cities of Türkiye, such as İstanbul, Ankara and İzmir and eventually showed a wide distribution all around the country. The first routine medical practice in the area of nuclear medicine mostly involved diagnostic radioisotopic scans with rectilinear scanners, radionuclide therapy mostly with radioiodine for thyroid disease and plenty of *in vitro* studies, most of which are replaced by non-isotopic counters by time and not being applied currently. The wide use of radioisotopic diagnostic and therapeutic applications as well as the meticulous assays for various hormones, metabolites, vitamines and others with radioimmunoassay and immunoradiometric assay methods gained wide acceptance throughout the medical professionals and absolutely provided strong roots to bloom as modern nuclear medicine practice in Türkiye at the upcoming years (1,2).

As the earlier nuclear medicine practice in Türkiye gave rise to a more established and wide use of radioisotopes both *in vivo* and *in vitro* studies, there came a time to be united under a society and to support this beneficial discipline and the needs of all professionals in the field of nuclear medicine. For such main initiatives and many more, the Turkish Society of Nuclear Medicine (TSNM) was founded in the year of 1975. The headquarter office tor TSNM was chosen to be located in Ankara, the capital of Türkiye and the city where Republic of Türkiye had been founded on 29th of October 1923 (1,2).

Address for Correspondence: Prof. Murat Fani Bozkurt, MD, Hacettepe University Faculty of Medicine, Department of Nuclear Medicine, Ankara, Türkiye
E-mail: fanibozkurt@gmail.com ORCID ID: orcid.org/0000-0003-2016-2624
Received: 03.10.2023 **Accepted:** 03.10.2023

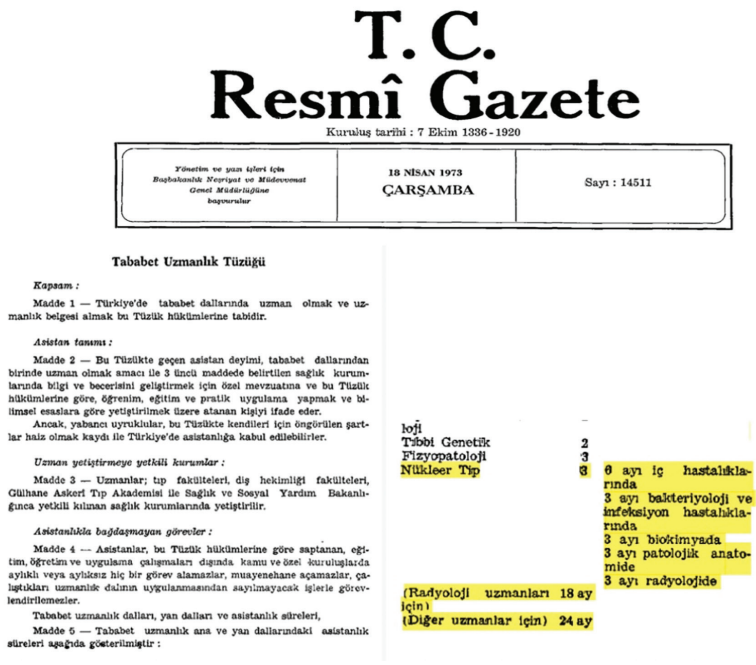

T. C.
Resmî Gazete

Kuruluş tarihi : 7 Ekim 1336 - 1920

Yönetim ve yazı işleri için Başbakanlık Neşriyat ve Müdevvenat Genel Müdürlüğüne başvurulur | 18 NİSAN 1973 ÇARŞAMBA | Sayı : 14511

Tababet Uzmanlık Tüzüğü

Kapsam :

Madde 1 — Türkiye'de tababet dallarında uzman olmak ve uzmanlık belgesi almak bu Tüzük hükümlerine tabidir.

Asistan tanımı :

Madde 2 — Bu Tüzükte geçen asistan deyimi, tababet dallarından birinde uzman olmak amacı ile 3 üncü maddede belirtilen sağlık kurumlarında bilgi ve becerisini geliştirmek için özel mevzuatına ve bu Tüzük hükümlerine göre, öğrenim, eğitim ve pratik uygulama yapmak ve bilimsel esaslara göre yetiştirilmek üzere atanan kişiyi ifade eder.

Ancak, yabancı uyruklular, bu Tüzükte kendileri için öngörülen şartlar hariz olmak kaydı ile Türkiye'de asistanlığa kabul edilebilirler.

Uzman yetiştirmeye yetkili kurumlar :

Madde 3 — Uzmanlar; tıp fakülteleri, diş hekimliği fakülteleri, Gülhane Askeri Tıp Akademisi ile Sağlık ve Sosyal Yardım Bakanlığınca yetkili kılınan sağlık kurumlarında yetiştirilir.

Asistanlıkla bağdaşmayan görevler :

Madde 4 — Asistanlar, bu Tüzük hükümlerine göre saptanan, eğitim, öğretim ve uygulama çalışmaları dışında kamu ve özel kuruluşlarda aylıklı veya aylıksız hiç bir görev alamazlar, muayenehane açamazlar, çalıştıkları uzmanlık dalının uygulanmasından sayılmayacak işlerle görevlendirilemezler.

Tababet uzmanlık dalları, yan dalları ve asistanlık süreleri,

Madde 5 — Tababet uzmanlık ana ve yan dallarındaki asistanlık süreleri aşağıda gösterilmiştir :

loji
Tıbbi Genetik 2
Fizyopatoloji 3
Nükleer Tıp 3

6 ayı iç hastalıklarında
3 ayı bakteriyoloji ve infeksiyon hastalıklarında
3 ayı biokimyada
3 ayı patolojik anatomide
3 ayı radyolojide

(Radyoloji uzmanları 18 ay için)
(Diğer uzmanlar için) 24 ay

Figure 1. The official recognition of nuclear medicine as an individual residency program in Türkiye, documented on the official paper of the Turkish Republic issued on 18th April 1973

Nuclear medicine has evolved to a more clinical manner in Türkiye like elsewhere in the world where this medical practice was taking place. As parallel to the developments and achievements in the technology and industrial production of both radiopharmaceuticals and imaging systems, clinical nuclear medicine has made its way to rapid rise among other clinical disciplines. Nuclear medicine is so unique that it is not a pure basic or a clinical discipline, but contains naturally basic science and clinical science within its intrinsic structure. This feature as bridging between basic and clinical science for nuclear medicine is also unique in a way that it does not only apply for academic work but also daily routine practice.

How Nuclear Medicine Started in Türkiye?: A Short History Back in Time

The first nuclear medicine practice in Türkiye started with extraordinary personal efforts of Prof. Suphi Artunkal (Figure 2), an internal medicine specialist in the beginning of 1950s in İstanbul. Prof. Artunkal and his team had first used I-131 to treat hyperthyroidism in the Radioisotope Laboratory within Haseki Hospital in İstanbul, of which he was the founder. This success was a real turning point for the rapid development of nuclear medicine practice in Türkiye in the following years.

Türkiye is not only among a few countries in which nuclear medicine applications had found use in routine

Figure 2. Professor Suphi Artunkal, the founder of nuclear medicine in Türkiye

clinical practice but also one of the first countries in which nuclear medicine supplies mainly radionuclides and radiopharmaceuticals had been locally produced. The first local radionuclide production in Türkiye took place at Çekmece Nuclear Training and Research Center in İstanbul in the year 1961, by which Türkiye became one of the first countries to use locally produced Tc-99m-pertechnetate.

Prof. Fevzi Renda and his team founded Radiobiology Institute within Ankara University in Ankara, with support

from International Agency of Atomic Energy in the year 1962. Just a few years after, the first rectilinear scanner was installed in Radioisotope Laboratory at İstanbul University in 1965, which gave rise to the foundation of Nuclear Medicine Institute in the following years. Prof. Fevzi Renda in Ankara, Prof. İrfan Urgancıoğlu in İstanbul, Prof. Nail Tartaroğlu in İzmir and Prof. Coşkun Bekdik in Ankara are among the pioneer medical doctors who started nuclear medicine applications in 1960s in Türkiye (1-3).

Short History of TSNM

TSNM was founded by the following nuclear medicine physicians on 9th May 1975:

Prof. Fevzi Renda

Prof. A. İrfan Urgancıoğlu

Prof. Ali Tan Işıtman

Prof. Ali Nail Tartaroğlu

Prof. Coşkun Bekdik

Prof. Münir Telatar

Prof. Asım Akın

Dr. Güner Tokuz

Dr. Ergun Ergun

Dr. Behçet İzbırak

Presidents of TSNM

Prof. Fevzi Renda	1975-1990
Prof. Coşkun Bekdik	1990-1994
Prof. İrfan Urgancıoğlu	1994-1996
Prof. Sema Cantez	1996-1998
Prof. Ali Tan Işıtman	1998-2002
Prof. Hatice Durak	2002-2006
Prof. Haluk B. Sayman	2006-2008
Prof. Mustafa Ünlü	2008-2010
Prof. Ömer Uğur	2010-2014
Prof. Zehra Özcan	2014-2018
Prof. Gamze Çapa Kaya	2018-2021
Prof. Tevfik Fikret Çermik	2021-2023
Prof. Murat Fani Bozkurt	2023-current

Short History of Annual Congresses of TSNM

The first annual congress of TSNM was held as "The 1st National Nuclear Medicine and Biological Sciences Congress" on 28-29 October 1981 in İstanbul and the first congress president was Prof. İrfan Urgancıoğlu.

Türkiye is one of the few countries in which European Association of Nuclear Medicine (EANM) Congress was held. The EANM Congress was hosted in İstanbul by the congress president Prof. Hatice Durak in the year of 2005 with great success.

Since the first annual congress in 1981, a total of 35 congresses were held by TSNM until present time.

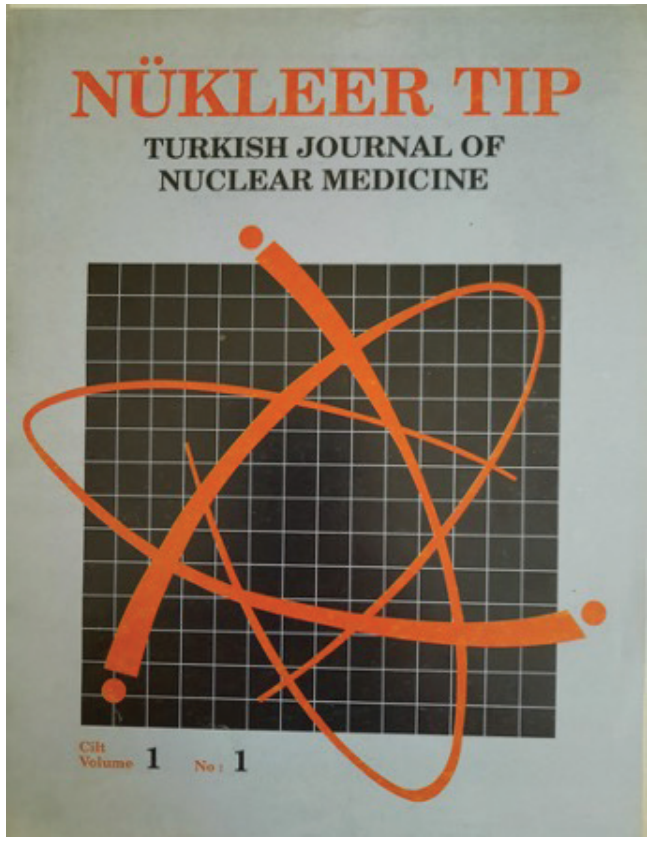

Figure 3. The cover page of the first issue of "Nükleer Tıp-Turkish Journal of Nuclear Medicine", published in 1992

The Offical Journals of TSNM: Historical Look-back from Molecular Imaging and Radionuclide Imaging

The first official journal of TSNM was published as "Nükleer Tıp-Turkish Journal of Nuclear Medicine" (Figure 3) on 30th March 1992 by then-president of TSNM Prof. Coşkun Bekdik as the owner and Prof. Hikmet Bayhan as the first editor. In the year 2011, the name of the Journal was changed as "Molecular Imaging and Radionuclide Imaging (MIRT)" (Figure 4) and went on regular-based publication fully in English language as an international journal by the editor Prof. Hatice Durak of that period. MIRT Journal was indexed in Pub-Med Medline Central as the first time in 2014 and has increased its range of citation indexes at both national and international level since then. Prof. Belkıs Erbaş and Prof. Zehra Özcan were the editors-in-chief before the current editor-in-chief Prof. M. Fani Bozkurt.

Figure 4. The cover page of the first issue of "Molecular Imaging and Radionuclide Therapy (MIRT)" in 2011

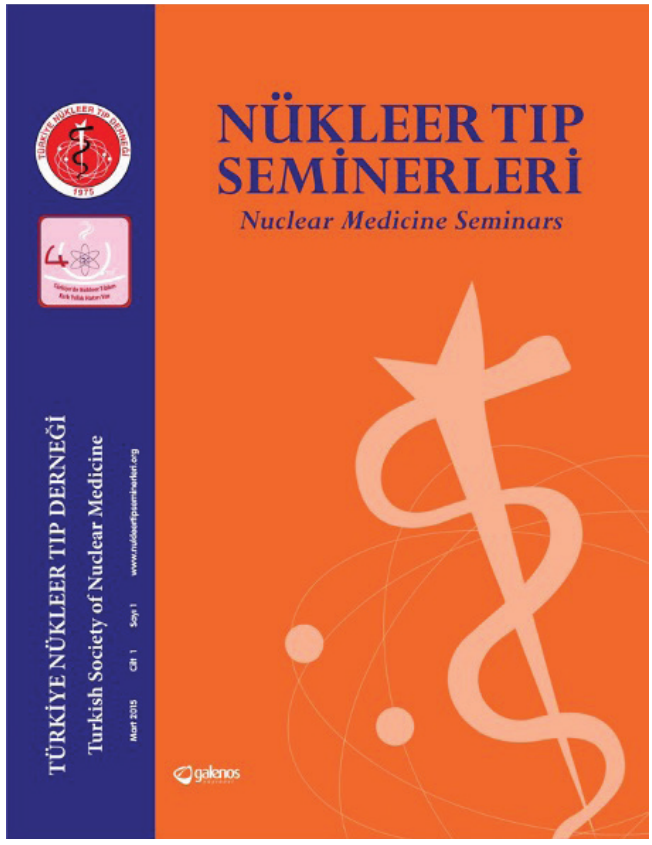

Figure 5. The cover page of the first issue of "Nükleer Tıp Seminerleri Nuclear Medicine Seminars" in 2015

In addition to MIRT, another journal of TSNM with the name of "Nükleer Tıp Seminerleri (Nuclear Medicine Seminars)" (Figure 5) started its publication in Turkish language in the year 2015, on the occasion of 40th anniversary of TSNM and is still being published on regular basis in order to support nuclear medicine training in Türkiye. The first editor of this journal was Prof. Zeynep Burak, followed with Prof. Tamer Özülker as the current editor-in-chief.

Last Words from the TSNM President

Nuclear medicine in Türkiye has a long history for more than 70 years back from the first medical use of radioisotopes and nuclear medicine professionals in Türkiye are so proud to celebrate the 50th anniversary of official recognition of nuclear medicine as an individual medical branch and a residency program along with a very nice occasion of celebrating the 100th anniversary of the Turkish Republic in October 2023. Nuclear medicine in Türkiye will definitely proceed its journey with great achievements in future too, owing to enormous efforts and dedication of not only nuclear medicine physicians but also a great team of radiochemists, radiopharmacists, physicists, technologists and industry.

On behalf of TSNM Executive Board, I would like to express my sincere gratitude to all of our senior pioneers, colleagues and all team members for their great contributions to nuclear medicine in Türkiye.

Long live Turkish Nuclear Medicine, long live Turkish Republic!

References

1. Bozkurt MF, Çermik TF, Sarı O, Çapa Kaya G, Sayit Bilgin E, Güngör F, Özcan Z. Türkiye'de Nükleer Tıp "Tarihsel Yolculuğumuzda Dönüm Noktaları". Nükleer Tıp Seminerleri / Nuclear Medicine Seminars 2015;1(Supplement).
2. Ozcan Z, Bozkurt MF, Erbaş B, Durak H. Nuclear medicine training and practice in Türkiye. Eur J Nucl Med Mol Imaging 2017;44:903-908.
3. Bozkurt MF. Nuclear Theranostics in Türkiye. Nucl Med Mol Imaging 2019;53:11-13.

Original Article
Mol Imaging Radionucl Ther 2023;32:195-205 DOI:10.4274/mirt.galenos.2022.60024

Relationship Between Metabolic Activity, Cellularity, Histopathological Features of Primary Tumors and Distant Metastatic Potential in Breast Cancer

Meme Kanserinde Primer Tümörün Metabolik Aktivitesinin, Hücreselliğinin ve Histopatolojik Özelliklerinin Uzak Metastaz Potansiyeli ile İlişkisi

Uğuray Aydos[1], Seda Gülbahar Ateş[2], Osman Kurukahvecioğlu[3], Ümit Özgür Akdemir[1], Pınar Uyar Göçün[4], Lütfiye Özlem Atay[1]

[1]*Gazi University Faculty of Medicine, Department of Nuclear Medicine, Ankara, Türkiye*
[2]*University of Health Sciences Türkiye, Dr. Abdurrahman Yurtaslan Ankara Oncology Training and Research Hospital, Clinic of Nuclear Medicine, Ankara, Türkiye*
[3]*Gazi University Faculty of Medicine, Department of General Surgery, Ankara, Türkiye*
[4]*Gazi University Faculty of Medicine, Department of Medical Pathology, Ankara, Türkiye*

Abstract

Objectives: The aim of this study was to evaluate the relationship between the types of distant metastatic spread, histopathological features, and imaging features of primary tumor on positron emission tomography/magnetic resonance imaging (PET/MRI) for primary staging in newly diagnosed breast invasive ductal carcinoma (IDC) patients.

Methods: Data from 289 female patients were retrospectively evaluated. Maximum standardized uptake value, metabolic tumor volume (MTV), total lesion glycolysis (TLG), and minimum apparent diffusion coefficient (ADC_{min}) values of primary tumors were obtained from PET/MRI. The patients were grouped as non-metastatic, oligometastatic (1-5 metastatic lesions) and multimetastatic (>5 metastatic lesions) disease according to the number of distant metastases, and divided into two groups as isolated bone metastasis (IBM) and mixed/soft tissue metastasis (M-SM) groups according to the sites of metastatic spread.

Results: Metabolic parameters had higher values and ADC_{min} had lower values in the multimetastatic and oligometastatic groups than in the non-metastatic group. MTV was the only parameter that showed significant difference between the multimetastatic and oligometastatic groups. MTV and TLG were significantly higher in the M-SM group than in the IBM group. ^{18}F-fluorodeoxyglucose PET parameters had significantly higher values in grade 3, hormone receptor negative, human epidermal growth factor receptor 2 positive, triple negative, and highly proliferative (Ki-67 ≥14%) tumors. The prediction models that included imaging parameters to predict the presence of distant metastasis had higher discriminatory powers than the prediction models that included only histopathological parameters.

Conclusion: Primary tumors with higher metabolic-glycolytic activity and higher cellularity were more aggressive and had higher metastatic potential in breast IDC. Compared with histopathological parameters alone, the combination of imaging parameters and histopathological features of primary tumors may help to better understand tumor biology and behavior.

Keywords: ^{18}F-FDG PET/MRI, breast cancer, oligometastasis, multimetastasis, bone metastasis, soft tissue metastasis

Öz

Amaç: Bu çalışmanın amacı, yeni tanı meme invaziv duktal karsinom (İDK) hastalarında primer evreleme pozitron emisyon tomografisi/manyetik rezonans görüntüleme (PET/MRG) görüntülerinden elde edilen görüntüleme parametrelerinin, histopatolojik özelliklerin ve uzak metastatik yayılım tipleri arasındaki ilişkinin değerlendirilmesidir.

Address for Correspondence: Asst. Prof. Uğuray Aydos, Gazi University Faculty of Medicine, Department of Nuclear Medicine, Ankara, Türkiye
Phone: +90 312 202 45 42 **E-mail:** uguray23@gmail.com ORCID ID: orcid.org/0000-0003-0582-5020
Received: 15.11.2022 **Accepted:** 18.12.2022

Yöntem: İki yüz seksen dokuz kadın hastanın verileri retrospektif olarak değerlendirildi. Primer tümörün maksimum standartlaştırılmış alım değeri, metabolik tümör volümü (MTV), toplam lezyon glikolizisi (TLG) ve minimum görünür difüzyon katsayı (ADC_{min}) değerleri PET/MRG'lerden elde edildi. Uzak metastaz sayısına göre hastalar non-metastatik, oligometastatik (OM) (1-5 metastatik lezyon) ve multimetastatik (>5 metastatik lezyon) olarak gruplandı. Uzak metastazı bulunan hastalar ayrıca metastatik yayılım bölgelerine göre izole kemik metastazı (İKM) ve mikst/yumuşak doku metastazı (M-YDM) olarak iki gruba ayrıldı.

Bulgular: Multimetastatik ve oligometastatik gruplarında non-metastatik grubuna göre metabolik parametreler daha yüksek değerler gösterirken, ADC_{min} değeri anlamlı olarak daha düşüktü. MTV, multimetastatik ve oligometastatik grupları arasında anlamlı farklılık gösteren tek parametreydi. M-YDM grubunda MTV ve TLG değerleri İKM grubuna göre anlamlı olarak daha yüksekti. ^{18}F-florodeoksiglukoz PET parametreleri grade 3, hormon reseptör negatif, insan epidermal büyüme faktörü reseptör 2 pozitif, triple negatif ve yüksek proliferatif (Ki-67 ≥%14) tümörlerde anlamlı olarak daha yüksek değerlere sahipti. Uzak metastaz varlığını öngörmek için oluşturulan ve görüntüleme parametrelerini içeren modellerin ayırıcılık gücü, sadece histopatolojik özellikleri içeren öngörü modelinden daha yüksek olarak bulundu.

Sonuç: Meme İDK'de yüksek metabolik-glikolitik aktivite ve yüksek hücresellik gösteren primer tümörler daha agresif ve daha yüksek metastatik potansiyele sahiptir. Tek başına histopatolojik parametrelere kıyasla primer tümörün histopatolojik özelliklerinin ve görüntüleme parametrelerinin kombinasyonu tümör biyolojisi ve davranışının daha iyi anlaşılmasına yardımcı olabilir.

Anahtar kelimeler: ^{18}F-FDG PET/MRG, meme kanseri, oligometastaz, multimetastaz, kemik metastazı, yumuşak doku metastazı

Introduction

Breast cancer is the most common type of malignancy in women and is one of the most common causes of cancer-related deaths (1). Invasive ductal carcinoma (IDC) is the most common subtype and constitutes approximately 75% of all breast cancers (2). Distant metastasis (stage IV disease) at the time of diagnosis can be detected in approximately 3.5% to 7% of newly diagnosed patients (3). The median overall survival times may vary significantly in patients with distant metastasis (4). Some prognostic factors that may affect survival include tumor biology, metastatic tumor load, and the localization of distant metastases (5).

Breast carcinoma is one of the most common osteotropic tumors, along with prostate cancer. In addition, bone is the first site of relapse in approximately 50% of patients with breast cancer (6). Breast cancer can also metastasize to soft tissues such as distant lymph nodes, liver, and lung (7). Localization of distant organs where breast cancer metastasizes has clinical and prognostic importance. Although there are several complications such as bone pain, hypercalcemia, and pathologic fractures in patients with isolated bone metastasis (IBM), survival rates are higher in this patient group than in those with soft tissue metastasis (SM) (5,6,8).

Although metastatic breast cancers are generally considered incurable, patients with higher survival rates can be observed within this group. This clinical condition can also be associated with oligometastatic disease. In 1995, Hellman and Weichselbaum (9) conceptualized oligometastatic disease as an intermediate state with a limited number of metastases in malignant tumors. In their view, oligometastatic tumors may not have the genetic and biological features to rapidly develop multimetastasis (9,10). Approximately 1-10% of newly diagnosed patients with metastatic breast cancer have "*de novo*" oligometastatic disease (3). With the combined use of systemic and aggressive local treatment options in patients with oligometastatic disease, higher progression-free and overall survival rates can be achieved. Recently, the use of imaging modalities has increased the frequency of detection of oligometastatic disease in various types of malignancies, such as ^{18}F-fluorodeoxyglucose (FDG) positron emission tomography/computed tomography (PET/CT) or PET/magnetic resonance imaging (MRI).

IBM and oligometastatic disease may be related to different biological features of the primary tumor in breast carcinomas, such as hormone receptor status, human epidermal growth factor receptor 2 (HER2) status, and proliferation index (6,11,12). ^{18}F-FDG PET-derived metabolic parameters also have significant relationships with histopathological features (molecular subtypes, proliferation and tumor grade) of primary tumors (13,14,15). However, to the best of our knowledge, studies that evaluated the relationship between ^{18}F-FDG PET/MRI-derived quantitative parameters, the number of distant metastatic lesions (oligometastatic vs. multimetastatic disease), and the localization of distant metastases [IBM vs. mixed/soft tissue metastasis (M-SM)] in primary staging are not numerous. Therefore, this study aimed to evaluate the relationship between the types of distant metastatic spread and the imaging features of the primary tumor on PET/MRI for primary staging in newly diagnosed patients with breast IDC. This study also aimed to evaluate the relationship between histopathological features, imaging parameters, and metastasis types.

Materials and Methods

Patients

We retrospectively reviewed patients with newly diagnosed, histopathologically confirmed breast cancer

who underwent ^{18}F-FDG PET/MRI for primary staging before surgery or neoadjuvant treatment in our department between 2016 and 2020. Patients who (a) had a history of another malignancy, (b) had a diagnosis of breast cancer other than IDC, (c) received any neoadjuvant treatment before ^{18}F-FDG PET/MRI were excluded from the study. A total of 289 female patients (mean age: 51.5±12.2 years) were included in the analysis. The histopathological data of the patients were recorded. This study was approved by the Gazi University Local Ethical Committee (decision no: 296, date: 11.05.2020).

^{18}F-FDG PET/MRI

PET/MRI of all patients was performed in accordance with the protocols recommended in international guidelines. According to the protocol used, patients fasted for 4-6 h and blood glucose levels were confirmed to be 180 mg/dL before intravenous injection of ^{18}F-FDG. All patients received a single injection of ^{18}F-FDG (median activity: 170 MBq; range: 78-310 MBq). PET/MRI were acquired using an integrated 3 Tesla PET/MRI scanner (GE Signa PET/MRI, GE Healthcare, Waukesha, Wisconsin, USA) with a time-of-flight PET detector 60 min after injection. Both whole body and breast dedicated PET/MRI protocols included an initial localizer scan and a 3D dual-echo fast spoiled gradient recalled echo liver-accelerated volume acquisition sequence (LAVA-FLEX) for MRI-based attenuation correction (MRAC). Whole-body PET/MRI was followed by a high-resolution axial T1-weighted 3D LAVA-FLEX sequence, coronal T2-weighted fast-recovery fast spin echo sequence, whole -body diffusion-weighted images (DWI) (b values: 50, 1000 s/mm^2), and apparent diffusion coefficient (ADC) mapping. The whole-body protocol included 5 or 6 bed positions. PET emission scans were recorded together with MRI sequences, and the acquisition time per bed position was 3 min. Breast-dedicated PET/MRI with an 8-channel breast coil included axial T1-weighted and high-resolution T2-weighted sequences, axial DWI (b values: 50, 800 s/mm^2), and ADC mapping in 1 bed position, with an acquisition time of 15 min. For the attenuation correction, an atlas-based attenuation correction map was used for the head, and a vendor-based algorithm using MRI-based attenuation correction data was used for the remaining body parts. The whole-body and breast-dedicated PET/MR images were acquired without contrast material injection.

^{18}F-FDG PET/MRI Image Analysis

All PET/MRI were visually and quantitatively evaluated by one experienced nuclear medicine specialist using vendor-based workstations (AW volume share 5, GE Medical Systems). For visual assessment, the number of ^{18}F-FDG-positive lesions that displayed pathological correlates on MRI and were consistent with distant metastasis at follow-up were recorded for each patient. The pathological correlates of ^{18}F-FDG-positive metastatic lesions on MRI were hypointensity on T1-w images and hyperintensity on T2-w images associated with increased signal intensity on DWI and diffusion restriction on ADC maps. Patients were grouped as non-metastatic, oligometastatic, and multimetastatic according to the number of distant metastatic lesions. For the definition of "*de novo*" oligometastatic disease, we used a cut-off of maximum of five PET-positive distant metastatic lesions (3). Patients with distant metastasis were also divided into two groups according to the localization of metastatic lesions: i) IBM, ii) M-SM. For quantitative evaluation, the maximum standardized uptake value (SUV_{max}), metabolic tumor volume (MTV), total lesion glycolysis (TLG), and minimum ADC (ADC_{min}) of primary tumors were extracted from PET/MRI data. SUV_{max}, MTV, and TLG were calculated on whole body images. For the calculation of MTV and TLG, the volumes of interest were automatically drawn over primary tumors using the program with a 42% threshold of SUV_{max}. ADC_{min} values (using b value: 800 s/mm^2) were extracted by manually drawing the region of interest around each primary tumor. There were no patients with bilateral breast tumors in the patient population. In patients with more than one tumor in the same breast, quantitative measurements were obtained from the tumor focus with the most intense ^{18}F-FDG uptake.

Statistical Analysis

Differences in categorical variables between metastatic groups were assessed using the chi-square test and Fisher's exact test. Differences in continuous variables between metastatic groups were analyzed using the Mann-Whitney U test and the Kruskal-Wallis test, with corrections for multiple pairwise comparisons. The likelihood of the presence of distant metastasis was modeled with logistic regression analyses using histopathological and imaging parameters. The discriminatory abilities of the prediction models were assessed by receiver operating characteristic (ROC) curve analysis. All statistical analyses were performed using IBM SPSS Statistics for Windows (version 23.0, IBM Corp., Armonk, New York) software. For all analyses a p value <0.05 was considered statistically significant.

Results

Patient Characteristics

The clinical and imaging characteristics of the patients are summarized in Table 1. The patients had a mean age of 51.5±12.2 years. There were no distant metastatic lesions in 220 patients (76.1%). Twenty-six patients (9%)

had oligometastatic disease, and 43 patients (14.9%) had multimetastatic disease. Of the 69 patients with distant metastasis, 29 (42%) had IBM and 40 (58%) had M-SM. Of the patients with oligometastasis (n=26), 20 had IBM and 6 had M-SM. Of the patients with multimetastasis (n=43), 9 had IBM and 34 had M-SM. While IBM was seen in 76.9% of the patients in the OM group, M-SM was seen in 79.1% of the patients in the MM group. This difference between the OM and MM groups was significant (p<0.001). Of the patients with M-SM, 27 had distant lymph node metastases, 25 had lung metastases, 13 had liver metastases, and 2 had brain metastases. Histopathological and/or clinical axillary lymph node metastasis was observed in 67.2% of patients (178/265). While there were no patients with distant metastasis in the axillary lymph node negative group, distant metastasis was detected in 33.7% of patients with axillary lymph node metastasis (p<0.001).

Table 1. The characteristics of patients

Age (mean ± SD) (range)	51.5±12.2 years (26-86 years)
	n (%)
Tumor grade	
Grade 1	32 (11.1%)
Grade 2	134 (46.4%)
Grade 3	114 (39.4%)
Missing	9 (3.1%)
Molecular subtype	
Luminal A	60 (20.8%)
Luminal B (HER2 negative)	133 (46%)
Luminal B (HER2 positive)	41 (14.2%)
HER2 overexpressed	23 (8%)
Triple negative	32 (11%)
Hormone receptor status	
Hormone receptor positive	234 (81%)
Hormone receptor negative	55 (19%)
HER2 status	
HER2 positive	64 (22.2%)
HER2 negative	225 (77.8%)
Ki-67 index	
Low (<14%)	67 (23.2%)
High (≥14%)	222 (76.8%)
Metastatic status	
Non-metastatic group (M0)	220 (76.1%)
Oligometastatic group	26 (9%)
Multimetastatic group	43 (14.9%)
The type of distant metastasis	
Isolated bone metastasis	29 (42%)
Mixed-soft tissue metastasis	40 (58%)

HER2: Human epidermal growth factor receptor 2, SD: Standard deviation

Relationship Between Imaging Parameters and Metastasis Groups

SUV_{max}, MTV, TLG, and ADC_{min} values of primary breast tumors had significant differences among metastatic groups (Table 2). SUV_{max}, MTV, and TLG were higher and ADC_{min} was lower in the multimetastatic group than in the oligometastatic and non-metastatic groups (Figures 1, 2). For the comparison between the multimetastatic and non-metastatic groups, SUV_{max}, MTV, TLG, and ADC_{min} demonstrated significant differences (p=0.01, p<0.001, p<0.001, and p<0.001, respectively). For the comparison between the oligometastatic and non-metastatic groups, SUV_{max}, MTV, TLG, and ADC_{min} had significant differences (p=0.021, p<0.001, p<0.001, p=0.033, respectively). For the comparison between the multimetastatic and oligometastatic groups, MTV was the only parameter with significantly higher values in the multimetastatic group (p=0.048). The median values of MTV and TLG were significantly higher in patients with M-SM than in those with IBM (Table 2). In patients with oligometastasis, TLG was the only imaging parameter that had a significant difference between the IBM and M-SM groups, with higher median values in the M-SM group (70.7 vs. 42.3, p=0.02).

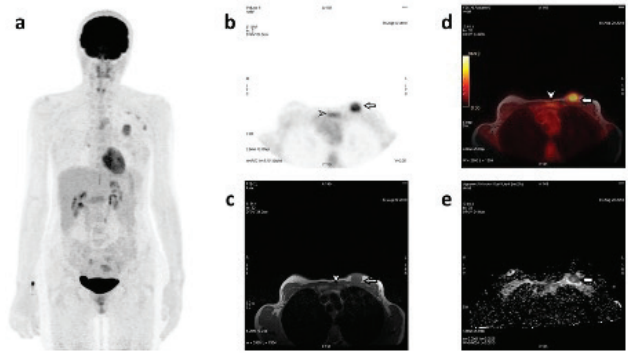

Figure 1. MIP (a), axial ^{18}F-FDG PET (b), axial T1 weighted MRI (c), axial fusion (d), and ADC mapping (e) whole body and breast dedicated PET/MRI of a 41-year-old female patient with invasive ductal carcinoma in left breast (arrows). SUV_{max}, MTV, TLG, ADCmin values of tumors were 5.9, 6.9 cm^3, 25.7 g, $0.42x10^{-3}$ mm^2/s, respectively. Histopathological features of tumor: grade 2, Ki-67 expression level 30%, ER and PR positive, HER2 negative. ^{18}F-FDG uptakes in left axillary lymph nodes were also seen on MIP image. The patient was included in oligometastatic and isolated bone metastasis groups, with one distant metastatic focus on manubrium of sternum (arrowheads)

MIP: Maximum intensity projection, ^{18}F-FDG: ^{18}F-fluorodeoxyglucose, PET: Positron emission tomography, MRI: Magnetic resonance imaging, ADC: Apparent diffusion coefficient, SUV_{max}: Maximum standardized uptake value, MTV: Metabolic tumor volume, TLG: Total lesion glycolysis, ER: Estrogen receptor, PR: Progesterone receptor, HER2: Human epidermal growth factor receptor 2

Relationship Between Histopathological Parameters and Metastasis

There was no significant association between tumor grade categories (low-intermediate grade: grade 1-2 vs. high grade: grade 3) and metastatic groups (p>0.05). In patients with distant metastasis (n=69), a significant association was found between hormone receptor status and distant metastatic sites (p=0.01). In metastatic patients with hormone receptor-positive tumors (n=57), the proportions of IBM and M-SM were 49.1% (28/57) and 50.9% (29/57), respectively. However, in metastatic patients with hormone receptor negative tumors (n=12), these proportions were 8.3% (1/12) and 91.7% (11/12), respectively. Distant metastasis was observed in 20.5% (46/224) of HER2-negative patients. This ratio was 35.4% (23/65) in patients with HER2 positivity (p=0.02). In patients with distant metastasis, patients with HER2 amplification had a significantly higher ratio of having M-SM (18/23, 78.3%) than those without HER2 amplification (22/46, 47.8%) (p=0.02). In the triple negative cancer group (n=32), distant metastasis was seen in only 3 patients, and all of these patients had M-SM.

Distant metastasis was observed in 7.8% (5/64) of the patients with low proliferation index levels (Ki-67 <14%), and this ratio was 27.8% (61/219) in the patients with high proliferation index (Ki-67 ≥14%) (p<0.001). In patients with oligometastasis, Ki-67 index levels were significantly higher in the M-SM group than in the IBM group (60% vs. 25%, respectively; p=0.015). However, in patients with multimetastasis, Ki-67 index levels did not demonstrate significant differences between the IBM and M-SM groups (30% vs. 30%, respectively; p>0.05).

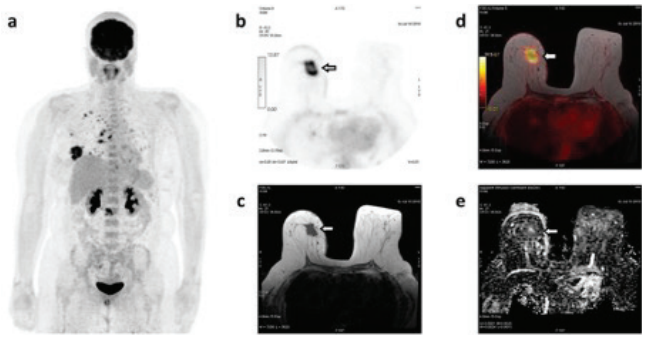

Figure 2. MIP (a), axial ^{18}F-FDG PET (b), axial T1 weighted MRI (c), axial fusion (d) and ADC mapping (e) whole body and breast dedicated PET/MRI images of a 50-year-old female patient with invasive ductal carcinoma in right breast (arrows). SUV_{max}, MTV, TLG, ADC_{min} values of tumors were 16.0, 12.2 cm^3, 109.7 g, 0.67x10^{-3} mm^2/s, respectively. Histopathological features of tumor: grade 2, Ki-67 expression level 50%, ER and PR positive, HER2 positive. ^{18}F-FDG uptakes in right axillary lymph nodes were also seen on MIP image. The patient was included in multimetastatic and mixed-soft tissue metastasis groups, with multiple distant metastatic foci on mediastinal lymph nodes, bilateral lungs, manubrium of sternum and L2 vertebra

MIP: Maximum intensity projection, ^{18}F-FDG: ^{18}F-fluorodeoxyglucose, PET: Positron emission tomography, MRI: Magnetic resonance imaging, ADC: Apparent diffusion coefficient, SUV_{max}: Maximum standardized uptake value, MTV: Metabolic tumor volume, TLG: Total lesion glycolysis, ER: Estrogen receptor, PR: Progesterone receptor, HER2: Human epidermal growth factor receptor 2

Relationship Between the Histopathological and Imaging Parameters

SUV_{max} and TLG were found to be significantly higher in grade 3 tumors than in grade 1-2 tumors, in hormone receptor -negative tumors than in positive tumors, in HER2-positive tumors than in negative tumors, and in triple-negative tumors than in non-triple-negative tumors. Higher MTV and lower ADC_{min} values were found in high-grade tumors, with marginal significance (p=0.06 and p=0.054, respectively). SUV_{max}, MTV, and TLG were significantly

Table 2. The relationship between imaging parameters of primary tumors, metastatic groups and distant metastasis types

	Median SUV_{max} (range)	p	Median MTV (range) (cm^3)	p	Median TLG (range) (g)	p	Median ADC_{min} (x10^{-3} mm^2/s) (range)	p
Metastatic groups								
Non-metastatic (M0) group (n=220)	6.2 (0.6-31.7)	**0.001**	3.0 (0.3-152.0)	**<0.001**	10.1 (0.2-1126.3)	**<0.001**	0.71 (0.1-1.11)	**<0.001**
Oligometastatic group (n=26)	8.8 (3.0-32.6)	-	8.3 (1.3-59.0)	-	52.1 (3.3-885.6)	-	0.51 (0.02-0.89)	-
Multimetastatic group (n=43)	10.0 (1.4-26.0)	-	14.4 (0.7-220.0)	-	64.6 (1.8-2076.8)	-	0.46 (0.01-0.73)	-
Distant metastasis types								
IBM group (n=29)	8.1 (3.0-32.6)	0.141	8.2 (0.7-220.0)	**0.008**	41.5 (1.8-2076.8)	**0.01**	0.46 (0.02-0.89)	0.502
M-SM group (n=40)	10.4 (1.4-30.8)	-	16.3 (2.1-104.0)	-	100.8 (6.8-1456.3)	-	0.53 (0.01-0.89)	-

The bold entries indicate a significant result. SUV_{max}: Maximum standardized uptake value, MTV: Metabolic tumor volume, TLG: Total lesion glycolysis, ADC: Apparent diffusion coefficient, IBM: Isolated bone metastasis, M-SM: Mixed or soft tissue metastasis

higher, and ADC_{min} was significantly lower in tumors with high Ki-67 index compared with tumors with low Ki-67 index (Table 3).

Regression Analyses and Prediction Models

In multivariate regression analysis using only histopathological parameters (model 1), Ki-67 index category (<14% vs. ≥14%) and HER2 positivity were significant predictive factors for distant metastasis [odds ratio (OR) with 95% confidence interval (CI): 4.57 with 1.66-12.6, p=0.003 for higher Ki-67 category, and 5.0 with 1.1-22.8, p=0.036 for HER2 positivity]. In multivariate analysis using only PET/MRI parameters (model 2), SUV_{max} (OR with 95% CI 1.12 with 1.03-1.22, p=0.006), MTV (1.08 with 1.02-1.15, p=0.007), TLG (1.02 with 1.0-1.04, p=0.025), and ADC_{min} (0.6 with 0.48-0.75, p<0.001) were found to be significant predictive factors. In another multivariate analysis using histopathological parameters and imaging parameters together (model 3), imaging parameters of primary tumors were found to be significant predictive factors.

In ROC curve analysis, the area under the curve (AUC) values of the prediction models for distant metastasis were 0.66 (95% CI, 0.56-0.75; p=0.008) in model 1, 0.85 (95% CI, 0.78-0.92; p<0.001) in model 2, and 0.90 (95% CI, 0.84-0.95; p<0.001) in model 3. These values indicated the strong discriminatory ability of models 2 and 3. The AUCs of prediction models 2 and 3 were higher than those of model 1 (Figure 3).

Discussion

Distant metastasis causes most cancer-related deaths. There are some important theories about the metastatic spread of tumors. In 1889, Paget's "seed and soil" hypothesis stated that circulating tumor cells released from primary tumors would seed to an amenable organ microenvironment. In 1894, Halstead stated that cancer metastasis was a progressive anatomical process of contiguous seeding by direct spread from the primary tumor to the regional lymph nodes and then to distant sites. The "systemic theory of metastasis", suggested by Keynes, stated that widespread dissemination occurs from the beginning of cancer and primary tumor is an early manifestation of systemic disease (16,17). In contrast to these theories, in 1994, Hellman developed the "spectrum theory" of cancer metastases, which was first described for breast cancers. According to

Table 3. The relationship between imaging parameters and histopathological features of primary tumors

	Median SUV_{max} (range)	p	Median MTV (range) (cm^3)	p	Median TLG (range) (g)	p	Median ADC_{min} ($x10^{-3}$ mm^2/s) (range)	p
Histopathological tumor grade								
Low-intermediate grade (grade 1-2) (n=166)	5.6 (0.6-31.7)	**<0.001**	3.6 (0.3-152.0)	0.06	11.2 (0.2-1456.3)	**0.001**	0.69 (0.01-1.11)	0.054
High grade (n=114)	9.7 (0.8-32.6)	-	4.9 (0.5-220.0)	-	31.8 (0.7-2076.8)	-	0.66 (0.1-0.97)	-
Steroid hormon receptor status								
Hormone receptor positive (ER and/or PR +) (n=234)	6.7 (0.6-32.6)	**<0.001**	3.8 (0.3-220.0)	0.399	14.5 (0.2-2076.8)	**0.034**	0.67 (0.01-1.11)	0.198
Hormone receptor negative (ER and PR -) (n=55)	9.9 (0.8-30.8)	-	4.8 (0.5-152.0)	-	28.4 (0.7-1126.3)	-	0.73 (0.24-0.97)	-
HER2 status								
HER2 negative (n=225)	6.8 (0.6-32.6)	**0.002**	3.7 (0.3-220.0)	0.125	14.4 (0.2-2076.8)	**0.017**	0.67 (0.01-1.11)	0.456
HER2 positive (n=64)	8.9 (1.1-29.2)	-	5.5 (0.6-82.5)	-	27.4 (0.7-643.8)	-	0.73 (0.24-0.97)	-
Triple negative status								
Triple negative (n=32)	10.4 (0.8-30.8)	**0.005**	5.8 (0.5-152.0)	0.119	43.2 (0.7-1126.3)	**0.032**	0.69 (0.50-0.97)	0.367
Non-triple negative (n=257)	6.9 (0.6-32.6)	-	3.9 (0.3-220.0)	-	14.8 (0.2-2076.8)	-	0.68 (0.01-1.11)	-
Ki-67 index status								
<14% (n=67)	3.6 (0.7-17.0)	**<0.001**	2.2 (0.3-43.8)	**<0.001**	6.4 (0.2-271.2)	**<0.001**	0.75 (0.01-0.99)	**0.005**
≥14% (n=222)	8.7 (0.6-32.6)	-	4.8 (0.3-220.0)	-	27.0 (0.3-2076.8)	-	0.66 (0.02-1.11)	-

The bold entries indicate a significant result. SUV_{max}: Maximum standardized uptake value, MTV: Metabolic tumor volume, TLG: Total lesion glycolysis, ADC: Apparent diffusion coefficient, ER: Estrogen receptor, PR: Progesterone receptor, HER2: Human epidermal growth factor receptor 2

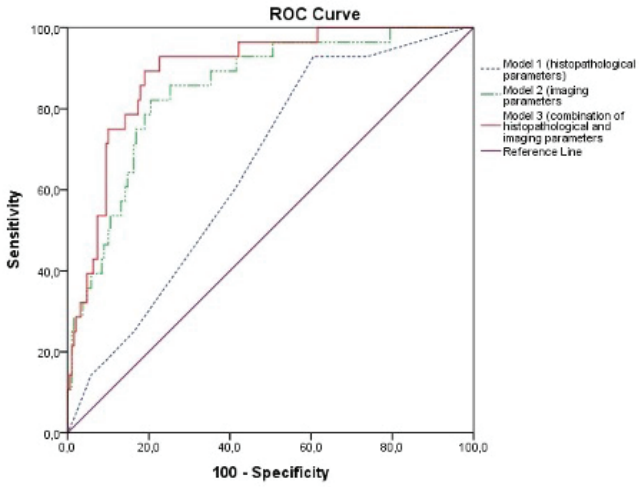

Figure 3. Receiver operating characteristic curves for multivariable prediction models in discriminating the presence of distant metastasis. The AUCs were 0.66 for model 1, 0.85 for model 2 and 0.90 for model 3, respectively
ROC: Receiver operating characteristic, AUC: Area under the curve

this evolutionary theory, cancer progression is a multistep process, ranging from indolent disease to widespread metastasis (16,18). Based on this theory, in 1995, Hellman and Weichselbaum (9) described oligometastatic disease as an intermediate state in the spectrum of metastatic disease. At the oligometastatic stage, tumors may not have aggressive biological features adequate to develop widespread metastasis, and the metastatic potential is limited with low burden disease. With the combined use of systemic and aggressive local treatment options in patients with oligometastatic disease, higher progression-free and overall survival rates can be achieved compared with multimetastatic disease (19). The biological characteristics of primary tumors are considered to be one of the most important factors in determining the type of metastatic spread due to the microenvironmental conditions in the primary tumor and the circulating tumor cells released from the primary tumor (16). Therefore, we aimed to investigate the relationship between histopathological markers, ^{18}F-FDG PET/MRI-derived imaging parameters of primary tumors as *in vivo* markers, and the types of distant metastases. There is no consensus on a strict definition of oligometastatic disease, and different cut-offs were used in the literature. For the definition of oligometastatic disease, we used the cut-off of maximum five ^{18}F-FDG PET-positive metastatic lesions (3). To obtain a more homogeneous patient population, only patients with IDC of the breast were included in our study because ^{18}F-FDG uptakes of primary tumors were found to be different among various histopathological types of breast carcinoma in previous studies (14,20).

Lactate is considered a metabolic key player in tumor metabolism. Altered glucose metabolism is pivotal for tumor growth. Warburg reported that cancer cells could maintain a high rate of glycolysis and their capacity to convert glucose to lactate at high speed, which was closely related to tumor aggressiveness, known as the "Warburg effect" (21). Lactate reduces cytotoxic T-cell function and contributes to the escape of tumor cells from immune cells. Furthermore, tumor cell motility is enhanced by lactate-induced mechanisms, and it was found that the lactate content of tumors was significantly correlated with the incidence of distant metastasis (22). In our study, we found that primary tumors in the multimetastatic state had higher metabolic-glycolytic activity compared with those in other groups and in the oligometastatic state compared with those in the non-metastatic disease. Our results suggest that the presence and number of distant metastatic lesions may be related to the degree of metabolic and glycolytic activity of the primary tumor. This may be explained by higher glycolysis and lactate production that stemmed from the primary tumor, and other biological factors. Besides ^{18}F-FDG PET-derived metabolic parameters, ADC_{min} also had significant differences among metastasis groups in our study. We found that the ADC_{min} values of primary tumors decreased with increased metastatic spread. ADC, which inversely correlates with tissue cellularity, represents a different aspect of the biological features of tumor cells from glucose metabolism (23). In a previous study using a breast cancer mouse model (24), it was shown that the reduction in tumor burden via primary tumor resection stopped metastatic progression and increased the immune response to cancer cells. Considering the literature and our results, it can be concluded that some of the important factors that determine the metastatic potential and metastatic spread are biological and metabolic features of the primary tumor.

In the oligometastatic state, the selectivity of tumor cells for metastatic organs is high. The metastatic potential of oligometastatic tumors is limited to certain distant sites that are the most suitable and receptive organs for tumor cells (16,18,19). Similar to this knowledge, in our study, we found that IBM was significantly higher than M-SM in patients with oligometastasis. In addition in multimetastatic patients, M-SM was observed to be significantly higher than IBM. Our results suggest that primary breast tumors, which have not yet reached their maximum metastatic potential, seem to metastatize primarily to the bones rather than soft visceral organs in an oligometastatic state. This may be related to the fact that bone is the most frequent site of distant metastasis in breast cancer and is the most amenable target organ for circulating tumor cells.

Our results also showed that high metastatic potential, which can be observed as widespread multimetastasis, had a significant relationship with metastatic spread to soft visceral tissues in breast cancer. These findings resemble the "seed and soil" and "spectrum" hypotheses of distant metastasis (16,18). In our study, the absence of distant metastasis in the axillary lymph node negative patient group may also bring Halstead's "contiguous seeding" hypothesis to mind (16,17).

Localization of distant organs where breast cancer metastasizes has clinical and prognostic importance. Patients with visceral metastases have a worse prognosis than those with IBM (5,25,26). The biology of the primary breast tumor was associated with the type of distant metastatic sites (6). As we expected, it was found that MTV and TLG of the primary tumor were significantly higher in patients with visceral metastasis (M-SM) than in those with IBM. SUV_{max} was also higher in the M-SM group, but this difference did not reach statistical significance. This finding seems to be related to the fact that SUV_{max} is based on a single voxel measurement. Unlike SUV_{max}, MTV and TLG, which were the combination of metabolic and volumetric features of the tumor, differed significantly between the groups. These results may be related to the aggressiveness and higher metastatic potential of the tumors, which had higher glycolytic activity and larger volumes. Similar to this finding, in oligometastatic patients (n=26), TLG was the only parameter that reached statistical significance, with higher values in the M-SM group than in the IBM group. TLG can provide information on both the tumor metabolic activity and tumor volume. This finding suggests that the presence of SM in oligometastatic patients is also associated with higher glycolytic activity and more aggressive tumor behavior.

Tumor grade, hormone receptor status, HER2 status, and proliferation index are considered important histopathological factors that determine the biological behavior of breast tumors. In our study, the metabolic-glycolytic activity of the primary tumor was positively correlated with tumor grade. This finding is in agreement with previous studies (14,27,28). In a previous study, it was reported that the expression of glucose transporter 1 (GLUT-1) was significantly associated with histological tumor grade (29) and our finding may be related to increased GLUT-1 expression in high-grade tumors. Tissue cellularity is another important component of tumor grade (30). Choi et al. (31) found that patients with high-grade tumors showed lower ADC mean values than those with low-grade tumors. Zhao et al. (32) also reported that lower ADC_{min} values were associated with higher histological grades. Similar to these studies, we found that ADC_{min} had lower values in high-grade tumors than in low-intermediate-grade tumors, but with marginal significance (p=0.054).

Steroid hormone receptor negativity in the primary tumor was significantly associated with GLUT-1 expression (33). Our study showed that hormone receptor-negative tumors had higher SUV_{max} and TLG than hormone receptor-positive tumors. This finding is similar to the findings of previous studies (14,20,27).

HER2 positivity in breast cancer is defined by high expression levels of the HER2 tyrosine kinase receptor as determined by immunohistochemistry and/or amplification of the *HER2* gene by fluorescence *in situ* hybridization. HER2-positive tumors have a highly aggressive disease course. Previous studies have demonstrated significant upregulation of glycolysis-related pathways in tumors with high HER2 expression (34,35). Groheux et al. (14) did not find a significant association between the HER2 status and SUV_{max} of primary tumors. We found a significant relationship between HER2 status and metabolic imaging parameters, with higher SUV_{max} and TLG in HER2-positive tumors, similar to previous studies (20,27,28). One of the anticancer effects of trastuzumab, an anti-HER2 agent, is the inhibition of glycolytic metabolism in HER2-positive breast cancer (36). Triple-negative breast tumors are considered very aggressive tumors with poor prognosis and lacking targeted therapy. GLUT-1 upregulation has also been reported in triple-negative breast cancer (33,37). Expression of other glycolysis markers, such as monocarboxylate transporters and carbonic anhydrase IX, was also found to be higher in triple-negative breast cancer than in other subtypes (29). Our study showed that triple-negative tumors had significantly higher SUV_{max} and TLG than non-triple-negative tumors. Increased tumor cell glycolysis rate, known as the Warburg effect, is one of the most important indicators of biological aggressiveness in triple negative breast cancer, and glycolytic markers may be possible molecular targets for therapy in this patient group (29,33).

Ki-67 expression is correlated with the tumor cell proliferation rate, and the Ki-67 index is considered a prognostic marker for breast cancer (38,39). A significant and positive relationship between the Ki-67 index and ^{18}F-FDG uptake in breast cancer has been reported in previous studies (20,40,41,42). Similar to previous studies, we found that breast tumors with a higher Ki-67 index (≥14%) demonstrated higher metabolic and glycolytic activity than those with a low Ki-67 index (<14%). This relationship between the Ki-67 index and ^{18}F-FDG uptake can be explained by the increased glucose consumption during the G1, G2, and S phases of the cell cycle. We also

found that ADC_{min} was significantly lower in tumors with a high Ki-67 index than in those with a low Ki-67 index. ADC values are inversely correlated with tumor cell density and tissue cellularity; therefore, it can be thought that increased cell proliferation rate has a significant relationship with lower ADC values.

Unlike metabolic imaging parameters, ADC_{min} values did not differ significantly between groups based on hormone receptor status, HER2 status, and triple negativity in our study. These results are in line with those of previous studies (20,27,43). This finding may be explained by the ^{18}F-FDG PET metabolic parameters and ADC values reflecting the different biological features of tumor cells. Hormone receptor status and HER2 status have major influences on glucose metabolism and glycolytic pathways. Therefore, it can be expected that ^{18}F-FDG uptake levels differ according to the biological characteristics of breast tumors. However, ADC represents the tumor cell density, not the metabolic activity of tumor cells. In addition, the ADC value also depends on the stromal components of tumors and cellularity (44).

Tumor histological grade, hormone receptor status, HER2 status, and Ki-67 index are considered biological factors that influence the distant metastasis type in breast carcinoma. In a previous study, it was reported that high-grade tumors were associated with SM and low-grade tumors were correlated with bone metastases (45). However, we did not find a significant association between tumor grade categories and metastatic groups. Wei et al. (6) reported that ER and PR expression was higher in patients with IBM than in those with visceral metastasis. In accordance with this study, we found that the ratio of patients with IBM was higher in the hormone receptor positive group than in the negative group (49.1% vs. 8.3%, respectively), while the ratio of M-SM was higher in the hormone receptor negative group than in the positive group (91.7% vs. 50.9%, respectively). We also found that the ratio of M-SM was significantly higher in the HER2-positive group than in the negative group (78.3% vs. 47.8%, respectively). Hormone receptor negativity and HER2 positivity are known to be poor prognostic factors and induce angiogenic pathways (46,47). High levels of Ki-67 indicate an aggressive tumor. In our study, the ratio of distant metastasis was higher in patients with a high proliferation rate (≥14%) than in those with a low proliferation rate (<14%) (27.8% vs. 7.8%, respectively). This finding is similar to that of a previous study (48). The Ki-67 index also seems to be related to distant metastatic sites. In our study, the Ki-67 index demonstrated significant differences between the IBM and M-SM groups (25% vs. 60%, respectively) in oligometastatic patients. Nishimura et al. (49) reported that Ki-67 index values of primary breast tumors for recurrent sites were lower in patients with bone metastasis than in those with liver or brain metastasis. We also obtained similar results in newly diagnosed patients.

In our study, it was found that multivariable prediction models that included imaging parameters (models 2 and 3) had strong discriminatory abilities for distant metastatic disease (the AUCs were 0.85 and 0.90, respectively). The discriminatory powers of these two prediction models were found to be higher than those of the prediction model that included only histopathological parameters (model 1). These findings show that imaging parameters that reflect the metabolic-glycolytic activity and cellularity of the primary tumor may be more effective than histopathological markers alone in explaining the aggressive biological behavior of the tumor in breast cancer patients.

Study Limitations

There are some limitations to our study. First, this was a retrospective single-center study. The second limitation was the lack of histopathological confirmation of distant metastatic lesions detected by ^{18}F-FDG PET/MRI. Although most of the PET positive findings were not histopathologically confirmed in patients with distant metastasis, PET positive lesions displayed pathological correlates on MRIs. Third, breast-dedicated PET/MRI were acquired without contrast injection; therefore, the contrast enhancement patterns and signal enhancement ratios of primary breast tumors could not be evaluated in our study. Therefore, this study did not provide full MRI information. Fourth, the immunohistochemical results of patients were obtained by tru-cut biopsy in 102 of 289 cases (35.3%); therefore, the histopathological features of the entire tumor might not have been evaluated in some patients. Fifth, we did not perform survival analysis because of the short follow-up time in most patients. Finally, although there was no distant metastatic lesion that was ^{18}F-FDG negative but was detected on MRI in our study, some millimetric metastases without ^{18}F-FDG uptake might have been missed and we might have underestimated the presence and number of metastatic lesions in some patients. Despite these limitations, our study included imaging and histopathological data of a large patient cohort in primary staging with PET/MRI. Simultaneous PET/MRI combines high-resolution anatomic and functional information from MRI with metabolic information from PET within the same imaging session. The combination of different imaging parameters of PET/MRI representing different biological features may allow better *in vivo* characterization of breast tumors.

Conclusion

Quantitative imaging parameters of primary tumors obtained from PET/MRI were associated with tumor biology, metastatic tumor load, and localization of distant metastases. Primary tumors with higher metabolic-glycolytic activity and higher cellularity were more aggressive and had a higher metastatic potential in breast IDC. While ^{18}F-FDG PET-derived metabolic-volumetric parameters had a strong relationship with histopathological prognostic factors, ADC only demonstrated a significant association with proliferation rate. Compared with histopathological parameters alone, the combination of PET/MRI parameters and histopathological features of primary tumors may help to better understand tumor biology and clinical course in breast carcinoma.

Ethics

Ethics Committee Approval: This study was approved by the Gazi University Local Ethical Committee (decision no: 296, date: 11.05.2020).

Informed Consent: Not applicable (Retrospective study).

Peer-review: Externally and internally peer-reviewed.

Authorship Contributions

Surgical and Medical Practices: U.A., S.G.A., O.K., Ü.Ö.A., P.U.G., L.Ö.A., Concept: U.A., O.K., P.U.G., L.Ö.A., Design: U.A., O.K., L.Ö.A., Data Collection or Processing: U.A., S.G.A., O.K., P.U.G., Analysis or Interpretation: U.A., S.G.A., Ü.Ö.A., Literature Search: U.A., S.G.A., Ü.Ö.A., Writing: U.A.

Conflict of Interest: No conflict of interest was declared by the authors.

Financial Disclosure: The authors declared that this study has received no financial support.

References

1. Gradishar WJ, Anderson BO, Balassanian R, Blair SL, Burstein HJ, Cyr A, Elias AD, Farrar WB, Forero A, Giordano SH, Goetz MP, Goldstein LJ, Isakoff SJ, Lyons J, Marcom PK, Mayer IA, McCormick B, Moran MS, O'Regan RM, Patel SA, Pierce LJ, Reed EC, Salerno KE, Schwartzberg LS, Sitapati A, Smith KL, Smith ML, Soliman H, Somlo G, Telli M, Ward JH, Shead DA, Kumar R. NCCN Guidelines Insights: Breast Cancer, Version 1.2017. J Natl Compr Canc Netw 2017;15:433-451.
2. Corben AD. Pathology of invasive breast disease. Surg Clin North Am 2013;93:363-392.
3. Kwapisz D. Oligometastatic breast cancer. Breast Cancer 2019;26:138-146
4. Pagani O, Senkus E, Wood W, Colleoni M, Cufer T, Kyriakides S, Costa A, Winer EP, Cardoso F; ESO-MBC Task Force. International guidelines for management of metastatic breast cancer: can metastatic breast cancer be cured? J Natl Cancer Inst 2010;102:456-463.
5. Largillier R, Ferrero JM, Doyen J, Barriere J, Namer M, Mari V, Courdi A, Hannoun-Levi JM, Ettore F, Birtwisle-Peyrottes I, Balu-Maestro C, Marcy PY, Raoust I, Lallement M, Chamorey E. Prognostic factors in 1,038 women with metastatic breast cancer. Ann Oncol 2008;19:2012-2019.
6. Wei S, Li Y, Siegal GP, Hameed O. Breast carcinomas with isolated bone metastases have different hormone receptor expression profiles than those with metastases to other sites or multiple organs. Ann Diagn Pathol 2011;15:79-83.
7. Hess KR, Varadhachary GR, Taylor SH, Wei W, Raber MN, Lenzi R, Abbruzzese JL. Metastatic patterns in adenocarcinoma. Cancer 2006;106:1624-1633.
8. Chiedozi LC. Prognostic significance of exclusive skeletal metastases in stage IV primary carcinoma of the breast. Surg Gynecol Obstet 1988;167:303-306.
9. Hellman S, Weichselbaum RR. Oligometastases. J Clin Oncol 1995;13:8-10.
10. Weichselbaum RR, Hellman S. Oligometastases revisited. Nat Rev Clin Oncol 2011;8:378-382.
11. Abbott DE, Brouquet A, Mittendorf EA, Andreou A, Meric-Bernstam F, Valero V, Green MC, Kuerer HM, Curley SA, Abdalla EK, Hunt KK, Vauthey JN. Resection of liver metastases from breast cancer: estrogen receptor status and response to chemotherapy before metastasectomy define outcome. Surgery 2012;151:710-716.
12. Kobayashi T, Ichiba T, Sakuyama T, Arakawa Y, Nagasaki E, Aiba K, Nogi H, Kawase K, Takeyama H, Toriumi Y, Uchida K, Kobayashi M, Kanehira C, Suzuki M, Ando N, Natori K, Kuraishi Y. Possible clinical cure of metastatic breast cancer: lessons from our 30-year experience with oligometastatic breast cancer patients and literature review. Breast Cancer 2012;19:218-237.
13. Ekmekcioglu O, Aliyev A, Yilmaz S, Arslan E, Kaya R, Kocael P, Erkan ME, Halac M, Sonmezoglu K. Correlation of 18F-fluorodeoxyglucose uptake with histopathological prognostic factors in breast carcinoma. Nucl Med Commun 2013;34:1055-1067.
14. Groheux D, Giacchetti S, Moretti JL, Porcher R, Espié M, Lehmann-Che J, de Roquancourt A, Hamy AS, Cuvier C, Vercellino L, Hindié E. Correlation of high 18F-FDG uptake to clinical, pathological and biological prognostic factors in breast cancer. Eur J Nucl Med Mol Imaging 2011;38:426-435.
15. Jung NY, Kim SH, Choi BB, Kim SH, Sung MS. Associations between the standardized uptake value of (18)F-FDG PET/CT and the prognostic factors of invasive lobular carcinoma: in comparison with invasive ductal carcinoma. World J Surg Oncol 2015;13:113.
16. Reyes DK, Pienta KJ. The biology and treatment of oligometastatic cancer. Oncotarget 2015;6:8491-8524.
17. Tait CR, Waterworth A, Loncaster J, Horgan K, Dodwell D. The oligometastatic state in breast cancer: hypothesis or reality. Breast 2005;14:87-93.
18. Makhlin I, Fox K. Oligometastatic Breast Cancer: Is This a Curable Entity? A Contemporary Review of the Literature. Curr Oncol Rep 2020;22:15.
19. Zhang L, Li Z, Zhang J, Wu Y, Zhu Y, Tong Z. De novo metastatic breast cancer: Subgroup analysis of molecular subtypes and prognosis. Oncol Lett 2020;19:2884-2894.
20. Kitajima K, Yamano T, Fukushima K, Miyoshi Y, Hirota S, Kawanaka Y, Miya M, Doi H, Yamakado K, Hirota S. Correlation of the SUVmax of FDG-PET and ADC values of diffusion-weighted MR imaging with pathologic prognostic factors in breast carcinoma. Eur J Radiol 2016;85:943-949.
21. Danhier P, Bański P, Payen VL, Grasso D, Ippolito L, Sonveaux P, Porporato PE. Cancer metabolism in space and time: Beyond the Warburg effect. Biochim Biophys Acta Bioenerg 2017;185:556-572.
22. Hirschhaeuser F, Sattler UG, Mueller-Klieser W. Lactate: a metabolic key player in cancer. Cancer Res 2011;71:6921-6925.
23. Razek AA, Gaballa G, Denewer A, Nada N. Invasive ductal carcinoma: correlation of apparent diffusion coefficient value with pathological prognostic factors. NMR Biomed 2010;23:619-623.
24. Rashid OM, Nagahashi M, Ramachandran S, Graham L, Yamada A,

Spiegel S, Bear HD, Takabe K. Resection of the primary tumor improves survival in metastatic breast cancer by reducing overall tumor burden. Surgery 2013;153:771-778.

25. Milano MT, Zhang H, Metcalfe SK, Muhs AG, Okunieff P. Oligometastatic breast cancer treated with curative-intent stereotactic body radiation therapy. Breast Cancer Res Treat 2009;115:601-608.
26. Coleman RE, Smith P, Rubens RD. Clinical course and prognostic factors following bone recurrence from breast cancer. Br J Cancer 1998;77:336-340.
27. Karan B, Pourbagher A, Torun N. Diffusion-weighted imaging and (18) F-fluorodeoxyglucose positron emission tomography/computed tomography in breast cancer: Correlation of the apparent diffusion coefficient and maximum standardized uptake values with prognostic factors. J Magn Reson Imaging 2016;43:1434-1444.
28. Nakajo M, Kajiya Y, Kaneko T, Kaneko Y, Takasaki T, Tani A, Ueno M, Koriyama C, Nakajo M. FDG PET/CT and diffusion-weighted imaging for breast cancer: prognostic value of maximum standardized uptake values and apparent diffusion coefficient values of the primary lesion. Eur J Nucl Med Mol Imaging 2010;37:2011-2020.
29. Choi J, Kim DH, Jung WH, Koo JS. Metabolic interaction between cancer cells and stromal cells according to breast cancer molecular subtype. Breast Cancer Res 2013;15:R78.
30. Yoshikawa MI, Ohsumi S, Sugata S, Kataoka M, Takashima S, Mochizuki T, Ikura H, Imai Y. Relation between cancer cellularity and apparent diffusion coefficient values using diffusion-weighted magnetic resonance imaging in breast cancer. Radiat Med 2008;26:222-226.
31. Choi JH, Lim I, Noh WC, Kim HA, Seong MK, Jang S, Seol H, Moon H, Byun BH, Kim BI, Choi CW, Lim SM. Prediction of tumor differentiation using sequential PET/CT and MRI in patients with breast cancer. Ann Nucl Med 2018;32:389-397.
32. Zhao S, Guo W, Tan R, Chen P, Li Z, Sun F, Shao G. Correlation between minimum apparent diffusion coefficient values and the histological grade of breast invasive ductal carcinoma. Oncol Lett 2018;15:8134-8140.
33. Hussein YR, Bandyopadhyay S, Semaan A, Ahmed Q, Albashiti B, Jazaerly T, Nahleh Z, Ali-Fehmi R. Glut-1 Expression Correlates with Basal-like Breast Cancer. Transl Oncol 2011;4:321-327.
34. Castagnoli L, Iorio E, Dugo M, Koschorke A, Faraci S, Canese R, Casalini P, Nanni P, Vernieri C, Di Nicola M, Morelli D, Tagliabue E, Pupa SM. Intratumor lactate levels reflect HER2 addiction status in HER2-positive breast cancer. J Cell Physiol 2019;234:1768-1779.
35. Schafer ZT, Grassian AR, Song L, Jiang Z, Gerhart-Hines Z, Irie HY, Gao S, Puigserver P, Brugge JS. Antioxidant and oncogene rescue of metabolic defects caused by loss of matrix attachment. Nature 2009;461:109-113.
36. Walsh AJ, Cook RS, Manning HC, Hicks DJ, Lafontant A, Arteaga CL, Skala MC. Optical metabolic imaging identifies glycolytic levels, subtypes, and early-treatment response in breast cancer. Cancer Res 2013;73:6164-6174.
37. Kaida H, Azuma K, Toh U, Kawahara A, Sadashima E, Hattori S, Akiba J, Tahara N, Rominger A, Ishii K, Murakami T, Ishibashi M. Correlations between dual-phase 18F-FDG uptake and clinicopathologic and biological markers of breast cancer. Hell J Nucl Med 2018;21:35-42.
38. Yerushalmi R, Woods R, Ravdin PM, Hayes MM, Gelmon KA. Ki67 in breast cancer: prognostic and predictive potential. Lancet Oncol 2010;11:174-183.
39. de Azambuja E, Cardoso F, de Castro G Jr, Colozza M, Mano MS, Durbecq V, Sotiriou C, Larsimont D, Piccart-Gebhart MJ, Paesmans M. Ki-67 as prognostic marker in early breast cancer: a meta-analysis of published studies involving 12,155 patients. Br J Cancer 2007;96:1504-1513.
40. Buck A, Schirrmeister H, Kühn T, Shen C, Kalker T, Kotzerke J, Dankerl A, Glatting G, Reske S, Mattfeldt T. FDG uptake in breast cancer: correlation with biological and clinical prognostic parameters. Eur J Nucl Med Mol Imaging 2002;29:1317-1323.
41. Shimoda W, Hayashi M, Murakami K, Oyama T, Sunagawa M. The relationship between FDG uptake in PET scans and biological behavior in breast cancer. Breast Cancer 2007;14:260-268.
42. Koo HR, Park JS, Kang KW, Cho N, Chang JM, Bae MS, Kim WH, Lee SH, Kim MY, Kim JY, Seo M, Moon WK. 18F-FDG uptake in breast cancer correlates with immunohistochemically defined subtypes. Eur Radiol 2014;24:610-618.
43. Choi BB. Associations Between Apparent Diffusion Coefficient Values and the Prognostic Factors of Breast Cancer. J Comput Assist Tomogr 2019;43:931-936.
44. Matsubayashi RN, Fujii T, Yasumori K, Muranaka T, Momosaki S. Apparent Diffusion Coefficient in Invasive Ductal Breast Carcinoma: Correlation with Detailed Histologic Features and the Enhancement Ratio on Dynamic Contrast-Enhanced MR Images. J Oncol 2010;2010:821048.
45. Porter GJ, Evans AJ, Pinder SE, James JJ, Cornford EC, Burrell HC, Chan SY, Cheung KL, Robertson JF. Patterns of metastatic breast carcinoma: influence of tumour histological grade. Clin Radiol 2004;59:1094-1098.
46. Makkat S, Luypaert R, Stadnik T, Bourgain C, Sourbron S, Dujardin M, De Greve J, De Mey J. Deconvolution-based dynamic contrast-enhanced MR imaging of breast tumors: correlation of tumor blood flow with human epidermal growth factor receptor 2 status and clinicopathologic findings--preliminary results. Radiology 2008;249:471-482.
47. Fuckar D, Dekanić A, Stifter S, Mustać E, Krstulja M, Dobrila F, Jonjić N. VEGF expression is associated with negative estrogen receptor status in patients with breast cancer. Int J Surg Pathol 2006;14:49-55.
48. Soliman NA, Yussif SM. Ki-67 as a prognostic marker according to breast cancer molecular subtype. Cancer Biol Med 2016;13:496-504.
49. Nishimura R, Osako T, Nishiyama Y, Tashima R, Nakano M, Fujisue M, Toyozumi Y, Arima N. Prognostic significance of Ki-67 index value at the primary breast tumor in recurrent breast cancer. Mol Clin Oncol 2014;2:1062-1068.

Original Article
Mol Imaging Radionucl Ther 2023;32:206-213 DOI:10.4274/mirt.galenos.2023.75046

A Different Scintigraphic Perspective on the Systolic Function of the Left Ventricle-I

Sol Ventrikülün Sistolik Fonksiyonuna Sintigrafik Olarak Farklı Bir Bakış Açısı-I

Alper Özgür Karaçalıoğlu, Alev Çınar

University of Health Sciences Türkiye, Gülhane Faculty of Medicine, Department of Nuclear Medicine, Ankara, Türkiye

Abstract

Objectives: The aim of this study was to analyze the systolic part of the left ventricular (LV) volume curve obtained by gated myocardial perfusion imaging with the formula used in exponential decay and to investigate the clinical value of the results.

Methods: One hundred fifty eight patients were retrospectively enrolled in the study. The study group was divided into three groups as normal, ischemia, and infarct. The systolic portion of the LV volume curve was also analyzed using the exponential decay formula. The scintigraphic parameter obtained using this formula is called the ejection constant (Ec).

Results: The Ec results were 1.8±0.8, 2.7±0.9, 3.5±1 in infarct, ischemia, and normal groups, respectively, and the difference in Ec results between the groups was statistically significant (p≤0.001).

Conclusion: It appears that Ec may play a clinical role as a scintigraphic parameter in the evaluation of systolic functions of the left ventricle.

Keywords: Exponential decay, time-volume curve, the left ventricle, gMPI

Öz

Amaç: Bu çalışmanın amacı, üstel bozulmada kullanılan formül ile gated miyokard perfüzyon görüntülemeI ile elde edilen sol ventrikül (LV) hacim eğrisinin sistolik kısmını analiz etmek ve sonuçların klinik değerini araştırmaktı.

Yöntem: Yüz elli sekiz hasta geriye dönük olarak çalışmaya alındı. Çalışma grubu normal, iskemi ve enfarktüs olmak üzere üç gruba ayrıldı. LV hacim eğrisinin sistolik kısmı da üstel bozulma formülü ile analiz edildi. Bu formülle elde edilen sintigrafik parametreye ejeksiyon sabiti (Ec) adı verilmiştir.

Bulgular: Enfarktüs, iskemi ve normal gruplarda Ec sonuçları sırasıyla 1,8±0,8, 2,7±0,9, 3,5±1 idi ve gruplar arasındaki Ec sonuçları farkı istatistiksel olarak anlamlıydı (p≤0,001).

Sonuç: Sonuç olarak, Ec'nin LV'nin sistolik fonksiyonlarının değerlendirilmesinde sintigrafik bir parametre olarak klinik bir rolü olabileceği görünmektedir.

Anahtar kelimeler: Üstsel azalma, zaman-hacim eğrisi, sol ventrikül, gMPS

Introduction

Electrocardiography (ECG)-gated myocardial perfusion imaging (gMPI) is the most widely used nuclear imaging modality for the diagnosis and management of coronary artery disease because in addition to the assessment of regional myocardial perfusion, it allows the simultaneous evaluation of left ventricular (LV) volumes, synchronization of the onset of mechanical contraction of the left ventricle, and regional ventricular systolic and diastolic functions at

Address for Correspondence: Alper Özgür Karaçalıoğlu MD, University of Health Sciences Türkiye, Gülhane Faculty of Medicine, Department of Nuclear Medicine, Ankara, Türkiye
Phone: +90 312 304 48 04 **E-mail:** aokaracali@yahoo.com ORCID ID: orcid.org/0000-0003-2683-804X
Received: 15.09.2022 **Accepted:** 26.02.2023

post-stress gated examination (1,2,3,4,5). The 16-phase gMPI allows for the automatic generation of the time-volume curve of the left ventricle (6,7,8). The portion of the time-volume curve of the left ventricle corresponding to systole is non-linear (Figure 1) and shows a continuous exponential decrease. Since, in exponential decay, the decay factor relies on a percentage of the original amount, which means that the actual number by which the original amount might be reduced will change over time, it is different from linear decay in which the original number decreases by the same amount every time (9,10,11,12). Therefore, the systolic part of the LV volume curve can be analyzed with a formula of continuous exponential decay.

The aim of this study was to analyze the systolic part of the LV volume curve obtained by gMPI using the formula used in exponential decay and to investigate the clinical value of the results.

Materials and Methods

Patients

From March 2021 to March 2022, 158 patients (67 women, 42.4%, mean age: 62 years, age range: 31-79 years, 91 men 57.6%, mean age: 61 years, age range: 34-87) who were referred to our department for stress-rest gMPI for suspected coronary artery disease were retrospectively enrolled in the study. Patients had a history of one or more of the following findings: previous positive treadmill test, atypical chest pain, shortness of breath with or without atypical chest pain, typical chest pain, or respiratory distress alone. The height and weight of the patients were recorded to calculate the body surface area (BSA). Technical failure to evaluate the scans and infidelity to instructions were the reasons for patients to be excluded from the study. Patients with bundle branch block, cardiac pacemaker, atrial fibrillation, valve disease, and images that were not evaluated for technical reasons were excluded from the study. According to our acquisition protocols, all patients were instructed to discontinue beta-blockers, calcium antagonists, and nitrates at least 24 h before testing. The University of Health Sciences Türkiye, Gülhane Scientific Research Ethics Committee approved the study protocol (decision no: 2022-278, date: 12.09.2022).

The study group was divided into three groups as normal, ischemia, and infarct, according to their history of heart disease and quantitative and qualitative evaluation of gMPI images. In the gMPI images of the normal group of 51 patients, the biological distribution of the radiopharmaceutical in the left ventricle was within normal physiological limits and the total stress score (SSS) was <4. In the ischemia group of 54 patients, reversible perfusion defects were detected in the gMPI images. Loss and reductions in radiopharmaceutical uptake detected in the left ventricle in stress gMPI images of the ischemia group were normalized in resting single photon emission computed tomography (SPECT) images. The SSS was ≥4 in this group. In the infarct group of 53 patients, perfusion defects detected in stress gMPI images persisted in resting SPECT images. In addition, past infarct findings were found in the histories or ECG records of these patients. The SSS was also ≥4 in this group. Demographic data of the subgroups of the study population are presented in Table 1.

Stress and Acquisition Protocols

One hundred forty one (~89%) patients underwent an exercise stress test and 17 (~11%) adenosine (Apoteket

Table 1. Demographic data of the study population

	Patient groups					
	Normal (51)		Ischemia (54)		Infarct (53)	
	W (27)	M (24)	W (24)	M (30)	W (14)	M (39)
Age (years)	63	57	62	63	62	63
Height (cm)	160.5	172.4	160	169.8	157	172.6
Weight (kg)	76.9	80.6	79	82.6	74	85
Diabetes	15	6	14	10	8	16
Hypertension	21	12	20	20	14	33
Hyperlipidemia	2	6	10	11	8	19
Family history	9	11	8	11	8	12
Infarct history	1	4	6	8	7	22
Stent history	2	4	9	10	8	21
Bypass history	0	1	4	8	2	8

W: Woman, M: Man

Produktion & Laboratorier AB, Formvagen, Sweden) pharmacologic stress tests. Depending on the patient's ability to exercise and to reach at least 85% of the maximal age-predicted heart rate, symptom-limited treadmill exercise test according to the standard Bruce protocol (stepwise increments of velocity and slope every 3 min) with continuous 12-lead ECG assessment or adenosine (140 µ gr/kg/min intravenously over 4 min) was chosen. Of the 141 patients who were submitted to the exercise stress test, 140 reached at least 85% of the expected maximal heart rate. Suboptimal exercise (75%) was administered to one patient in the infarct group where adenosine was contraindicated. According to our two-day stress-rest gMPI clinical protocol, each patient underwent stress gMPI for the first day. The intravenously injected dose of Tc-99m MIBI (Cardio-SPECT, Medi-Radiopharma, Budapest, Hungary) was 222-296 MBq (6-8 mCi) when the patients reached maximum exercise. All ECG-gated SPECT acquisitions were initiated 30±10 min while the patients were in the supine position with arms placed over the head. The next day, rest SPECT imaging was performed 45±15 minutes after the same dose of Tc-99m MIBI was applied to the subjects with perfusion defects on their stress images.

Daily quality control of the gamma camera was performed routinely before the first study of the day. A dedicated cardiac gamma camera (Discovery NM 530c, GE Healthcare, Chicago, Illinois, USA) equipped with a multiple pinhole collimator and 19 stationary cadmium-zinc-telluride detectors was used for patient acquisition. Each detector contained 32x32 pixelated 5 mm thick (2.46x2.46 mm) elements. A window of 15% was centered on the 140 keV gamma peak, and gating was performed with 16 frames per RR interval cycle. List mode files were acquired and stored. Images were reconstructed on the same workstation used for standard SPECT acquisition (Xeleris II, GE Healthcare, Haifa, Israel) using a new dedicated iterative algorithm. A Butterworth postprocessing filter (frequency 0.37, order 7) was applied to the reconstructed slices. Images were reconstructed without scatter or attenuation correction. The R-R acceptance window was set to 25%. Attenuation correction was not used.

Data Analysis

Scintigraphic images were analyzed visually and semi-numerically in consensus by 2 experienced nuclear medicine physicians who were unaware of the content of the study. The LV time-volume curves of the patients were obtained from stress-gMPI scans (Figure 1). Data from the gated SPECT studies of all patients were analyzed using Quantitative Gated SPECT and Quantitative Perfusion SPECT softwares (QGS, QPS, Cedars Sinai Medical center, Los Angeles, CA, USA). Myocardial segmentation was based on a 20-segment model, and SSS was calculated based on 0-4 points in each segment (0, normal to 4, defect). The ejection fraction (EF), volumes of end-diastolic (EDV) and end-systolic (ESV) were automatically determined using QGS software, and heart rate as beats per minute (BPM) were noted.

Calculations

All continually and exponentially decreasing systems are scaled versions of a common constant represented by "e" (Euler's constant). In addition to a constant, four variables (percent change, time, the amount at the beginning of the time period, and the amount at the end of the time period) play roles in exponential functions. In exponential decreases, the original amount is reduced at a consistent rate over a period of time. The systolic portion of the LV volume curve was also analyzed using this formula, as it shows a continuous exponential decrease pattern.

Systole time was calculated for each patient based on their heart rate using the following method:

If the pulse rate of the patient is 60 beats/min, the duration of each beat is 1000 milliseconds (ms).

Cardiac cycle time (ms) = (1000 ms x 60)/BPM of the patient

Cardiac cycle time (ms) / 16 (total frame number) = Frame time (ms) (Figure 1)

Systolic frame number frame time (ms) = Systole time (ms)

Thus, each patient's systole time, and therefore, the ejection constant (Ec), was indexed to their own BPM.

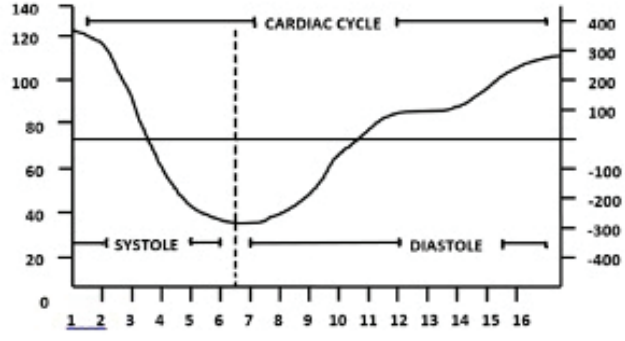

Figure 1. An example of the volume curve of the left ventricle over time in 16-frame gMPI, which was derived using QGS software. It shows that the cardiac cycle is divided into 16 frames. The systolic part of the time-volume curve can be seen as not linear
gMPI: Gated myocardial perfusion imaging, QGS: Quantitative Gated SPECT

Systole time in seconds (s) was used in the formula instead of "t".

The original continuous exponential decay formula is $\mathbf{A_f = A_i\, e^{-kt}}$ where,

A_i= Initial amount or EDV in our study

A_f= Final amount or ESV in our study

e= Euler's constant (2.718...)

k= decay constant, or Ec in this study

t= Time or systole time (s) in this study

The exponential decrease analysis formula used to evaluate the systolic part of the LV volume curve in our study is as following.

$ESV = EDV \times e^{-kt}$

Using this formula, the LV emptying rate was calculated for each patient.

BSA is a more accurate indicator of metabolic mass and is used in various clinical settings, such as dosages for chemotherapy or determining the cardiac index, which relates a person's heart performance to their body size. The most widely used of these is the Du Bois formula, which is $BSA = 0.007184 \times W^{0.425} \times H^{0.725}$, where BSA is represented in m^2, W is weight in kg, and H is height in cm. Each patient's BSA was calculated by using this formula and each result was divided by average BSA of 1.73 m^2.

Ec is also indexed to BSA using the following method. Indexing measurements by body size is thought to establish limits of normality among individuals varying in body habits.

BSA indexing: Ec result of patient X (BSA of the patient/1.73 m^2).

If the Ec is multiplied by 100, the unit of the result is given as percent reduction per second (Ec x 100= % decrease/second). It is necessary to change the name of the Ec to ejection rate, but we preferred not to multiply by 100 and to use the Ec in this study.

Statistical Analysis

Descriptive analysis was performed to examine the pertinent variables in the study group. Continuous variables are expressed as mean ± standard deviation (SD). One-Way ANOVA was used to compare the results of the measurements between the groups. The linear relationship between the groups was investigated using the Pearson correlation test. The sensitivity and specificity of Ec in the differential diagnosis between the groups were investigated by receiver operating characteristic (ROC) curve analysis. All p values were two-tailed with a p value <0.05 set priori and used as the level of significance. Statistical analyzes were performed with using SPSS version 22.0 for Windows (SPSS Inc., Chicago, IL, USA).

Results

The demographic data of the study population and its subgroups are summarized in Table 1. There was no statistically significant difference between the groups in terms of age, gender, and BSA. The statistical results of the study are summarized in Table 2.

The differences in EF, ESV, EDV, and Ec (with or without BSA index) between the groups were statistically significant. (p<0,001). In post-hoc tests, it was revealed that this difference was due to the statistically significant difference in the mean of each group. There was no statistically significant difference between the groups in terms of other parameters (Table 2). The mean and SD of the Ec and EF results between the groups are compared in Figures 2, 3, respectively.

Table 2. Results data of the study groups

	Patients (158)	Patient groups			p
		Normal (51)	Ischemia (54)	Infarct (53)	
Age (years)	61±10	60±11	62±10	62±10	0.425
Height (cm)	166.5±8.9	166±8.7	165.3±8	168.3±9.8	0.199
Weigth (kg)	80.8±13.3	78.7±10.9	81±14	82.4±14.6	0.343
BSA (m^2)	1.9±0.2	1.9±0.2	1.9±0.2	2±0.2	0.303
EF (%)	56.3±14.2	64.9±9.6	58.2±12	45.8±13.4	<0.001
EDV (mL)	100.3±40.8	76±19	96.9±36.7	127±44.7	<0.001
ESV (mL)	48.8±35	27.2±11.9	43.6±28.8	74.8±39.2	<0.001
BPM	74±12	73±12	72±11	74±14	0.565
Ec*	2.4±1	3.2±1	2.4±0.9	1.6±0.7	<0.001
Ec	2.6±1.1	3.5±1	2.7±0.9	1.8±0.8	<0.001

BSA: Body surface area, EF: Ejection fraction, EDV: Volumes of end-diastolic, ESV: Volumes of end-systolic, BPM: Beats per minute, Ec: Ejection constant, Ec*: Not BSA indexed

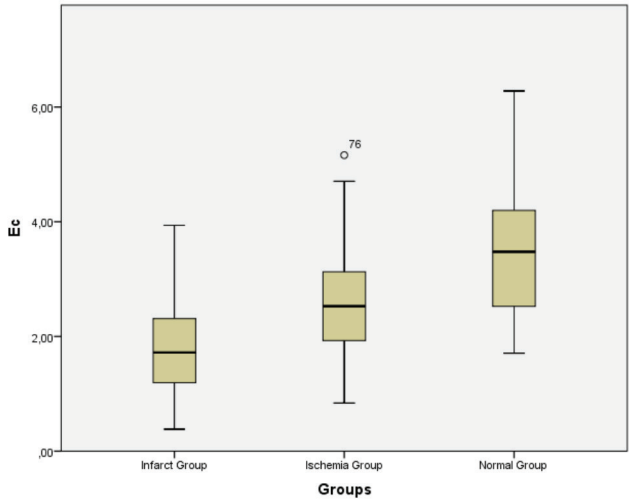

Figure 2. Box and whisker plots of Ec results among the groups
Ec: Ejection constant

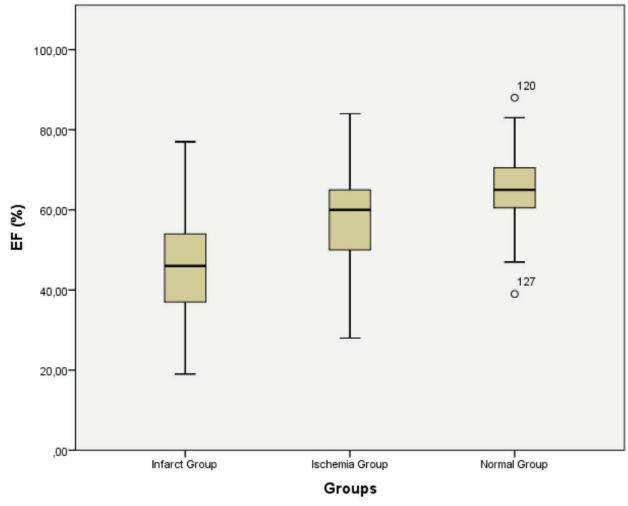

Figure 3: Box and whisker plots of EF results among the groups
EF: Ejection fraction

The correlation coefficient between Ec and EF was excellent (r= 0.792, p<0.001) (Figure 4).

If the value of 2.34 is taken as the cut-off, the sensitivity of Ec is 88% and the specificity is 62% in the differential diagnosis between the normal group and others (Figure 5). Area under the ROC curve is 0.805. If the value of 2.47 was taken as the cut-off, the sensitivity of Ec in the differential diagnosis between the ischemia and normal groups was calculated as 80% and the specificity as 50% (Figure 6). The area under the ROC curve is 0.719. If the value of 2.17 is taken as the cut-off, the sensitivity of Ec is 90% and the specificity is 74% in the differential diagnosis of normal and others (Figure 7). Area under the ROC curve is 0.892.

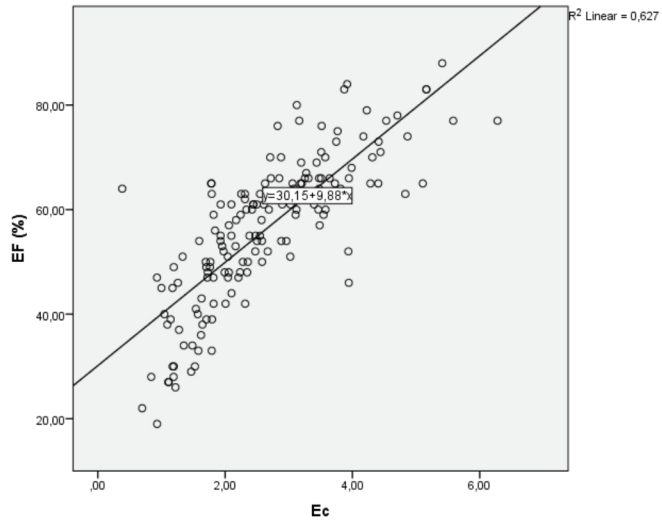

Figure 4. Scatter plot of the correlation between EF and Ec
EF: Ejection fraction, Ec: Ejection constant

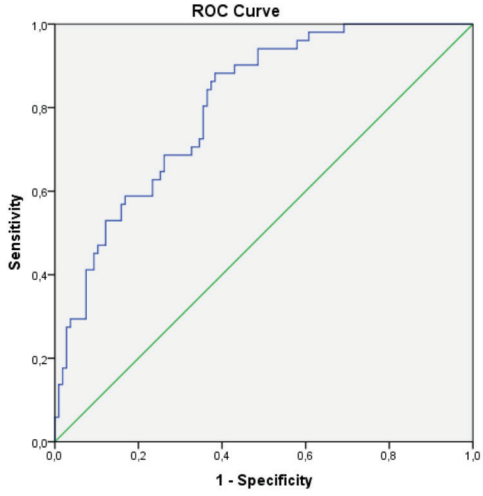

Figure 5. ROC curve between the normal group and others
ROC: Receiver operating characteristic

According to the ROC curves, it was noticed that the differential diagnosis of those in the normal group (Figure 8A) and the infarct group (Figure 8B) can be made more easily with Ec compared to those between the ischemia (Figure 8C) and normal groups. The underlying cause may be structural changes that change the shape of the systolic part of the LV time-volume curve more significantly than functional changes.

Discussion

In this study, because the systolic part of the LV volume curve obtained with gMPI shows a continuous exponential

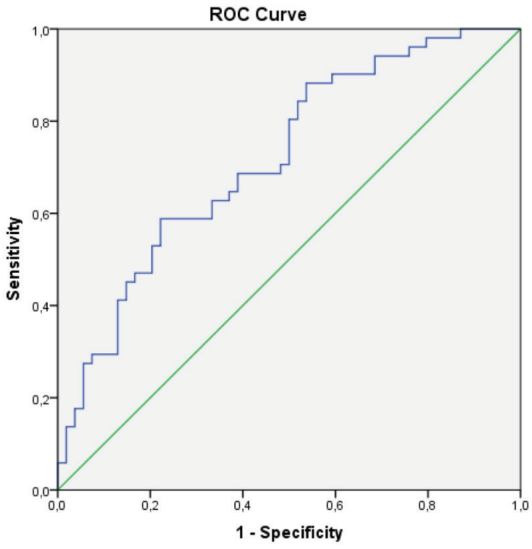

Figure 6. ROC curve between the ischemia and normal groups
ROC: Receiver operating characteristic

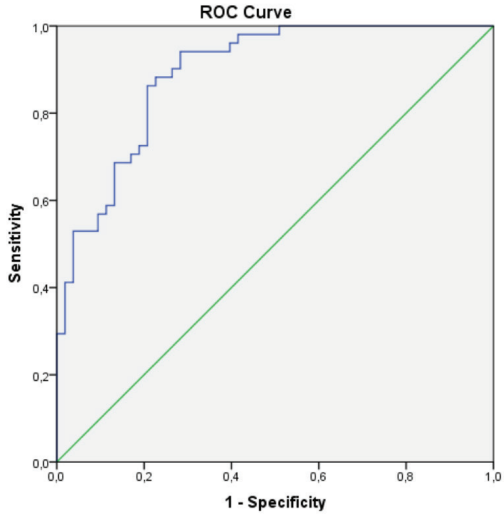

Figure 7. ROC curve between the normal and infarct groups
ROC: Receiver operating characteristic

decrease pattern, it was analyzed mathematically using the exponential decay formula. The parameter obtained using the formula used was named the Ec of the left ventricle. This parameter showed a statistically significant difference between the normal, ischemia, and infarct groups and correlated very well with the EF results of the patients in the study group.

EF is defined as the stroke volume indexed to the EDV, which is calculated from the input (EDV) and output (ESV) data and is one of the most frequently measured variables in clinical practice (13). In addition to contractility of the LV preload and afterload, EF is also affected by changes in heart rate (1). The exponential decay formula in this study gives the percent reduction per unit time, which is constant as the LV moves from EDV to ESV and is indexed to the heart rate and BSA (14,15). The percentage of decreasing volume of the left ventricle per unit time given by the formula seems to indirectly reflect the contraction or myocardial inotropy and afterload of the LV as a whole. We believe that Ec in the exponential decay formula is a scintigraphic parameter that will act like EF in the evaluation of the systolic functions of the left ventricle. The LV EF, a measure of LV systolic performance, reflects the contractility of the LV if abnormal afterload or valvular diseases are absent (16). According to our results, the presence of a excellent correlation between Ec and EF may support this idea.

The LV preload, which is the length of the muscle at the onset of contraction, is clinically assessed by measurements of the pulmonary capillary wedge pressure (6). LV preload can also be assessed from the LV filling pressure, LV EDV, or LV end-diastolic stress (17). In the healthy heart, increases in preload lead to an increase in stroke volume and cardiac output without major change in EF due to the Frank-Starling mechanism, in which myocyte stretch causes a more forceful systolic contraction (1,18). The exponential decay formula used in this study includes the EDV/ESV ratio; therefore, even the same amount of changes in the EDV and ESV values will change the results. On the basis of

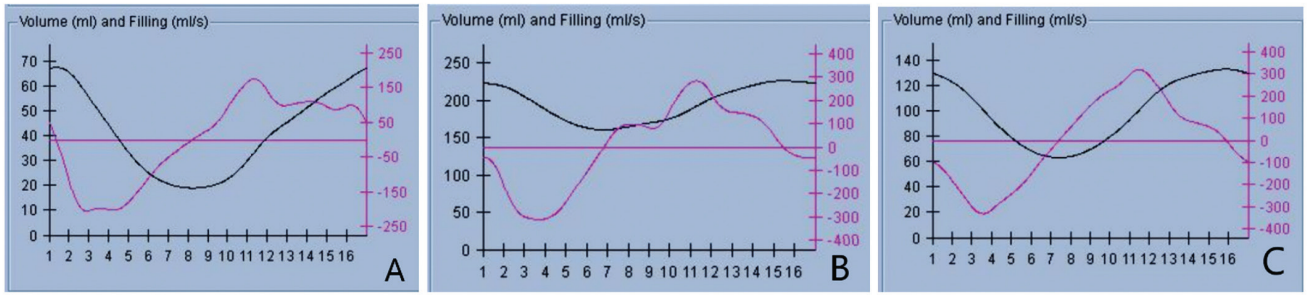

Figure 8. (A) Time-volume curve of a patient in the normal group. (B) Time-volume curve of a patient in the infarct group. (C) Time-volume curve of a patient in the ischemia group

these findings, the exponential decay formula appears to be sensitive to preload changes.

LV afterload may be defined as the tension or stress developed in the LV wall during ejection due to the force against which the myocardium contracts. LV afterload is determined by arterial pressure as well as the volume and thickness of the LV according to Laplace's law (19). Clinically, the level of LV afterload can be estimated by the systolic arterial pressure in the presence of a normal aortic valve (19,20). Afterload affects the workload of the heart and the contractility of the myocardium against this workload. This situation results in structural changes in the myocardium of the left ventricle. Accordingly, the parameters that determine the afterload according to Laplace's law also determine the shape of the systolic curve of the left ventricle. Even if EDV and ESV do not change under these conditions, the shape of the systolic part of the LV time-volume curve changes, and this change can be detected by the exponential decay formula used in this study. The exponential analysis of the systolic part of the LV volume curve seems to can evaluate the combined effect of parameters determining the afterload simultaneously. In fact, it has been reported that LV afterload is determined by complex, time-varying phenomena that affect the pressure and flow patterns produced by the pumping ventricle and cannot be expressed as a single numerical measure or defined in terms of pressure alone (20). However, exponential analysis of the systolic curve seems to have the potential to shed light on this issue.

In addition to contractility of the LV, preload, and afterload, EF is affected by changes in heart rate (1). Because heart rate affects the diastole duration of the cardiac cycle, it also affects the LV filling time or preload. Increased venous return increases ventricular filling, and increasing preload increases the active tension developed by the muscle fiber and increases the velocity of fiber shortening at a given afterload and inotropic state. Therefore, the time interval during ejection of the left ventricle in the exponential decay formula in this study has also been indexed to beat per minute of the LV. Thus, the differences caused by changes in heart rhythm are eliminated. Similarly, the results obtained using the formula were also indexed to the BSA of each patient. Thus, it has been aimed to eliminate the changes that will arise from the mass differences in the patients.

The presence of a statistically significant difference in the Ec results between the patient groups formed according to the presence of perfusion defects and whether they are reversible suggests that this parameter has diagnostic potential. In the ischemia group, myocardial stunning or subendocardial ischemia caused by reversible perfusion defects probably played a role in the statistically significant difference between the normal and ischemia groups. In the infarct group with irreversible perfusion defects, the presence of myocardial fibrosis or hibernated myocardium, which are indicative of structural changes, may be responsible for an even more statistically significant difference between the normal and infarct groups. According to these results, structural and functional changes affecting inotropy of the left ventricle seem to gradually change the shape of the systolic part of the left ventricle time-volume curve The presence of a very good linear correlation between EF and Ec may also support this view. Furthermore, sensitivity and specificity analyses of the results seem to support the existence of such a diagnostic potential.

Study Limitations

As a limitation of the study, although it was planned to obtain all parameters from scintigraphic data, the systole time could have been calculated more precisely using ECG, and Ec results would have been more precise.

Conclusion

Because the systolic part of the LV volume curve obtained using gMPI shows a non-linear decrease, it was analyzed using the exponential decrease formula. Thus, with a formula that includes output (ESV) and input (EDV), it was possible to examine the decreasing pattern of the volume curve as it progressed from EDV to ESV. The scintigraphic parameter obtained with this formula has been called the Ec, and it has been detected that this parameter showed a statistically significant progressive decrease trend in patients with reversible and irreversible perfusion defects compared with the normal group. Besides, it seems that Ec may have a clinical role as a scintigraphic parameter in the evaluation of systolic functions of the left ventricle.

Acknowledgement

I would like to thank Nuclear Medicine Specialist Doctor Alev Nar and Nuclear Medicine Specialization Student Beyza Bedi, who contributed to the collection, classification, and tabulation of patient data.

Ethics

Ethics Committee Approval: The University of Health Sciences Türkiye, Gülhane Scientific Research Ethics Committee approved the study protocol (decision no: 2022-278, date: 12.09.2022).

Informed Consent: Not applicable.

Peer-review: Externally peer-reviewed.

Authorship Contributions

Concept: A.Ö.K., A.Ç., Design: A.Ö.K., A.Ç., Data Collection or Processing: A.Ö.K., A.Ç., Analysis or Interpretation: A.Ö.K., A.Ç., Literature Search: A.Ö.K., A.Ç., Writing: A.Ö.K., A.Ç.

Conflict of Interest: No conflict of interest was declared by the authors.

Financial Disclosure: The authors declared that this study has received no financial support.

References

1. Halliday BP, Senior R, Pennell DJ. Assessing left ventricular systolic function: from ejection fraction to strain analysis. Eur Heart J 2021;42:789-797.
2. Cuocolo A, Petretta M, Acampa W, De Falco T. Gated SPECT myocardial perfusion imaging: the further improvements of an excellent tool. Q J Nucl Med Mol Imaging 2010;54:129-144.
3. Shojaeifard M, Ghaedian T, Yaghoobi N, Malek H, Firoozabadi H, Bitarafan-Rajabi A, Haghjoo M, Amin A, Azizian N, Rastgou F. Comparison of gated SPECT myocardial perfusion imaging with echocardiography for the measurement of left ventricular volumes and ejection fraction in patients with severe heart failure. Res Cardiovasc Med 2015;5:e29005.
4. Noordzij W, Slart RH. Clinical value of quantitative measurements derived from GATED SPECT: motion and thickening, volumes and related LVEF. Q J Nucl Med Mol Imaging 2018;62:321-324.
5. Puente-Barragán A. Coronary atherosclerotic disease evaluation by nuclear cardiology procedures: Gate-SPECT and PET myocardial perfusion imaging. Cardiovascular and Metabolic Science 2021;32:258-262.
6. Rozental O, Thalappillil R, White RS, Tam CW. To Swan or Not to Swan: Indications, Alternatives, and Future Directions. J Cardiothorac Vasc Anesth 2021;35:600-615.
7. Kasai T, DePuey EG, Sponder I. "W-shaped" volume curve with gated myocardial perfusion single photon emission computed tomography. Ann Nucl Med 2005;19:59-64.
8. Abidov A, Germano G, Hachamovitch R, Berman DS. Gated SPECT in assessment of regional and global left ventricular function: major tool of modern nuclear imaging. J Nucl Cardiol 2006;13:261-279.
9. Annamalai C. Applications of exponential decay and geometric series ineffective medicine dosage. Advances in Bioscience and Biotechnology 2010:1;51-54.
10. Strickland JC, Lile JA, Rush CR, Stoops WW. Comparing exponential and exponentiated models of drug demand in cocaine users. Exp Clin Psychopharmacol 2016;24:447-455.
11. Available from: https://courses.lumenlearning.com/ivytech-collegealgebra/chapter/model-exponential-growth-and-decay/
12. Available from: http://www.montereyinstitute.org/courses/DevelopmentalMath/COURSE_TEXT2_RESOURCE/U18_L1_T1_text_final.html
13. Marwick TH. Ejection Fraction Pros and Cons: JACC State-of-the-Art Review. J Am Coll Cardiol 2018;72:2360-2379.
14. Evans JM, Wang S, Greb C, Kostas V, Knapp CF, Zhang Q, Roemmele ES, Stenger MB, Randall DC. Body Size Predicts Cardiac and Vascular Resistance Effects on Men's and Women's Blood Pressure. Front Physiol 2017;8:561.
15. LaBounty TM, Bach DS, Bossone E, Kolias TJ. Indexing left ventricular wall thickness to body surface area improves prognostic value. Echocardiography 2019;36:824-830.
16. Antohi EL, Chioncel O. Understanding cardiac systolic performance beyond left ventricular ejection fraction. Explor Med 2020:1:75-84.
17. Peverill RE. Understanding preload and preload reserve within the conceptual framework of a limited range of possible left ventricular end-diastolic volumes. Adv Physiol Educ 2020;44:414-422.
18. Han JC, Pham T, Taberner AJ, Loiselle DS, Tran K. Solving a century-old conundrum underlying cardiac force-length relations. Am J Physiol Heart Circ Physiol 2019;316:H781-H793.
19. Fukuta H, Little WC. The cardiac cycle and the physiologic basis of left ventricular contraction, ejection, relaxation, and filling. Heart Fail Clin 2008;4:1-11.
20. Chirinos JA, Segers P. Noninvasive evaluation of left ventricular afterload: part 1: pressure and flow measurements and basic principles of wave conduction and reflection. Hypertension 2010;56:555-562.

Original Article
Mol Imaging Radionucl Ther 2023;32:214-220 DOI:10.4274/mirt.galenos.2023.55707

A Study of CT-derived Radiation Dose Calculation in Lung Q-SPECT/CT Imaging

Akciğer Q-SPECT/BT Görüntülemede BT Kaynaklı Radyasyon Doz Hesabı Çalışması

Güler Silov, Fatih Boğa

Samsun Gazi State Hospital, Clinic of Nuclear Medicine, Samsun, Türkiye

Abstract

Objectives: To investigate the amount of effective dose (ED) due to the computed tomography (CT) component of lung perfusion-single-photon emission computed tomography (Q-SPECT)/CT.

Methods: In this single-center retrospective study, imaging data were collected from the clinic database for the period 2016-2022. The 327 patients identified were aged between 20 and 94 years. Tube voltage, tube current, pitch, gantry rotation time, volume CT dose index, and dose-length product (DLP) were recorded. The DLP was then converted to an ED using the conversion factors. The comparison of the ED between two groups was performed using the Mann-Whitney U non-parametric test.

Results: ED (mean ± standard deviation, mSv) was 1.20±0.70 for the pulmonary embolism (PE) (-) and 1.54±1.04 for the PE (+) cases ($p<0.05$). It was observed that there was a 28% increase in the ED for the PE (+) cases. In addition, each of the PE (-) and PE (+) cases was divided into two groups according to the use of the computed tomography dose reduction (CTDR): without CTDR protocol group (non-CTDR) and with CTDR protocol group (CTDR). For those groups, ED were obtained as 0.87±0.72 and 1.55±0.47 for PE (-) cases ($p<0.05$); 1.56±1.17 and 1.49±0.54 for PE (+) cases ($p>0.05$) correspondingly. For a deeper understanding, ED was calculated for all three groups formed with different tube voltage values applied for the non-CTDR and CTDR groups.There was a 42% decrease in the ED for group 1 PE (+) compared to group 2 PE (+) (1.21±0.28, 2.07±0.91, $p<0.05$) and there was a 41% decrease in the ED for group 1 PE (-) compared to group 2 PE (-) cases (1.17±0.32, 1.97±0.65, $p<0.05$).

Conclusion: It could be concluded that the effective DR protocol is the non-CTDR protocol for the PE (-) cases and the application of the tube voltage at the level of 100 kVp for the PE (+) cases.

Keywords: Lung Q-SPECT/CT, effective dose, dose reduction, pulmonary embolism

Öz

Amaç: Akciğer perfüzyon-tek foton emisyonlu bilgisayarlı tomografi/bilgisayarlı tomografinin (Q-SPECT/BT) BT komponenti kaynaklı maruz kalınan etkin doz (ED) miktarını araştırmaktır.

Yöntem: Bu tek merkezli ve retrospektif çalışmada, görüntüleme verileri 2016-2022 dönemi için klinik veri tabanından toplandı. Tanımlanan 327 hastanın yaşları 20 ile 94 arasındaydı. Tüp voltajı, tüp akımı, pitch, gantri rotasyon süresi, hacim BT doz indeksi ve doz-uzunluk çarpımı (DLP) kaydedildi. DLP daha sonra dönüştürme faktörleri kullanılarak ED'ye dönüştürüldü. İkili gruplar arasındaki ED karşılaştırması Mann-Whitney U non-parametrik test ile yapıldı.

Bulgular: ED (ortalama ± standart sapma, mSv) pulmoner emboli (PE) (-) olgular için 1,20±0,70 ve PE (+) olgular için 1,54±1,04 idi ($p<0,05$). PE (+) olgularda ED'de %28'lik bir artış olduğu gözlendi. Ayrıca, PE (-) ve PE (+) olguların her biri bilgisayarlı tomografi doz azaltımı (CTDR) kullanımına göre iki gruba ayrıldı: CTDR protokolü olmayan grup (non-CTDR) ve CTDR protokolü olan grup (CTDR). Bu gruplar için ED sırasıyla PE (-) olgular için 0,87±0,72 ve 1,55±0,47 ($p<0,05$); PE (+) olgular için 1,56±1,17 ve 1,49±0,54 ($p>0,05$) olarak elde edildi. Daha derin bir anlayış için ED, non-CTDR ve CTDR grupları için uygulanan farklı tüp voltaj değerleri ile oluşturulan üç grup için de hesaplandı. Grup 1 PE (+) için, grup 2 PE (+) ile

Address for Correspondence: Güler Silov MD, Samsun Gazi State Hospital, Clinic of Nuclear Medicine, Samsun, Türkiye
Phone: +90 362 311 30 30 **E-mail:** gulersilov@yahoo.com ORCID ID: orcid.org/0000-0002-4658-8634
Received: 08.12.2022 **Accepted:** 02.04.2023

karşılaştırıldığında ED'de %42 azalma (1,21±0,28, 2,07±0,91, p<0,05) ve grup 1 PE (-) için, grup 2 PE (-) ile karşılaştırıldığında ED'de %41 azalma (1,17±0,32, 1,97±0,65, p<0,05) vardı.

Sonuç: Etkin DR protokolünün PE (-) olgular için non-CTDR protokol ve PE (+) olgular için 100 kVp düzeyinde tüp voltajı uygulaması ile olduğu sonucuna varılabilir.

Anahtar kelimeler: Akciğer Q-SPECT/BT, etkin doz, doz azaltma, pulmoner emboli

Introduction

Single photon emission computed tomography/computed tomography (SPECT/CT) is recently preferred in nuclear medicine studies due to its superior features such as anatomical correlation and attenuation correction. SPECT/CT uses the body density map obtained from the CT scan and performs attenuation correction depending on the energy of the photon. Lung ventilation/perfusion (V/Q) scintigraphy or only perfusion single photon emission computed tomography/computed tomography (Q-SPECT/CT) is a widely used tool for the diagnosis of acute pulmonary embolism (PE) and for the follow-up of chronic PE because of its lower radiation doses with almost no contraindications (1).

Currently, an enhanced computed tomography pulmonary angiography (CTPA) study is recommended by the American College of Radiology as a primary diagnostic method for the detection of PE (2). However, V/Q SPECT is strongly recommended by the European Association of Nuclear Medicine as the first imaging choice for PE diagnosis (3). In the literature, a wide range for the effective dose (ED) of CTPA has been reported, which varies from 1.8 to 20 mSv, and the absorbed breast dose lies within the range of 2.8-70 mGy (4,5,6). The estimated ED range from V/Q SPECT is substantially lower, 0.6-3 mSv, and the absorbed breast dose is 1.1-1.5 mGy (6,7,8).

The best standard for the practice of imaging using ionizing radiation requires compliance with the As Low As Reasonably Achievable (ALARA) principle (9). Therefore, if CT is used for only attenuation correction and anatomical localization, low-dose CT should be preferred to avoid unnecessary radiation exposure. Low-dose CT is generally recommended in cases where concurrent diagnostic CT is available and in cases where treatment response is being evaluated. It is recommended that low-dose CT should be performed immediately after SPECT imaging. The amount of dose organ received in CT depends on many factors. The most important parameters are patient body mass index, slice thickness, number of slices, gantry rotation time, pitch value, tube voltage, and tube current value. Low-dose CT parameters may vary according to the technical specifications of the device. Dose reduction (DR) techniques are available in many systems. In addition, most of the CT acquisition parameters can also be changed by technicians during the CT examination (10).

There are a large number of studies in the literature that have attempted to determine the ED and absorbed breast dose for V/Q SPECT and CTPA studies (11). To the best of our knowledge, there is a single study reporting CT-derived ED in the Chronic Thromboembolic Pulmonary Hypertension (CTEPH) study group that underwent lung Q-SPECT/CT (12). However, we could not find any study using different CT parameters for DR in lung Q-SPECT/CT imaging. This study aimed to investigate the amount of radiation dose due to the CT component to which the patient is exposed during lung Q-SPECT/CT.

Materials and Methods

Study Population

The regional institutional Ondokuz Mayıs University Clinical Research Ethics Committee approved this retrospective study protocol (decision no: 2022/512, date: 23.11.2022). This single-center study was based on the data from lung V/Q-SPECT/CT imaging of patients under the suspicion of acute PE or chronic PE in follow-up using the Nuclear Medicine Department database. The final diagnosis was established with a composite reference standard that included electrocardiogram, ultrasound of lower extremity veins, D-dimer levels, CTPA, and clinical follow-up for at least 6 months. Imaging data from 2016 to 2022 were reviewed. All 327 patients were aged between 20 and 94 years and had undergone at least one lung Q-SPECT/CT imaging.

As of January 2022, a working system that is assumed to be more in line with the ALARA principles has been implemented. For CTDR protocol the rotation time applied to 132 cases was manually set as 0.66s, tube current as 120 mA, and pitch value as 1. Of these 132 cases, 61 patients received a tube voltage of 100 kVp (group 1) and 71 patients received a tube voltage of 120 kVp (group 2). The remaining 195 patients in the non-CTDR group received a rotation time of 1s, tube current of 160 mA, pitch value of 0.75, and tube voltage of 120 kVp (group 3). ED was then calculated for all three groups.

Acquisition Protocol

Five minutes after the intravenous injection of 200 MBq (5.4 mCi) of Tc-99m MAA in the supine position, acquisition started applying AnyScan® SC, combined SPECT gamma-camera and CT (Mediso Ltd., Budapest, Hungary) system. SPECT imaging specifications included an energy window of 140 keV 20%, single energy window scatter correction of 5% around the 120 keV peak, low energy high-resolution collimator, 128x128 matrix, 32 projections over 360°, and time per projection of 30 s for perfusion imaging. Low-dose CT scans of the chest were recorded during free breathing at 100-120 kVp and 80-160 mAs without intravenous contrast administration. Helical low-dose CT imaging of the thorax was acquired in dose modulation and the cephalocaudal direction, using settings of 0.66-1 s rotation time, helical thickness of 5 mm, pitch of 0.75-1, 512x512 matrix and collimation of 20x1.25. Q-SPECT images were reconstructed using ordered subset expectation maximization reconstruction, then fused with the corresponding CT image slices.

CT Dose Calculation

SPECT, CT, and fused images were interpreted simultaneously using InterView™ Fusion software (version: 3.08.008.0000; Mediso Ltd., Budapest, Hungary). This study was conducted using CT dose data from only Q-SPECT/CT images. Peak tube voltage (kVp), tube current (mA), pitch value, gantry rotation time, volume computed tomography dose index (CTDIvol), and dose-length product (DLP) were recorded for CT dose calculation. CT radiation dose assessment is performed by estimating the CTDIvol measured during a single rotation of the X-ray source. This index represents the absorbed dose along the longitudinal axis of the CT scanner. The unit of CTDIvol is mGy. To calculate the total absorbed dose in a full CT scan based on the scanned range (L) and the DLP was calculated as CTDIvolxL (mGy*cm) (13,14).

DLP was converted to an ED value using the conversion factor recommended by the ICRP publication 102 and AAPM report no. 96 (15,16). Therefore, a value of 0.014 was accepted as the conversion factor for the thoracic region and used throughout all ED analyzes corresponding to the results in Tables 1 and 2.

For the results in Table 3, note that the conversion factor for the male gender was taken as 0.0104 for the tube voltage of 100 kVp and 0.0105 for 120 kVp, and for the female gender was taken as 0.0183 for the tube voltage of 100 kVp and 0.0185 for 120 kVp, as reported in ICRP 103 (17).

TTo achieve the same image quality at a lower dose in this study, a dose modulation system was used. The CT scanner applied the tube current at a level appropriate to the patient's tissue attenuation.

Statistical Analysis

SPSS 22.0 software was used for statistical analysis of the data, which are presented as mean ± standard deviation (SD) and overall percentages. The non-parametric Mann-Whitney U test was used for CT-induced ED comparisons. A p-value of 0.05 was considered to indicate a statistically significant difference.

Results

One hundred thirty patients (40%, 86 female and 44 male) were diagnosed with PE. The embolism group consisted of acute and chronic cases. One hundred ninety-seven patients (60%, 109 female and 88 male) were diagnosed as negative for PE.

The data for the PE (-) and PE (+) cases are summarised in Table 1. ED (mean ± SD) was 1.20±0.7 mSv for the PE (-) cases and 1.54±1.04 mSv for the PE (+) cases, and there was a statistically significant difference between the ED of the PE (-) and PE (+) cases ($p<0.05$). It was observed that there was a 28% increase in the ED for the PE (+) cases. The measurements for non-CTDR and CTDR groups of PE (-) and PE (+) cases are summarized in Table 2. ED (mean± SD) was 0.87±0.72 mSv and 1.55±0.47 mSv for non-CTDR and CTDR groups of PE (-) cases ($p<0.05$); 1.56±1.17 mSv and 1.49±0.54 mSv for non-CTDR and CTDR groups of PE (+) cases ($p>0.05$), respectively. While the ED values presented similarity between the PE (+) non-CTDR and PE (+) CTDR groups, an increase in the ED was observed for the PE (-)

Table 1. CT parameters and calculated dose values in PE (-) and PE (+) cases

CT acquisition parameters and calculated dose values	Range	PE (-) (n=197) (mean ± SD)	PE (+) (n=130) (mean ± SD)
Peak tube voltage (kVp)	100-120	-	-
Tube current (mA)	120-160	-	-
Gantry rotation time (s)	0.66-1	-	-
Pitch value	0.75-1	-	-
CTDIvol (mGy)	1.21-13.65	3.1±1.7	4.5±3.1
DLP (mGy*cm)	9.49-399.46	85.8±49.7	110±74
ED (mSv)*	0.13-5.59	1.20±0.70	1.54±1.04

*p<0.05, DLP: Dose-length product, CTDIvol: Volume computed tomography dose index, ED: Effective dose, PE: Pulmonary embolism, SD: Standard deviation

CTDR group in comparison to the PE (-) non-CTDR group.

The measurements for groups 1-3 and the results of the pairwise ED comparison within the groups are shown in Table 3.

For pairwise comparisons between group 1 PE (-) and group 2 PE (-), group 1 PE (-) and group 3 PE (-), group 2 PE (-) and group 3 PE (-), and group 1 PE (+) and group 2 PE (+) cases, a statistically significant difference in ED was observed ($p<0.05$). However, no statistically significant difference ($p>0.05$) was observed between group 1 PE (+) and group 3 PE (+) and group 2 PE (+) and group 3 PE (+) cases (Table 3).

Noting the only difference between group 1 and group 2 that is the tube voltage of 100 kVp and 120 kVp, respectively, the analyzes regarding these two groups revealed that there was a 42% decrease in the ED in group 1 PE (+) compared to group 2 PE (+) cases (1.21±0.28 mSv, 2.07±0.91 mSv, $p<0.05$, respectively) and there was 41% decrease in the ED in group 1 PE (-) compared to group 2 PE (-) cases (1.17±0.32 mSv, 1.97±0.65 mSv, $p<0.05$, respectively).

Table 2. CT parameters and calculated ED results in the PE (-) and PE (+) cases with non-CTDR and CTDR protocol

CT acquisition parameters	PE (-) Non-CTDR (n=101)	PE (-) CTDR (n=96)	PE (+) Non-CTDR (n=94)	PE (+) CTDR (n=36)
Gantry rotation time (s)	1	0.66	1	0.66
Pitch value	0.75	1	0.75	1
Tube current (mA)	160	120	160	120
ED (mSv) (mean ± SD)	0.87±0.72	1.55±0.47	1.56±1.17	1.49±0.54
p-value (ED)	<0.05		>0.05	

Non-CTDR: Without CTDR protocol, CTDR: With CTDR protocol, ED: Effective dose, SD: Standard deviation

Discussion

In the examination and follow-up of pulmonary parenchymal lesions, it is now possible to perform a tomographic examination at doses close to the dose of chest radiography with low mAs values and other low-dose applications (18). Because a certain amount of noise can be tolerated in the detection of high-contrast lesions of the lung, mAs can be reduced. Low tube current-time product (mAs) images are especially useful for the examination of the lungs and paranasal sinuses, the investigation of urinary system stones, and CT-guided interventional procedures (19).

The dose varies linearly with gantry rotation time. A shorter gantry rotation time reduces the time the patient is exposed to radiation, thereby decreasing the dose and reducing the risk of motion artifacts. In most multislice computed tomography devices, the gantry rotation time is less than 1s. In our Q-SPECT/CT study, we applied two different values (0.66s and 1s) as the rotation time of the CT scanner. The pitch value is the ratio of the table advancement distance to the slice thickness in the complete rotation time of the tube. A high pitch factor reduces the dose by decreasing the X-ray exposure time of the examined area. However, this may negatively affect the image quality (20,21).

Tube voltage (kVp) determines the X-ray energy. It is a parameter that affects spatial and contrast resolution. The radiation dose is directly proportional to the square of the tube voltage. Therefore, small decreases in tube voltage significantly contribute to DR. In some examinations, this can be achieved by decreasing the tube voltage value without increasing noise and preserving image quality. Generally, tube voltage is used in the range of 70-140 kVp in clinical applications. Natural structures such as the lung, airway, and bone are high-density tissues that cause

Table 3. CT parameters and calculated ED results in the groups according to tube voltage

CT acquisition parameters	Group 1 CTDR 100 kVp		Group 2 CTDR 120 kVp		Group 3 Non-CTDR 120 kVp	
	PE (-) (n=44)	PE (+) (n=17)	PE (-) (n=52)	PE (+) (n=19)	PE (-) (n=101)	PE (+) (n=94)
Gantry rotation time (s)	0.66	0.66	0.66	0.66	1	1
Pitch value	1	1	1	1	0.75	0.75
Tube current (mA)	120	120	120	120	160	160
ED (mSv) (mean ± SD)	1.17±0.32	1.21±0.28	1.97±0.65	2.07±0.91	0.91±0.8	1.84±1.48
p-value (ED)	>0.05		>0.05		<0.05	

Non-CTDR: Without CTDR protocol, CTDR: With CTDR protocol, ED: Effective dose, SD: Standard deviation, PE: Pulmonary embolism, CT: Computed tomography

natural contrasts. Therefore, a low tube voltage in the range of 80-100 kVp can be applied more safely in the examination of these structures (20,21). In our study, the ED at tube voltages of 100 and 120 kVp was investigated in accordance with the values reported in the literature.

The tube current (mA) is related to the number of X-rays produced by the tube. Multiplying this with the gantry rotation time gives mAs. The radiation dose is directly proportional to the change in the tube current. However, careless and unplanned irradiation may lead to decreased image quality as a result of increased noise (20,22). In a Q-SPECT/CT study conducted with values of CT irradiation parameters, similar to our study (120 kVp, 1s gantry rotation time, 1.25 pitch), it was reported that embolism diagnostic accuracy was 94.9%, with a sensitivity of 98.6%, and specificity of 94.5% even at 30 mAs (23).

With the developing technology in CT devices, the optimum kVp and mAs values are calculated according to the region of the patient that can be examined in the contrast-to-noise ratio, especially in the first topogram images, and it is aimed to provide optimum image quality at low radiation dose. There are also studies indicating that automatic tube voltage selection provides more radiation DR than other methods (24). However, by creating group 1 (100 kVp) and group 2 (120 kVp) with manual selection of tube voltage in our study also revealed that a 41% reduction in ED can be achieved in group 1 PE (-) and a 42% reduction in group 1 PE (+) cases.

Referring to an embolism study (25) that applied the same DR as ours, we also do not expect a difference in sensitivity and specificity values to achieve adequate image quality. In a study the tube voltage value of 80 kVp used for CTPA in patients weighing less than 100 kg resulted in a 40% DR, compared to 100 kVp without deterioration in image quality (26).

While the average ED in a standard thorax CT is approximately 6 mSv, this value is approximately 1.6 mSv in low-dose thorax CT. In the literature, it has been reported that the tube current used in low-dose CT is less than 100 mAs and the tube voltage is usually 120 kVp (27,28,29). Roach et al. (28) showed that CT scans for chest/abdomen anatomical localization amount to up to 1-2 mSv.

It is thought that the unexpected increase in ED despite the lower value of the gantry rotation time and tube current and the higher value of the pitch in the CTDR studies may be due to the activation of the dose modulation system. CT parameters such as tube current, gantry rotation time, tube voltage, and pitch value are the factors that affect the radiation dose. If one of these parameters is changed, the dose modulation may increase the tube current to ensure adequate image quality (30). Decreasing the gantry rotation time may be compensated by an increase in mAs to maintain the mAs at a constant level (31). In our study, an increase in ED was observed in the group 2 PE (+), group 2 PE (-), and group 1 PE (-) cases, which may be caused by such compensations (Table 3).

In a Q-SPECT/CT study (12), CT was performed with a pitch value of 1.25, rotation time of 1s, tube current-time product of 30 mAs, and tube voltage of 120 kVp. Then, the ED (mean ± SD) was computed as 2.1±0.62 mSv (12), which is similar to the results obtained from group 2 in our study.

No statistically significant difference in ED was observed in the PE (+) cases with CTDR group compared to the non-CTDR group, whereas an increase in ED was observed in the PE (-) cases with CTDR group ($p<0.05$). In the group comparisons of PE (+) cases, effective DR was observed only in group 1 PE (+) cases with 100 kVp tube voltage compared to group 2 PE (+) cases with 120 kVp tube voltage ($p<0.05$) (Table 3). In addition, group 3 PE (-) has the lowest ED of all the groups considered. All these findings indicate that the best DR protocol for the PE (-) cases can be considered as a non-CTDR protocol and for the PE (+) cases, the application of tube voltage at the 100 kVp level. Regarding image acquisition protocols, it has been reported that nuclear medicine specialists should adjust the CT imaging procedure by considering the patient's clinical data (32). Lung Q-SPECT/CT is a hybrid application in which SPECT images are first obtained, followed by CT images. Therefore, in Q-SPECT/CT imaging, after the specialist comments on the possibility of PE from the SPECT image, a reduction in ED can be achieved in accordance with the ALARA principle. If the patient shows perfusion defect(s) in SPECT images, the application of tube voltage at 100 kvp level could be used. However, if the patient has no perfusion defect, the non-CTDR protocol should be preferred.

In our study, by applying 80 and 160 mAs and tube voltages of 100-120 kVp, ED (mean ± SD) were calculated as 1.20±0.70 mSv and 1.54±1.04 mSv for the PE (-) and PE (+) cases, respectively. It was observed that ED in the PE (+) was higher than that in the PE (-) cases. PE is a clinical condition that causes many histopathological changes in the lung parenchyma and bronchovascular system. In a recent study that compared pulmonary vascular resistance (PVR) and mean pulmonary arterial pressure (mPAP) values with a CT scoring system that included main pulmonary artery diameter and mosaic perfusion pattern, a highly significant statistical correlation was observed between the CT scoring and both mPAP and PVR ($p<0.05$). High

PVR and mPAP have been reported as a consequence of hemodynamic changes in the lung due to CTEPH (33). In another study, vascular attenuation was calculated using region of interest drawn on the main pulmonary arteries and their peripheral branches, and increased attenuation was found in both acute and chronic PE [33 Hounsfield unit (HU) for acute PE, 87 HU for chronic PE]. Similarly in our study, there were acute and chronic cases in the embolism positive group. It could be thought that the difference in tissue attenuation caused a statistically significant increase in ED in the embolism-positive group compared with the embolism-negative group (34). New studies are required to support this idea.

Study Limitations

Because our study was retrospective, the body mass index of the patients could not be included in the evaluation.

A subgroup evaluation using different voltage levels in the non-CTDR group would have added a new perspective to this study. However, in our study, only single voltage results were available in the non-CTDR group. Investigating this issue in future studies may allow for more objective evaluations.

Conclusion

As a result, it is concluded that reducing the tube voltage level alone rather than CTDR protocol might be sufficient to achieve an ED decrease in PE (+) patients.

Ethics

Ethics Committee Approval: The regional institutional Ondokuz Mayıs University Clinical Research Ethics Committee approved this retrospective study protocol (decision no: 2022/512, date: 23.11.2022).

Informed Consent: Data for this retrospective study were obtained from the medical records of the hospital, and patient consent was waived by the approval of the Institutional Review Board.

Peer-review: Externally and internally peer-reviewed.

Authorship Contributions

Surgical and Medical Practices: G.S., F.B., Concept: G.S., Design: G.S., Data Collection or Processing: F.B., Analysis or Interpretation: G.S., Literature Search: G.S., F.B., Writing: G.S., F.B.

Conflict of Interest: No conflict of interest was declared by the authors.

Financial Disclosure: The authors declared that this study has received no financial support.

References

1. Lu Y, Lorenzoni A, Fox JJ, Rademaker J, Vander Els N, Grewal RK, Strauss HW, Schöder H. Noncontrast perfusion single-photon emission CT/CT scanning: a new test for the expedited, high-accuracy diagnosis of acute pulmonary embolism. Chest 2014;145:1079-1088.
2. Expert Panels on Cardiac and Thoracic Imaging:; Kirsch J, Brown RKJ, Henry TS, Javidan-Nejad C, Jokerst C, Julsrud PR, Kanne JP, Kramer CM, Leipsic JA, Panchal KK, Ravenel JG, Shah AB, Mohammed TL, Woodard PK, Abbara S. ACR Appropriateness Criteria® Acute Chest Pain-Suspected Pulmonary Embolism. J Am Coll Radiol 2017;14:S2-S12.
3. Bajc M, Neilly JB, Miniati M, Schuemichen C, Meignan M, Jonson B; EANM Committee. EANM guidelines for ventilation/perfusion scintigraphy : Part 1. Pulmonary imaging with ventilation/perfusion single photon emission tomography. Eur J Nucl Med Mol Imaging 2009;36:1356-1370.
4. Hurwitz LM, Reiman RE, Yoshizumi TT, Goodman PC, Toncheva G, Nguyen G, Lowry C. Radiation dose from contemporary cardiothoracic multidetector CT protocols with an anthropomorphic female phantom: implications for cancer induction. Radiology 2007;245:742-750.
5. Schembri GP, Miller AE, Smart R. Radiation dosimetry and safety issues in the investigation of pulmonary embolism. Semin Nucl Med 2010;40:442-454.
6. Tonkopi E, Manos D, Ross A. DOES THE USE OF CONTEMPORARY CT SCANNERS ALTER THE RADIATION DOSE DEBATE IN THE IMAGING WORK UP FOR PULMONARY EMBOLISM? Radiat Prot Dosimetry 2019 31;187:353-360.
7. Stein PD, Freeman LM, Sostman HD, Goodman LR, Woodard PK, Naidich DP, Gottschalk A, Bailey DL, Matta F, Yaekoub AY, Hales CA, Hull RD, Leeper KV Jr, Tapson VF, Weg JG. SPECT in acute pulmonary embolism. J Nucl Med 2009;50:1999-2007.
8. Phillips JJ, Straiton J, Staff RT. Planar and SPECT ventilation/perfusion imaging and computed tomography for the diagnosis of pulmonary embolism: A systematic review and meta-analysis of the literature, and cost and dose comparison. Eur J Radiol 2015;84:1392-1400.
9. Brink JA, Amis ES Jr. Image Wisely: a campaign to increase awareness about adult radiation protection. Radiology 2010;257:601-602.
10. Işık Z, Selçuk H, Albayram S. Bilgisayarlı Tomografi ve Radyasyon. Klinik Gelişim Dergisi 2014;23:16-18.
11. Astani SA, Davis LC, Harkness BA, Supanich MP, Dalal I. Detection of pulmonary embolism during pregnancy: comparing radiation doses of CTPA and pulmonary scintigraphy. Nucl Med Commun 2014;35:704-711.
12. Wang L, Wang M, Yang T, Wu D, Xiong C, Fang W. A Prospective, Comparative Study of Ventilation-Perfusion Planar Imaging and Ventilation-Perfusion SPECT for Chronic Thromboembolic Pulmonary Hypertension. J Nucl Med 2020;61:1832-1838.
13. Sağsöz ME, Alper F. Kardiyak Multi Dedektör Bilgisayarlı Tomografide (MDBT) Radyasyon Dozu. Trd Sem 2013;1:16-25.
14. Sarpün İH, İnal A, Çeçen B. Voltaj ve Akım Değerlerinin Hasta Dozu Üzerindeki Etkilerinin CTDI Fantomu ile Araştırılması. Süleyman Demirel Üniversitesi Fen Edebiyat Fakültesi Fen Dergisi 2019;14:327-334.
15. International Commission on Radiological Protection: ICRP publication 102: Managing Patient Dose in Multi-Dedector Computed Tomography (MDCT). Oxford: Elsevier; 2007.
16. American Association of Physicists in Medicine, The Measurement, Reporting, and Management of Radiation Dose in CT, Rep. No. 96, AAPM, College Park, 2008.
17. Goo HW. CT radiation dose optimization and estimation: an update for radiologists. Korean J Radiol 2012;13:1-11.
18. Başar ve Karaarslan E. Bilgisayarlı tomografide doz hesaplama ve düşük doz uygulamaları. In Gelal F, editor. Radyoloji Fiziği. İstanbul, Nobel Tıp Kitabevleri, 2019;92-100.
19. Karabulut N, Ariyürek M. Low dose CT: practices and strategies of radiologists in university hospitals. Diagn Interv Radiol 2006;12:3-8.

20. Başekim CÇ, Arslanoğlu A. Bilgisayarlı Tomografide Radyasyon Doz Kontrolü ve Düşük Doz Çekim Teknikleri. Trd Sem 2020;8:129-147.
21. Kalra MK, Maher MM, Toth TL, Hamberg LM, Blake MA, Shepard JA, Saini S. Strategies for CT radiation dose optimization. Radiology 2004;230:619-628.
22. Cody DD, Moxley DM, Krugh KT, O'Daniel JC, Wagner LK, Eftekhari F. Strategies for formulating appropriate MDCT techniques when imaging the chest, abdomen, and pelvis in pediatric patients. AJR Am J Roentgenol 2004;182:849-859.
23. Yildirim N, Genc M. The efficiency of hybrid perfusion SPECT/CT imaging in the diagnostic strategy of pulmonary thromboembolism. Hell J Nucl Med 2020;23:304-311.
24. Seyal AR, Arslanoglu A, Abboud SF, Sahin A, Horowitz JM, Yaghmai V. CT of the Abdomen with Reduced Tube Voltage in Adults: A Practical Approach. Radiographics 2015;35:1922-1939.
25. Szucs-Farkas Z, Kurmann L, Strautz T, Patak MA, Vock P, Schindera ST. Patient exposure and image quality of low-dose pulmonary computed tomography angiography: comparison of 100- and 80-kVp protocols. Invest Radiol 2008;43:871-876.
26. Szucs-Farkas Z, Schaller C, Bensler S, Patak MA, Vock P, Schindera ST. Detection of pulmonary emboli with CT angiography at reduced radiation exposure and contrast material volume: comparison of 80 kVp and 120 kVp protocols in a matched cohort. Invest Radiol 2009;44:793-799.
27. Durhan G, Akpınar MG. Toraks İncelemelerinde İleri BT Teknikleri ve Protokolleri. Trd Sem 2020;8:38-53.
28. Roach PJ, Schembri GP, Ho Shon IA, Bailey EA, Bailey DL. SPECT/CT imaging using a spiral CT scanner for anatomical localization: Impact on diagnostic accuracy and reporter confidence in clinical practice. Nucl Med Commun 2006;27:977-987.
29. Mettler FA Jr, Huda W, Yoshizumi TT, Mahesh M. Effective doses in radiology and diagnostic nuclear medicine: a catalog. Radiology 2008;248:254-263.
30. Hamberg LM, Rhea JT, Hunter GJ, Thrall JH. Multi-detector row CT: radiation dose characteristics. Radiology 2003;226:762-772.
31. Smith AB, Dillon WP, Gould R, Wintermark M. Radiation dose-reduction strategies for neuroradiology CT protocols. AJNR Am J Neuroradiol 2007;28:1628-1632.
32. Salvatori M, Rizzo A, Rovera G, Indovina L, Schillaci O. Radiation dose in nuclear medicine: the hybrid imaging. Radiol Med 2019;124:768-776.
33. Leone MB, Giannotta M, Palazzini M, Cefarelli M, Martìn Suàrez S, Gotti E, Bacchi Reggiani ML, Zompatori M, Galiè N. A new CT-score as index of hemodynamic changes in patients with chronic thromboembolic pulmonary hypertension. Radiol Med 2017;122:495-504.
34. Wittram C, Maher MM, Halpern EF, Shepard JA. Attenuation of acute and chronic pulmonary emboli. Radiology 2005;235:1050-1054.

Original Article
Mol Imaging Radionucl Ther 2023;32:221-225 DOI:10.4274/mirt.galenos.2023.06078

Investigation of Clinical Histopathologic Features and Metabolic Parameters of ^{18}F-FDG PET/CT in Invasive Breast Carcinoma with a Micropapillary Component

Mikropapiller Komponentli İnvazif Meme Kanserinde Klinik, Histopatolojik Özellikler ile ^{18}F-FDG PET/BT Metabolik Parametrelerin İncelenmesi

Elife Akgün[1], Göksel Alçın[2], Esra Canan Kelten Talu[3], Tevfik Fikret Çermik[2], Tuçe Söylemez Akkurt[4], Ebru Şen[5], Esra Arslan[2]

[1]*University of Health Sciences Türkiye, Başakşehir Çam and Sakura City Hospital, Clinic of Nuclear Medicine, İstanbul, Türkiye*
[2]*University of Health Sciences Türkiye, İstanbul Training and Research Hospital, Clinic of Nuclear Medicine, İstanbul, Türkiye*
[3]*University of Health Sciences Türkiye, İzmir Tepecik Training and Research Hospital, Clinic of Pathology, İzmir, Türkiye*
[4]*University of Health Sciences Türkiye, Başakşehir Çam and Sakura City Hospital, Clinic of Pathology, İstanbul, Türkiye*
[5]*University of Health Sciences Türkiye, Başakşehir Çam and Sakura City Hospital, Clinic of General Surgery, İstanbul, Türkiye*

Abstract

Objectives: The aim of this study was to evaluate the correlation between clinical histopathologic features and micropapillary (MP) ratio with the maximum standardized uptake value (SUV_{max}) derived from ^{18}F-fluorodeoxyglucose positron emission tomography/computed tomography (^{18}F-FDG PET/CT) in treatment naïve breast cancer.

Methods: Twenty-nine patients diagnosed with breast cancer with a MP component who underwent PET/CT imaging before any local and/or systemic treatment were included in this retrospective study. All clinical histopathological features were recorded. SUV_{max} values were measured from ^{18}F-FDG PET images for primary tumors and metastatic axillary lymph nodes.

Results: MP component percentage did not correlate with any clinical histopathological features except age. At early ages, the MP component ratio was significantly higher. Our results showed that there is no significant correlation between the SUV_{max} value and MP component percentage.

Conclusion: A high SUV_{max} value is generally expected in aggressive malignancies. However, this assumption may not be valid for the MP subgroup, which has an aggressive course compared to other subgroups in breast cancer.

Keywords: ^{18}F-FDG, micropapillary, breast cancer, PET/CT, SUV_{max}

Öz

Amaç: Bu çalışmanın amacı, tedavi uygulanmamış meme kanserinde klinik, histopatolojik özellikler, mikropapiller (MP) komponent oranı ile ^{18}F-florodeoksiglukoz pozitron emisyon tomografisi/bilgisayarlı tomografiden (^{18}F-FDG PET/BT) elde edilen maksimum standardize tutulum değeri (SUV_{maks}) arasındaki ilişkiyi değerlendirmektir.

Yöntem: Bu retrospektif çalışmaya herhangi bir lokal ve/veya sistemik tedavi uygulanmadan önce PET/BT görüntülemesi yapılan MP komponentli meme kanseri tanılı 29 hasta dahil edildi. Tüm klinik, histopatolojik özellikler kaydedildi. Primer tümörlerin ve metastatik aksiller lenf nodlarının SUV_{maks} değerleri ^{18}F-FDG PET görüntülerinden ölçüldü.

Address for Correspondence: Elife Akgün, MD, University of Health Sciences Türkiye, Başakşehir Çam and Sakura City Hospital, Clinic of Nuclear Medicine, İstanbul, Türkiye
Phone: +90 534 711 67 76 **E-mail:** elifekaymak@hotmail.com ORCID ID: orcid.org/0000-0001-5625-9749
Received: 14.03.2023 **Accepted:** 21.05.2023

Bulgular: MP komponent oranı yaş dışında herhangi bir klinik-histopatolojik özellik ile korele değildi. Erken yaşlarda, MP komponent oranı anlamlı olarak daha yüksekti. Sonuçlarımız SUV_{maks} değeri ile MP komponent oranı arasında anlamlı bir ilişki olmadığını gösterdi.

Sonuç: Agresif malignitelerde genelde yüksek düzeyde SUV_{maks} değeri beklenir. Ancak bu varsayım meme kanserinde diğer alt gruplara kıyasla agresif seyir gösteren MP alt grup için geçerli olmayabilir.

Anahtar kelimeler: ^{18}F-FDG, mikropapiller, meme kanseri, PET/BT, SUV_{maks}

Introduction

Invasive micropapillary carcinoma (MPC) of the breast is an infrequent type of breast cancer. It was described as a different entity having 'exfoliative appearance' by Fisher et al. (1) in 1980 and included in the classification of breast tumors in 1993. These cases present with larger tumor volumes, higher histological grade, and a higher percentage of lymphovascular invasion (2,3).

^{18}F fluorodeoxyglucose positron emission tomography/computed tomography (^{18}F-FDG PET/CT) is an extensively used imaging modality that shows glucose metabolism. PET data could uncover underlying histopathologic features by revealing metabolic tumor characteristics. Whether the MP component ratio negatively influenced disease prognosis is not clear in the literature. High ^{18}F-FDG uptake generally indicates poor prognosis, as is well known. In this context, we planned a retrospective study to investigate the relationship between the percentage of MP component in treatment-naïve breast cancer patients and metabolic parameters derived from the primary tumor and lymph node metastases derived from the initial ^{18}F-FDG PET study.

Materials and Methods

Study Population

Cases diagnosed with invasive ductal carcinoma with MP features who did not receive any systemic/local therapy were included in the study. The study period of interest was from 2016 to 2021. The duration between pretreatment PET/CT imaging and histopathological analysis of the surgical specimen was 30 days. Cases with secondary malignancies were excluded from the study.

All clinical data of patients were recorded, including age, location of the tumor (right-left breast), percentage of MP component, histological grade, nuclear grade, Ki-67 value, estrogen receptor, progesterone receptor, human epidermal growth factor receptor 2 receptor statuses, molecular subtypes, axillary lymph node status, tumor size, and metastatic lymph node size (Table 1). All lymph node metastases were verified as histopathological.

Patient Imaging and PET/CT Data Analysis

Patients were injected with 3.7 MBq/kg of ^{18}F-FDG after fasting for at least 6 hours (h) with blood glucose level <180 mg/dL and scanned approximately 60 minutes after injection on PET/CT scanners (Ingenuity TF, Philips Healthcare, Cleveland, Ohio, USA). CT was first acquired using a low-dose technique without contrast agent injection, and a PET scan was obtained immediately after

Table 1. All patients clinical, histopathological, and PET characteristics

	No. of patients	SUV_{max} value median (range)
Lateralization		
Right breast	15	9.4 (2.0-20.2)
Left breast	14	8.3 (2.7-32.6)
Tumor size		
T1	11	6.9 (2.0-15.3)
T2	13	10.6 (2.1-21.4)
T3	2	14.6 (9.0-20.2)
T4	3	9.4 (6.6-32.6)
Hypermetabolic axillary lymph node		
Positive	18	8.0 (1.6-41.2)*
Negative	11	
Ki-67		
<15	3	9.7 (7.7-15.1)
>15	26	8.4 (2.0-32.6)
Subtypes		
Luminal A	4	12.4 (7.7-21.4)
Luminal B	24	7.7 (2.0-32.6)
HER-2 positive	0	-
Triple negative	1	20.2
MPC percentage		
100%	15	9.4 (2.0-32.6)
80%	1	2.1
50%	1	2.9
40%	2	9.1 (7.5-10.6)
25%	2	5.9 (4.5-7.2)
20%	4	7.8 (7.1-15.3)
15%	1	15.2
10%	3	11.4 (7.7-21.4)

SUV_{max} value of axillary lymph nodes. PET: Positron emission tomography, HER-2: Human epidermal growth factor receptor 2, MPC: Micropapillary carcinoma

the CT scan. Attenuation correction was performed on the PET images using the corresponding CT images.

The standardized uptake value (SUV) is a commonly used parameter for semi-quantitative analysis of PET images and is calculated either as the ratio of tissue radioactivity concentration to the injected dose adjusted by body weight. The maximum SUV (SUV_{max}) is obtained for a 1-pixel region of interest corresponding to the maximum pixel value in the tumor.

Initial PET/CT was analyzed by 2 experienced nuclear medicine specialists who were blinded to patients' clinicopathological information and percentage of MP component. SUV_{max} was measured separately for the primary tumor and metastatic lymph nodes. If there were multiple hypermetabolic primary tumors and metastatic lymph nodes, the lesion with the highest SUV_{max} was selected.

University of Health Sciences Türkiye, Başakşehir Çam and Sakura City Hospital Ethics Committee approved this study (decision no: 2023.01.43).

Statistical Analysis

The median values and ranges for quantitative variables are presented. The Mann-Whitney U test was used to compare MP component percentage between lymph node metastasis -positive and -negative cases. SUV_{max} clinicohistopathologic features were compared using Spearman correlation matrix. The r value was interpreted as 0.00-0.19 very weak, 0.20-0.39 weak, 0.40-0.59 moderate, 0.60-0.79 high, 0.80-1.0 very high level correlation. Statistical analyzes were performed using IBM SPSS-25 software (SPSS Inc, Chicago, IL, USA). Any p-value <0.05 was considered statistically significant.

Results

Twenty-nine patients with a median age of 55 (range: 27-76) were included in this study. All patients were female. In 52% of the cases (n=15), the tumor was located in the right breast. Bone metastases were detected in 3 patients, and bone and lung metastases were detected in 1 patient. The median tumor size was 2.5 cm (range: 0.4-14). Percentages of MP components ranged between 10-100%. SUV_{max} values of the tumor ranged between 2.0-32.6 (median 9.0). The median SUV_{max} value for patients with 100% MP component (n=15) was 9.4 (range: 2-32.6); for patients with 10% MP component (n=3) was 11.4 (range: 7.7-21.4). The clinical, histopathological, and PET characteristics are listed in Table 1.

In eighteen cases, hypermetabolic axillary lymph nodes were detected on PET images, which were histopathologically verified as metastasis. In one case, because of the temporal resolution, PET could not detect lymph node metastasis whose size was 0.2 cm. The median metastatic lymph node size was 1.9 cm (range: 0.2-4.0). SUV_{max} values of metastatic lymph nodes ranged from 1.6 and 41.2 g/mL (median 8.0 g/mL).

The median Ki-67 value was 33 (range: 10-70). Four cases were luminal A, only one was triple negative, and the rest were luminal B.

At early ages, Ki-67 values and probability of hypermetabolic lymph node detection were higher (r=-0.38, p=0.04; r=-0.39, p=0.03; respectively). Between Ki-67 value and nuclear grade, axillary lymph node metastasis had a moderate positive correlation (r=0.50, p=0.01; r=0.48, p=0.01; respectively).

Luminal B and triple-negative cases were prone to axillary lymph node metastasis (p=0.03). Tumor size was positively correlated with tumor SUV_{max} value (r=0.42, p=0.02). There were no data showing that more axilla lymph node metastases were detected in cases with high tumor SUV_{max} value (r=0.26, p=0.18).

There was no significant correlation between MPC percentage and tumor SUV_{max} value (r=-0.02, p=0.91). When the cases were grouped as positive and negative lymph node metastases, no significant difference was found in the percentages of MPC (p=0.50). No significant differences were detected between MPC percentage, clinical histopathologic features, and SUV_{max} values. There was a negative correlation between age and MPC (r=-0.40; p=0.03).

Two demonstrative cases are shown in Figures 1 and 2.

Discussion

The pure form of MP breast cancer is rare (0.9-2.0%) among other types of breast carcinoma (2). In our series, which included only patients with MPC, 51.7% (n=15) of cases presented with pure invasive MPC.

One of the largest studies with pure invasive MPC showed regional lymph node metastasis in 55.2% of the cases (4). This ratio was 65.5% in our study. This difference could be attributed to the fact that PET/CT was performed in patients with a high risk of metastasis.

Many previous studies have reported that MPC tends to be in the luminal B category (5,6,7). Consistent with the literature, most of our cases (82.8%, n=24) were in the luminal B category.

Vingiani et al. (8) reported that tumor size was higher in invasive MPC patients than in invasive ductal cancer

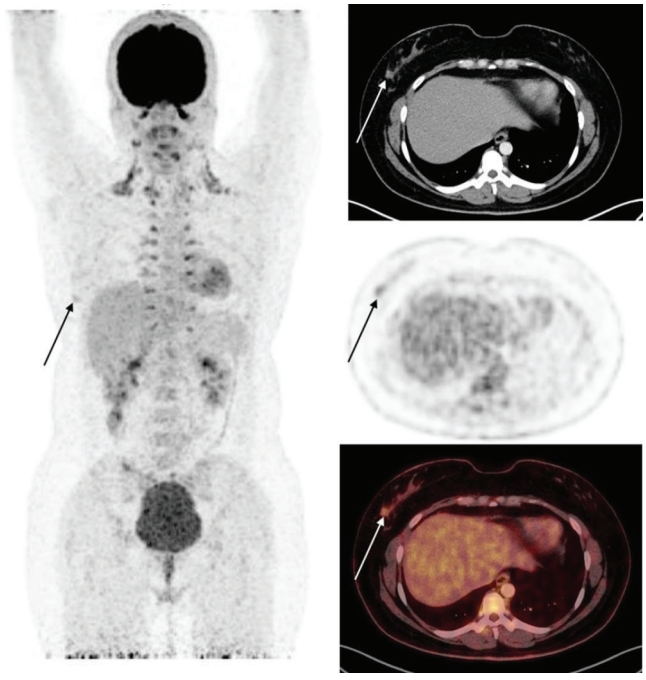

Figure 1. Twenty-seven-year-old-female, stage IIA 80% micropapillary component, 20% invasive ductal component breast cancer patient. Mildly hypermetabolic lesion located in the right breast was shown (SUV_{max}: 2.1 mg/dL; arrow)
Left column: MIP image, right column: Axial CT, PET, and fusion images.
CT: Computed tomography, MIP: Maximum intensity projection, PET: Positron emission tomography

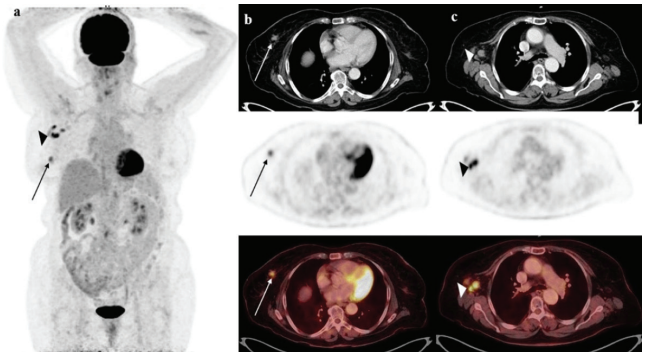

Figure 2. Seventy-six-year-old-female, stage IIIA 20% micropapillary component, 80% invasive ductal component breast cancer patient. Markedly hypermetabolic lesion located in the right breast was shown (SUV_{max}: 5.3 mg/dL; arrow). Metastatic axillary lymph nodes showed intense ^{18}F-FDG uptake (SUV_{max}: 10.1 mg/dL; arrow head).
Column a: MIP image, column b and c: Axial CT, PET, and fusion images
CT: Computed tomography, MIP: Maximum intensity projection, PET: Positron emission tomography, ^{18}F-FDG: ^{18}F-fluorodeoxyglucose

patients. Our data showed that tumor size did not significantly change with MPC percentage. In these cases, even if the MP component rate is low, close follow-up is important in terms of aggressive prognosis.

Breast cancer with MPC presents with a higher histological grade, lymphovascular invasion, and higher percentage of lymph node metastasis (2,3). Worse recurrence-free survival was attributed to a higher incidence of lymph node recurrence in the MPC group (9,10).

It is still not clear whether locoregional recurrence negatively influenced the overall survival of patients with MPC compared with other subtypes of breast cancer with similar nodal stage. Although there are some discrepancies in the literature, one recent meta-analysis demonstrated no statistically significant difference in overall survival and disease-free survival between patients with MPC and those with invasive ductal carcinoma (11). Our results showed that MPC percentage did not differ with any histopathologic features and SUV_{max} value of tumor/lymph nodes. Only younger patients had a statistically higher rate of MPC. These results led us to believe that there may not be a significant difference between the prognosis of cases with pure form and mixed components.

To our knowledge, the largest study in the literature with sixteen PET/CT imaging in MPC cases revealed that the mean SUV_{max} value of the primary tumor was 11.2, which is similar to our result 9.0 mg/dL (12). High ^{18}F-FDG uptake is an indicator of poor prognosis in breast cancer (13,14,15,16). SUV_{max} did not correlate with MPC ratio, only tumor size was positively correlated with SUV_{max} value. Kaya et al. (17) stated that there was no significant difference in demographic characteristics, tumor diameter, lymph node metastasis status, histological grade, multicentricity, local recurrence, distant metastasis, and overall survival between their groups (group 1: MPC ratio 10-75%; group 2: MPC ratio >75%). These findings made us think that MPC might not be an aggressive subtype in which to expect high ^{18}F-FDG uptake.

There is limited literature regarding the metabolic imaging features of breast carcinoma with MPC. As far as we know, this is the biggest cohort in the literature.

Study Limitations

The number of cases in our study may be considered small. It must be taken into consideration that the incidence of MPC is quite low. To increase the case number and statistical examination reliability, we included cases with under 1 cm tumor size. This could be considered a study limitation because of the partial volume effect.

Conclusion

Our results showed that the MPC percentage did not show a significant correlation with the tumor SUV_{max} value. In light of the ^{18}F-FDG PET findings, we believe that the MP

subtype ratio is not a poor prognostic factor for breast cancer. New studies are needed to evaluate whether a high SUV_{max} could indicate a poor prognosis with the same MPC percentage.

Ethics

Ethics Committee Approval: University of Health Sciences Türkiye, Başakşehir Çam and Sakura City Hospital Ethics Committee approved this study (decision no: 2023.01.43).

Informed Consent: Patient consent was obtained.

Peer-review: Externally and internally peer-reviewed.

Authorship Contributions

Surgical and Medical Practices: E.A., G.A., E.C.K.T., T.S.A., E.Ş., E.Ar., Concept: E.A., E.Ar., Design: E.A., E.Ar., Data Collection or Processing: E.A., G.A., E.C.K.T., Analysis or Interpretation: E.A., T.F.Ç., E.Ar., Literature Search: E.A., Writing: E.A.

Conflict of Interest: No conflicts of interest were declared by the authors.

Financial Disclosure: The authors declare that this study has received no financial support.

References

1. Fisher ER, Gregorio R, Redmond C, Dekker A, Fisher B. Pathologic findings from the national surgical adjuvant breast project (protocol no. 4). II. The significance of regional node histology other than sinus histiocytosis in invasive mammary cancer. Am J Clin Pathol 1976;65:21-30.
2. Akiyoshi T, Nagaie T, Tokunaga M, Tajima M, Morita M, Nakatsuka A, Taga S, Wakiyama S, Ikebe M, Nakanishi K, Hashimoto M, Toyomasu T, Nakanishi K. Invasive micropapillary carcinoma of the breast with minimal regional lymph node metastasis regardless of the huge size: report of a case. Breast Cancer 2003;10:356-360.
3. Chen H, Wu K, Wang M, Wang F, Zhang M, Zhang P. Invasive micropapillary carcinoma of the breast has a better long-term survival than invasive ductal carcinoma of the breast in spite of its aggressive clinical presentations: a comparison based on large population database and case-control analysis. Cancer Med 2017;6:2775-2786.
4. Lewis GD, Xing Y, Haque W, Patel T, Schwartz MR, Chen AC, Farach A, Hatch SS, Butler EB, Chang JC, Teh BS. The impact of molecular status on survival outcomes for invasive micropapillary carcinoma of the breast. Breast J 2019;25:1171-1176.
5. Stewart RL, Caron JE, Gulbahce EH, Factor RE, Geiersbach KB, Downs-Kelly E. HER2 immunohistochemical and fluorescence in situ hybridization discordances in invasive breast carcinoma with micropapillary features. Mod Pathol 2017;30:1561-1566.
6. Bandyopadhyay S, Bluth MH, Ali-Fehmi R. Breast Carcinoma: Updates in Molecular Profiling 2018. Clin Lab Med 2018;38:401-420.
7. Min SY, Jung E-J, Seol H, Park IA. Cancer subtypes of breast carcinoma with micropapillary and mucinous component based on immunohistochemical profile. Korean J Pathol 2011;45:125-131.
8. Vingiani A, Maisonneuve P, Dell'orto P, Farante G, Rotmensz N, Lissidini G, Del Castillo A, Renne G, Luini A, Colleoni M, Viale G, Pruneri G. The clinical relevance of micropapillary carcinoma of the breast: a case-control study. Histopathology 2013;63:217-224.
9. Yu JI, Choi DH, Huh SJ, Cho EY, Kim K, Chie EK, Ha SW, Park IA, Ahn SJ, Lee JS, Shin KH, Kwon Y, Kim YB, Suh CO, Koo JS, Kim JH, Jeong BG, Kim IA, Lee JH, Park W. Differences in Prognostic Factors and Failure Patterns Between Invasive Micropapillary Carcinoma and Carcinoma With Micropapillary Component Versus Invasive Ductal Carcinoma of the Breast: Retrospective Multicenter Case-Control Study (KROG 13-06). Clin Breast Cancer 2015;15:353-361.
10. Wu Y, Zhang N, Yang Q. The prognosis of invasive micropapillary carcinoma compared with invasive ductal carcinoma in the breast: a meta-analysis. BMC Cancer 2017;17:839.
11. Hao S, Zhao YY, Peng JJ, Ren F, Yang WT, Yu KD, Shao ZM. Invasive micropapillary carcinoma of the breast had no difference in prognosis compared with invasive ductal carcinoma: a propensity-matched analysis. Sci Rep 2019;9:286.
12. Yun SU, Choi BB, Shu KS, Kim SM, Seo YD, Lee JS, Chang ES. Imaging findings of invasive micropapillary carcinoma of the breast. J Breast Cancer 2012;15:57-64.
13. Guo X, Chen L, Lang R, Fan Y, Zhang X, Fu L. Invasive micropapillary carcinoma of the breast: association of pathologic features with lymph node metastasis. Am J Clin Pathol 2006;126:740-746.
14. Wong SI, Cheung H, Tse GM. Fine needle aspiration cytology of invasive micropapillary carcinoma of the breast. A case report. Acta Cytol 2000;44:1085-1089.
15. Gil-Rendo A, Martínez-Regueira F, Zornoza G, García-Velloso MJ, Beorlegui C, Rodriguez-Spiteri N. Association between [18F]fluorodeoxyglucose uptake and prognostic parameters in breast cancer. Br J Surg 2009;96:166-170.
16. Ueda S, Tsuda H, Asakawa H, Shigekawa T, Fukatsu K, Kondo N, Yamamoto M, Hama Y, Tamura K, Ishida J, Abe Y, Mochizuki H. Clinicopathological and prognostic relevance of uptake level using 18F-fluorodeoxyglucose positron emission tomography/computed tomography fusion imaging (18F-FDG PET/CT) in primary breast cancer. Jpn J Clin Oncol 2008;38:250-258.
17. Kaya C, Uçak R, Bozkurt E, Ömeroğlu S, Kartal K, Yazıcı P, İdiz UO, Mihmanlı M. The Impact of Micropapillary Component Ratio on the Prognosis of Patients With Invasive Micropapillary Breast Carcinoma. J Invest Surg 2020;33:31-39.

Original Article
Mol Imaging Radionucl Ther 2023;32:226-232 DOI:10.4274/mirt.galenos.2023.38258

Initial Findings on the Use of [^{225}Ac]Ac-DOTATATE Therapy as a Theranostic Application in Patients with Neuroendocrine Tumors

Nöroendokrin Tümörlü Hastalarda Bir Teranostik Uygulama Olarak [^{225}Ac]Ac-DOTATATE Tedavisi: İlk Bulgular

Emre Demirci[1], Nalan Alan Selçuk[2], Gamze Beydağı[2], Meltem Ocak[3], Türkay Toklu[2], Kaan Akçay[2], Levent Kabasakal[4]

[1]*University of Missouri, Department of Radiology, Columbia, Missouri, USA*
[2]*Yeditepe University Faculty of Medicine, Department of Nuclear Medicine, İstanbul, Türkiye*
[3]*University of Missouri, Molecular Imaging and Theranostics Center, Columbia, Missouri, USA*
[4]*İstanbul University-Cerrahpaşa, Cerrahpaşa Faculty of Medicine, Department of Nuclear Medicine, İstanbul, Türkiye*

Abstract

Objectives: This study aimed to evaluate the stability, safety, and efficacy of alpha-targeted therapy with [^{225}Ac]Ac-DOTATATE in patients with grade 1/2 metastatic neuroendocrine tumors (NETs).

Methods: This retrospective cohort included patients (n=11) with metastatic NETs from different primary sites (bronchial, pancreatic, non-pancreatic gastroenteropancreatic NETs, paraganglioma, and unknown primary site) treated with [^{225}Ac]Ac-DOTATATE with a mean activity of 8.2±0.6 MBq (range: 7.5-10.0 MBq) at our institution between November 2019 and March 2022. The *in vivo* and *in vitro* stability of [^{225}Ac]Ac-DOTATATE was calculated. The safety profile was evaluated according to the CTCAE-v5.0. Treatment efficacy was evaluated according to [^{68}Ga]Ga-DOTATATE positron emission tomography/computed tomography (PET/CT) images and the RECIST 1.1 criteria.

Results: Patients had 73% (n=8) lymph node metastases, 91% (n=10) liver metastases, 36% (n=4) lung metastases, and 73% (n=8) bone metastases. All but one patient was refractory to treatment with [^{177}Lu]Lu-DOTATATE. [^{225}Ac]Ac-DOTATATE was stable for at least 5 h *in vitro* (in saline) and 3 h *in vivo* (urine and blood samples). Grade 2 renal toxicity and grade 2 hematotoxicity were observed in one patient. No grade 3-4 toxicities were reported. According to post-treatment [^{68}Ga]Ga-DOTATATE PET/CT (n=9), 11% (n=1) had progressive disease, 44.4% (n=4) had stable disease, and 44.4% (n=4) had a partial response. The disease control rate was 89% (n=8). The median progression-free survival estimated according to Kaplan-Meier analysis was 12 months.

Conclusion: The preliminary results of this study suggest that [^{225}Ac]Ac-DOTATATE is stable, safe, and effective for treating advanced and [^{177}Lu]Lu-DOTATATE-refractory NETs. However, prospective studies are needed to determine the impact of treatment on overall survival and to uncover potential side effects.

Keywords: [^{225}Ac]Ac-DOTATATE, ^{225}Ac targeted alpha therapy, neuroendocrine tumors, peptide receptor radionuclide therapy, theranostic

Öz

Amaç: Bu çalışmanın amacı, grade 1/2 metastatik nöroendokrin tümörler (NET'ler) tanılı hastalarda [^{225}Ac]Ac-DOTATATE ile alfa hedefli tedavinin stabilitesini, güvenliğini ve etkinliğini değerlendirmektir.

Address for Correspondence: Levent Kabasakal Prof. MD, İstanbul University-Cerrahpaşa, Cerrahpaşa Faculty of Medicine, Department of Nuclear Medicine, İstanbul, Türkiye
Phone: +90 532 366 79 08 **E-mail:** lkabasakal@tsnm.org ORCID ID: orcid.org/0000-0002-4050-1972
Received: 06.05.2023 **Accepted:** 03.07.2023

Yöntem: Primer tanıları bulunan (bronşiyal, pankreatik, non-pankreatik gastroenteropankreatik NET'ler, paraganglioma ve primeri bilinmeyen) metastatik NET olan ve Kasım 2019 ile Mart 2022 arasında kliniğimizde tedavi edilen hastalar retrospektif olarak incelendi. Hastalara ortalama 8,2±0,6 MBq (aralık: 7,5-10,0 MBq) aktivite ile [225Ac]Ac-DOTATATE tedavisi uygulandı (n=11). [225Ac]Ac-DOTATATE'in *in vivo* ve *in vitro* stabilitesi hesaplandı. Güvenlik profili CTCAE-v5.0'a göre değerlendirildi. Tedavi etkinliği [68Ga]Ga-DOTATATE pozitron emisyon tomografisi/bilgisayarlı tomografi (PET/BT) görüntüleri ve RECIST 1.1 kriterlerine göre değerlendirildi.

Bulgular: Hastaların %73'ünde (n=8) lenf nodu metastazı, %91'inde (n=10) karaciğer metastazı, %36'sında (n=4) akciğer metastazı ve %73'ünde (n=8) kemik metastazı bulunuyordu. Hastaların bir tanesi hariç tümü, [177Lu]Lu-DOTATATE ile tedaviye dirençliydi. [225Ac]Ac-DOTATATE, in vitro (salin içinde) en az 5 saat ve in vivo (idrar ve kan örnekleri) en az 3 saat boyunca stabil kaldı. Bir hastada grade 2 böbrek toksisitesi ve grade 2 hematotoksisite gözlendi. Grade 3-4 toksisite izlenmedi. Tedavi sonrası [68Ga]Ga-DOTATATE PET/BT'ye (n=9) göre, %11'inde (n=1) progresyon, %44,4'ünde (n=4) stabil hastalık ve %44,4'ünde (n=4) kısmi yanıt gözlendi. Hastalık kontrol oranı %89 (n=8) idi. Kaplan-Meier'e göre tahmini medyan progresyonsuz sağkalım 12 aydı.

Sonuç: Bu çalışmanın ön sonuçları, [225Ac]Ac-DOTATATE'in ileri evre ve [177Lu]Lu-DOTATATE tedavisine dirençli NET'lerin tedavisinde stabil, güvenli ve etkili olduğunu ortaya koymaktadır. Bununla birlikte, tedavinin genel sağkalım üzerindeki etkisini belirlemek ve olası yan etkileri ortaya çıkarmak için prospektif çalışmalara ihtiyaç vardır.

Anahtar kelimeler: [225Ac]Ac-DOTATATE, 225Ac hedeflenmiş alfa tedavi, nöroendokrin tümörler, peptid reseptör radyonüklit tedavi, teranostik

Introduction

For neuroendocrine tumors (NETs), early-stage surgery remains the only treatment option for complete cure (1,2). Because of the clinically silent course of the disease at onset, approximately 50% of patients are not detected until the advanced stage (1,3). However, in the metastatic stage, there are few effective treatment options, including long-acting somatostatin analogs, sunitinib, a multicentric tyrosine kinase inhibitor, and everolimus, an mTOR inhibitor (4,5,6,7).

Peptide receptor radionuclide therapy (PRRT) is a molecularly targeted treatment approach in which radiolabeled peptides with high affinity for somatostatin receptors are administered systemically. In the last 20 years, it has been successfully used for metastatic and unresectable NETs (8). Among the numerous alternatives, Lutetium-177 [177Lu] has emerged as the preferred radionuclide due to its favorable toxicity profile. After 20 years of experience, there is a growing body of evidence supporting the efficacy of PRRT (9,10). NETTER-1, a phase 3 study with [177Lu]Lu-DOTATATE, is the most important study to date. Patients treated with [177Lu]Lu-DOTATATE had an estimated median progression-free survival (PFS) of 40 months in the NETTER-1 trial, whereas patients treated with 60 mg octreotide-LAR had a PFS of only 8.4 months (11). However, despite high somatostatin receptor expression, a substantial number of patients develop resistance to targeted beta therapy after intensive treatment with [177Lu]Lu-DOTATATE (9,10,11,12).

In PRRT, targeted alpha therapy (TAT) has proven to be a viable alternative to targeted beta therapy. The use of alpha emitters for cancer therapy has two advantages over the use of beta emitters in PRRT. Because alpha particles have a short range of only a few cell diameters (0.1 mm), they can selectively ablate cancer cells while sparing healthy tissue (13,14). In addition, the higher linear energy transfer (LET) compared with typical beta emitters causes complicated DNA double-strand and DNA cluster breaks that eventually lead to cell death. Despite these advantages, there are limited data on the efficacy of TAT for treating NETs (15). In this study, we aimed to evaluate the safety and efficacy of treatment with [225Ac]Ac-DOTATATE in patients who did not respond to all other available treatments, including [177Lu]Lu-DOTATATE.

Materials and Methods

Patients

From November 2019 to March 2022, patients (n=11) treated with [225Ac]Ac-DOTATATE were enrolled in this retrospective study. All patients had a histopathological diagnosis of NETs and tumor progression prior to alpha therapy. Institutional inclusion criteria for PRRT were white blood cell (WBC) count >2000, platelet (PLT) >75000, red blood cell >3,000,000, hemoglobin (Hb) >6 mmol/L, serum creatinine level <2 mg/dL, and Karnofsky performance status >50. All patients had high uptake in all metastatic lesions on [68Ga]Ga-DOTATATE positron emission tomography/computed tomography (PET/CT), which was higher than uptake in the liver. Radiological evidence of disease progression according to [68Ga]Ga-DOTATATE PET/CT and the Response Evaluation Criteria in Solid Tumors (RECIST) criteria 1.1 to determine tumor progression at baseline.

This study was approved by the Yeditepe University Clinical Research Ethics Committee (decision no: 1633, date: 06.07.2022).

Preparation of [225Ac]Ac-DOTATATE

[225Ac]$AcCl_3$ and [225Ac]$Ac(NO_3)_3$ were provided by ORNL, Oak Ridge USA IPPE JSC, Obninsk, Russia. In-house radiolabeling was performed in a hot cell using [225Ac]

(1 MBq/14 nmol ligand) with 0.1 M Tris buffer and 20% ascorbic acid. Radiolabeling was performed at 95 °C for 25 minutes (min). After cooling the reaction vessel to room temperature, 0.5-1.0 mL of sterile DTPA solution (3 mg mL-1 DTPA in saline) was added to the reaction vessel. This preparation was sterile filtered (0.22 µM) under aseptic conditions and then made up to 5-6 mL with sterile saline. The integrity of the filter was checked using a bubble point test. The radiochemical yield was determined by instant thin-layer chromatography (ITLC) on silica gel with 0.05 M citric acid as the solvent. The radiochemical yield was determined by measuring the activity of 218-keV-γ emission of [221Fr] on the upper and lower parts of the strip using a Captus 3000 well-type gamma counter (Capintec Inc, NJ, USA) after 45 min of labeling. The measured radiochemical yields of [225Ac]Ac-DOTATATE were over 97% after 45 min of labeling.

Stability of [225Ac]Ac-DOTATATE

One MBq of [225Ac]Ac-DOTATATE was incubated in saline at 37 °C for up to 5 h (n=3). At specific time points, the incubation solution sample was injected into reversed-phase high-pressure liquid chromatography (RP-HPLC) to investigate the *in vitro* stability of [225Ac]Ac-DOTATATE. The HPLC fractions were measured in the gamma counter at least 20 h after collection. The measured counts of the fractions with 440 keV γ-emission of [213Bi] were plotted in agreement with their tube counts obtained from RP-HPLC analysis. In the first 3 patients, in vivo stability was checked using blood samples obtained 0-10 min after injection of [225Ac]Ac-DOTATATE and urine samples obtained up to 3 h after injection. Blood samples collected from patients were precipitated with acetonitrile (1:1) and shaken. The precipitate was separated by centrifugation (5 min at 14,680 rpm). For analysis by RP-HPLC, the supernatant was diluted with double-distilled water (1:1) and then injected into RP-HPLC. The collected urine samples from patients were diluted with bi-distilled water, filtered, and immediately analyzed using RP-HPLC. The amount of [225Ac]Ac-DOTATATE excreted was calculated using standard samples prepared at the time of injection. The excretion rate was calculated using the injected amount of [225Ac]Ac-DOTATATE activity. The measured counts from the fractions were plotted according to their tube number from the analysis of RP-HPLC.

Treatment

All therapies were performed on an inpatient basis. To protect the kidneys, patients were administered a total of 500-1,000 mL of a 2.5% arginine and 2.5% lysine amino acid solution for 4 h starting 30 min before the injection of [225Ac]Ac-DOTATATE. Thirty min before therapy, 8 mg of ondansetron was administered to prevent nausea. [225Ac]Ac-DOTATATE was administered over 5 min with slow injection. The amount of injected activity was 100-120 kBq/kg, as adapted from Kratochwil et al. (16). Whole-body images were obtained 4 h after administration of therapies with gamma energies of [221Fr] and [213Bi]. Patients were observed every 60 min for 5 h to record vital signs such as blood pressure, fever, and pulse rate. In addition, patients were monitored for any complaints of pain, vomiting, and nausea for 24 h according to the standard institutional protocol for all inpatient treatments.

Response Evaluation, Survival, and Toxicity

Response to [225Ac]Ac-DOTATATE treatment was assessed by [68Ga]Ga-DOTATATE PET/contrast enhanced (ce) CT performed within 4 weeks before and 12-16 weeks after treatment. Treatment efficacy was assessed according to images from [68Ga]Ga-DOTATATE PET/CT and RECIST 1.1 criteria (17) using ceCT images from PET/CT. [68Ga]Ga-DOTATATE PET/CT was repeated 12-18 weeks after each treatment cycle and until clinical progression or death. PFS was calculated from the date of first administration of [225Ac]Ac-DOTATATE. The disease control rate was calculated as the percentage of patients who had a complete, partial, or stable response to treatment. Adverse events were documented three months after each cycle of [225Ac]Ac-DOTATATE treatment according to the Common Terminology Criteria for Adverse Events version 5 (18).

Statistical Analysis

The PFS calculation was based on Kaplan-Meier curves, whereas numerical outcome comparisons were performed with the Wilcoxon rank sum test using SPSS version 21 (IBM Corp., Armonk, NY, USA). Comparative assessment of response evaluation statistics was calculated using the chi-square test. A p-value of less than 0.05 was considered significant. Numerical results are presented as mean ± standard deviation.

Results

Patient Population

Within the patient cohort (n=11), 3 (27%) patients had pancreatic cancer NET, 1 (9%) had pulmonary NET, 3 (27%) had non-pancreatic gastroenteropancreatic-NET, 3 (27%) had NET with unknown primary tumor, and 1 had paraganglioma (Table 1). Ki-67 indexes were available only in 7 patients, and World Health Organization (WHO) classification was evaluated in 9 patients. Patients were previously treated with a median of 7.5 cycles of [177Lu]Lu-DOTATATE and multiple lines of chemotherapy. One patient received 3 cycles, 5 patients received 2 cycles, 6 patients

received 1 cycle of [225Ac]Ac-DOTATATE treatment. A total of 17 cycles of [225Ac]Ac-DOTATATE were administered. Patients received a median of one cycle of [225Ac]Ac-DOTATATE (range: 1-3) with mean activity of 8.2±0.6 MBq (range: 7.5-10.0 MBq). The mean time between different doses of [225Ac]Ac-DOTATATE treatment was 125±76 days. Some patients could not take up the treatment on time because of 225Ac supply shortages and travel restrictions during the coronavirus disease-2019 pandemic. At baseline, all patients showed tumor progression according to [68Ga]Ga-DOTATATE PET/CT. According to the WHO classification of NETs, 2 (20%) patients had grade 1, 7 (70%) patients had grade 2 (Ki-67 index range: 10-18%), 1 (10%) patient had unknown grade, and 1 patient had paraganglioma. The locations of metastases and previous therapies are listed in Table 1.

Table 1. Patient characteristic

Patients		
Age		
Mean (years)		59.0±11.9
Range		43-79
Gender	Male/female	8/3
Previous therapies		
Long acting somatostatin analogues		10 (91%)
Chemotherapy		11 (100%)
Radioembolizetion/chemoembolization to liver		6 (55%)
MIBG treatment		2 (18%)
[177Lu]Lu-DOTATATE		10 (91%)
WHO grade		
Grade 1 NET		2 (20%)
Grade 2 NET		7 (70%)
Unknown		1 (10%)
Location of primary tumor		
Lung		1 (9%)
Pancreas		3 (27%)
Non-pancreatic GEP-NET		3 (27%)
Paraganglioma		1 (9%)
Unknown primary		3 (27%)
Sites of metastases		
Lymph nodes		8 (73%)
Liver		10 (91%)
Lung		4 (36%)
Bone		8 (73%)

MIBG: Meta-iodobenzylguanidine, NET: Neuroendocrine tumor, GEP-NET: Gastroenteropancreatic neuroendocrine tumor

Stability of [225Ac]Ac-DOTATATE

RP-HPLC analyzes of the saline incubation samples showed a single radioactivity peak corresponding to [225Ac]Ac-DOTATATE. However, a slight decrease in the in vitro stability of [225Ac]Ac-DOTATATE was observed in the RP-HPLC analysis after 5 h of incubation in saline. A chromatogram of one of the samples RP-HPLC is shown in Figure 1. A slight decrease in the in vitro stability of [225Ac]Ac-DOTATATE was also observed in ITLC analysis, but the radiochemical yield was still higher than 96% after 5 h of incubation in saline solution.

RP-HPLC analyzes of the blood and urine samples showed a single radioactivity peak corresponding to [225Ac]Ac-DOTATATE, but a slight decrease in stability *in vivo* was also observed in the blood and urine samples after injection (Figure 2). The mean excretion rate of [225Ac]Ac-DOTATATE

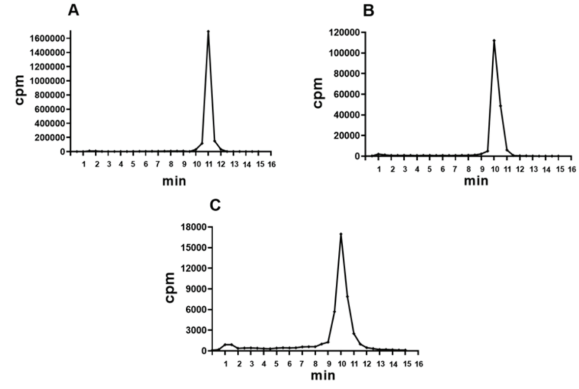

Figure 1. Reversed-phase high-pressure liquid chromatography profiles of 1 MBq [225Ac]Ac-DOTATATE from reaction vessel **A)** after incubation in saline, **B)** after 3 hours, **C)** after 5 hours

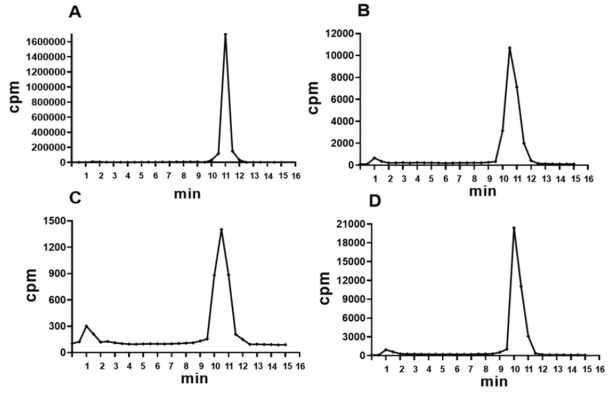

Figure 2. Reversed-phase high-pressure liquid chromatography profiles of [225Ac]Ac-DOTATATE A) from the reaction vial B) in blood after injection of 10 MBq of radioligand in a patient after 0-10 min C) in urine after injection of 10 MBq of radioligand in a patient after 1 h D) in urine after injection of 10 MBq of radioligand in a patient after 3 h

from the kidneys 24 h after injection was 56±9.7% (range, 40-65%) in 9 patients.

Toxicity and Side Effects

[225Ac]Ac-DOTATATE administration was well tolerated. We did not observe any acute side effects, such as nausea or vomiting, during the injection. No change in blood pressure, fever, or pulse rate was not observed for 5 h in our patient group.

Before [225Ac]Ac-DOTATATE therapy, 4 of 11 patients had grade 1/2 hematologic toxicity and 2 of 11 patients had grade 1/2 nephrotoxicity. Toxicity analysis could be performed in 8 patients. Nephrotoxicity and grade 2 hematotoxicity were observed in one patient after 3 cycles of treatment with [225Ac]Ac-DOTATATE. The patient had received multistep chemotherapy and 13 cycles of [177Lu]Lu-DOTATATE before treatment with [225Ac]Ac-DOTATATE. The nephrotoxicity rate was 12.5% (n=1), and the hematotoxicity rate was 12.5% (n=1). A transient decrease in lymphocyte count was observed in all patients ($p<0.05$). The patients' WBC counts decreased but were still within the normal range ($p=0.02$). The mean values of WBC, PLTs, Hb, and hematocrit are shown in Table 2. One patient with peritoneal carcinomatosis required 7 days of hospitalization, intravenous fluid administration, and steroid treatment to control symptoms. None of the patients required discontinuation of treatment with [225Ac]Ac-DOTATATE because of adverse reactions.

The mean parotid maximum standardized uptake value (SUV_{max}) values were 2.98±0.96 before therapy (baseline), 2.07±0.93 after the first cycle (n=9), 2.48±0.59 (n=6) after two cycles of [225Ac]Ac-DOTATATE treatments. There was no statistically significant change in parotid gland uptake from baseline ($p=0.93$ after the first cycle and $p=0.73$ after the second cycle). Patients did not complain of xerostomia (Table 2).

Efficacy and Survival

According to [68Ga]Ga-DOTATATE PET/CT images three months after treatment (n=9), 44% of patients (n=4) showed a partial response (PR), 44% (n=4) showed stable disease (SD), and 11% (n=1) showed progressive disease. The disease control rate of treatment was 89% (n=8). In all patients (n=9), [68Ga]Ga-DOTATATE PET images and ceCT images interpreted according to the RECIST criteria yielded the same results ($p>0.05$). The median PFS estimated by Kaplan-Meier analysis was 12 months from the time of first treatment. The patient survival times are shown in Figure 3. PET images of the selected patients before and after treatment are shown in Figure 4.

Table 2. Hematological, renal, liver parameters and [68Ga]Ga-DOTATATE uptake of parotid glands before and after the last cycle of [225Ac]Ac-DOTATATE treatment*

	Before treatment	After treatment
White blood cells (cnt/µL)	6.94±4.09	4.09±2.34
Platelets (cnt/µL)	226.00±109.12	237.00±86.26
Hemoglobin (g/dL)	11.13±1.57	10.40±1.58
Hematocrit (%)	32.93±4.52	30.88±4.79
Creatinine (mg/dL)	0.86±0.44	1.16±0.41
Total bilirubin (mg/dL)	0.54±0.48	0.58±0.51
Albumin (g/dL)	3.90±0.72	3.84±0.74
Parotid gland (SUV_{max})	2.98±0.96	2.07±0.93

*$p>0.05$
SUV_{max}: Maximum standardized uptake value

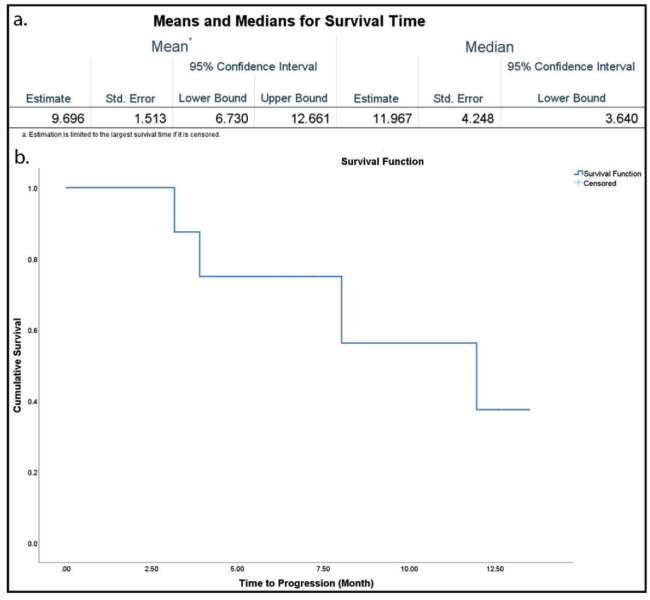

Figure 3. Kaplan Meier progression- free survival estimates **(a)** and patient progression-free survival curves **(b)**

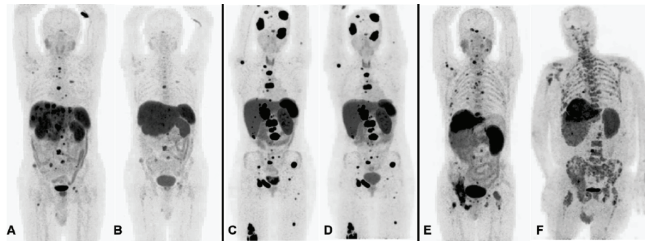

Figure 4. [68Ga]Ga-DOTATATE PET maximum intensity projection pre- and post-treatment images of selected patients with **A, B)** partial response, **C, D)** stable disease, **E, F)** progression
PET: Positron emission tomography

Discussion

There are limited treatment options for patients with metastatic NETs, especially after the failure of [^{177}Lu]Lu-DOTATATE therapy. Therefore, there is an urgent need for additional therapies for metastatic NETs. Targeted alpha therapies have several advantages over beta therapies, at least in theory. The most important finding is that high LET radiation has the ability to break DNA double strands and DNA clusters. In addition, alpha radiation isotopes are less dependent on tumor oxygen levels than beta radiation isotopes. These biological advantages may explain why TAT is superior to targeted beta therapy (15,19,20). Although [^{213}Bi] is only used in a limited number of patients, [^{225}Ac] is one of the leading alternatives to beta therapy (13,21). However, PRRT with [^{225}Ac]Ac-DOTATATE has not been clearly demonstrated in clinical trials. This study demonstrates the potential efficacy of [^{225}Ac]Ac-DOTATATE as an end-of-line treatment in patients who have experienced progression on therapy with [^{177}Lu]Lu-DOTATATE. According to our study, therapy with [^{225}Ac]Ac-DOTATATE may be a useful treatment option for patients with advanced metastatic NETs, increasing survival rates and providing disease management with few adverse effects. The disease control rate of 88.9% in our study is similar to the rates reported by Ballal et al. (22). In their report of 32 patients with NET treated with three cycles of [^{225}Ac]Ac-DOTATATE (100 kBq/kg), PR was 37.5% and SD was 62.5%. In a recent study of the same group, the disease control rate was 79.8% (23).

In our patient cohort, [^{225}Ac]Ac-DOTATATE therapy was generally well tolerated. Although patients were treated with intensive [^{177}Lu]Lu-DOTATATE and chemotherapy, none showed grade 3 hematotoxicity or nephrotoxicity. Grade 2 nephrotoxicity and hematotoxicity were observed in one patient after 3 cycles of treatment with [^{225}Ac]Ac-DOTATATE, who had previously been treated with intensive chemotherapy including cisplatin + etoposide and 13 cycles of [^{177}Lu]Lu-DOTATATE. Similar safety results have also been reported by Ballal et al. (22,23). In our study, none of the patients complained of xerostomia. SUV_{max} values before and after treatment with [^{225}Ac]Ac-DOTATATE showed no significant change. Tafreshi et al. (24) reported very low absorbed radiation doses in salivary glands in mice. Xerostomia does not appear to be a clinical problem in these patients. One patient who had not been previously treated with [^{177}Lu]Lu-DOTATATE required hospitalization 5 days after treatment with [^{225}Ac]Ac-DOTATATE for an ileus finding. The patient had received steroids to control her symptoms. This patient had an ileal NET and peritoneal metastasis. Strosberg et al. (25) reported 5 cases of bowel obstruction after treatment with [^{177}Lu]Lu-DOTATATE. All patients in this report also had ileal NETs and peritoneal metastases.

[^{225}Ac]Ac-DOTATATE had slightly decreased *in vitro* stability in saline, but the radiochemical yield was still higher than 96% after 5 h of incubation in saline. Thus far, DOTA has been shown to be the most suitable chelator for [^{225}Ac], but other studies have reported the loss of [^{225}Ac] from DOTA *in vitro* and *in vivo* (26,27). Because of rapid plasma clearance and volume distribution, stability in blood could be verified only 10 min after injection, and [^{225}Ac]Ac-DOTATATE remained stable in blood for up to 10 min. In urine samples, [^{225}Ac]Ac-DOTATATE remained stable for up to 3 h. More than half of the injected [^{225}Ac]Ac-DOTATATE was excreted by the kidneys 24 h after injection. However, organ dosimetry could not be performed because of the poor quality of the [^{225}Ac] whole-body images obtained 4 h after injection. It was not possible to delineate the organs although the kidneys had the highest physiological uptake of [^{225}Ac]Ac-DOTATATE (21).

This study has all the limitations of a retrospective design. The number of patients in this preliminary report is limited, and the results should be evaluated with caution. However, we believe that the results presented in this study are promising and that treatment with [^{225}Ac]Ac-DOTATATE appears to be a safe treatment option for patients who do not respond to treatment with [^{177}Lu]Lu-DOTATATE.

Conclusion

In conclusion, the results of the current study, together with the concordant literature, demonstrate that [^{225}Ac]Ac-DOTATATE is the treatment of choice and has a significant effect in patients with SSTR-2-positive metastatic NETs with high somatostatin receptor expression. Therapy with [^{225}Ac]Ac-DOTATATE did not cause significant toxicity in our heavily pretreated patient cohort. The preliminary results are very promising, and a multicenter randomized control trial of [^{225}Ac]Ac-DOTATATE therapy in NET patients is required.

Ethics

Ethics Committee Approval: This study was approved by the Yeditepe University Clinical Research Ethics Committee (decision no: 1633, date: 06.07.2022).

Informed Consent: Not applicable (retrospective study).

Peer-review: Externally peer-reviewed.

Authorship Contributions

Surgical and Medical Practices: E.D., N.A.S., G.B., M.O., K.A., Concept: E.D., N.A.S., L.K., Design: L.K., Data Collection or Processing: E.D., N.A.S., G.B., T.T., K.A., Analysis or Interpretation: E.D., N.A.S., T.T., Literature Search: E.D., N.A.S., L.K., Writing: E.D., N.A.S., T.T., L.K.

Conflict of Interest: No conflict of interest was declared by the authors.

Financial Disclosure: The authors declared that this study has received no financial support.

References

1. Yao JC, Hassan M, Phan A, Dagohoy C, Leary C, Mares JE, Abdalla EK, Fleming JB, Vauthey JN, Rashid A, Evans DB. One hundred years after "carcinoid": epidemiology of and prognostic factors for neuroendocrine tumors in 35,825 cases in the United States. J Clin Oncol 2008;26:3063-3072.
2. Norton JA, Warren RS, Kelly MG, Zuraek MB, Jensen RT. Aggressive surgery for metastatic liver neuroendocrine tumors. Surgery 2003;134:1057-1063; discussion 1063-1065.
3. Modlin IM, Lye KD, Kidd M. A 5-decade analysis of 13,715 carcinoid tumors. Cancer 2003;97:934-959.
4. Pape UF, Perren A, Niederle B, Gross D, Gress T, Costa F, Arnold R, Denecke T, Plöckinger U, Salazar R, Grossman A; Barcelona Consensus Conference participants. ENETS Consensus Guidelines for the management of patients with neuroendocrine neoplasms from the jejuno-ileum and the appendix including goblet cell carcinomas. Neuroendocrinology 2012;95:135-156.
5. Rinke A, Müller HH, Schade-Brittinger C, Klose KJ, Barth P, Wied M, Mayer C, Aminossadati B, Pape UF, Bläker M, Harder J, Arnold C, Gress T, Arnold R; PROMID Study Group. Placebo-controlled, double-blind, prospective, randomized study on the effect of octreotide LAR in the control of tumor growth in patients with metastatic neuroendocrine midgut tumors: a report from the PROMID Study Group. J Clin Oncol 2009;27:4656-4663.
6. Yao JC, Shah MH, Ito T, Bohas CL, Wolin EM, Van Cutsem E, Hobday TJ, Okusaka T, Capdevila J, de Vries EG, Tomassetti P, Pavel ME, Hoosen S, Haas T, Lincy J, Lebwohl D, *Öberg* K; RAD001 in Advanced Neuroendocrine Tumors, Third Trial (RADIANT-3) Study Group. Everolimus for advanced pancreatic neuroendocrine tumors. N Engl J Med 2011;364:514-523.
7. Raymond E, Dahan L, Raoul JL, Bang YJ, Borbath I, Lombard-Bohas C, Valle J, Metrakos P, Smith D, Vinik A, Chen JS, Hörsch D, Hammel P, Wiedenmann B, Van Cutsem E, Patyna S, Lu DR, Blanckmeister C, Chao R, Ruszniewski P. Sunitinib malate for the treatment of pancreatic neuroendocrine tumors. N Engl J Med 2011;364:501-513.
8. Baum RP, Kulkarni HR, Carreras C. Peptides and receptors in image-guided therapy: theranostics for neuroendocrine neoplasms. Semin Nucl Med 2012;42:190-207.
9. Sabet A, Biersack HJ, Ezziddin S. Advances in Peptide Receptor Radionuclide Therapy. Semin Nucl Med 2016;46:40-46.
10. Demirci E, Kabasakal L, Toklu T, Ocak M, Şahin OE, Alan-Selcuk N, Araman A. 177Lu-DOTATATE therapy in patients with neuroendocrine tumours including high-grade (WHO G3) neuroendocrine tumours: response to treatment and long-term survival update. Nucl Med Commun 2018;39:789-796.
11. Strosberg J, El-Haddad G, Wolin E, Hendifar A, Yao J, Chasen B, Mittra E, Kunz PL, Kulke MH, Jacene H, Bushnell D, O'Dorisio TM, Baum RP, Kulkarni HR, Caplin M, Lebtahi R, Hobday T, Delpassand E, Van Cutsem E, Benson A, Srirajaskanthan R, Pavel M, Mora J, Berlin J, Grande E, Reed N, Seregni E, *Öberg* K, Lopera Sierra M, Santoro P, Thevenet T, Erion JL, Ruszniewski P, Kwekkeboom D, Krenning E; NETTER-1 Trial Investigators. Phase 3 Trial of ^{177}Lu-Dotatate for Midgut Neuroendocrine Tumors. N Engl J Med 2017;376:125-135.
12. Ambrosini V, Kunikowska J, Baudin E, Bodei L, Bouvier C, Capdevila J, Cremonesi M, de Herder WW, Dromain C, Falconi M, Fani M, Fanti S, Hicks RJ, Kabasakal L, Kaltsas G, Lewington V, Minozzi S, Cinquini M, *Öberg* K, Oyen WJG, O'Toole D, Pavel M, Ruszniewski P, Scarpa A, Strosberg J, Sundin A, Taïeb D, Virgolini I, Wild D, Herrmann K, Yao J. Consensus on molecular imaging and theranostics in neuroendocrine neoplasms. Eur J Cancer 2021;146:56-73.
13. Morgenstern A, Apostolidis C, Kratochwil C, Sathekge M, Krolicki L, Bruchertseifer F. An Overview of Targeted Alpha Therapy with ^{225}Actinium and ^{213}Bismuth. Curr Radiopharm 2018;11:200-208.
14. Targeted Alpha Therapy Working Group; Parker C, Lewington V, Shore N, Kratochwil C, Levy M, Lindén O, Noordzij W, Park J, Saad F. Targeted Alpha Therapy, an Emerging Class of Cancer Agents: A Review. JAMA Oncol 2018;4:1765-1772.
15. Koh TT, Bezak E, Chan D, Cehic G. Targeted alpha-particle therapy in neuroendocrine neoplasms: A systematic review. World J Nucl Med 2021;20:329-335.
16. Kratochwil C, Bruchertseifer F, Giesel FL, Weis M, Verburg FA, Mottaghy F, Kopka K, Apostolidis C, Haberkorn U, Morgenstern A. 225Ac-PSMA-617 for PSMA-Targeted α-Radiation Therapy of Metastatic Castration-Resistant Prostate Cancer. J Nucl Med 2016;57:1941-1944.
17. Eisenhauer EA, Therasse P, Bogaerts J, Schwartz LH, Sargent D, Ford R, Dancey J, Arbuck S, Gwyther S, Mooney M, Rubinstein L, Shankar L, Dodd L, Kaplan R, Lacombe D, Verweij J. New response evaluation criteria in solid tumours: revised RECIST guideline (version 1.1). Eur J Cancer 2009;45:228-247.
18. Common Terminology Criteria for Adverse Events (CTCAE) v5.0. In: 2017. https://ctep.cancer.gov/protocoldevelopment/electronic_applications/docs/ctcae_v5_quick_reference_5x7.pdf
19. Marcu L, Bezak E, Allen BJ. Global comparison of targeted alpha vs targeted beta therapy for cancer: In vitro, in vivo and clinical trials. Crit Rev Oncol Hematol 2018;123:7-20.
20. Makvandi M, Dupis E, Engle JW, Nortier FM, Fassbender ME, Simon S, Birnbaum ER, Atcher RW, John KD, Rixe O, Norenberg JP. Alpha-Emitters and Targeted Alpha Therapy in Oncology: from Basic Science to Clinical Investigations. Target Oncol 2018;13:189-203.
21. Ocak M, Toklu T, Demirci E, Selçuk N, Kabasakal L. Post-therapy imaging of ^{225}Ac-DOTATATE treatment in a patient with recurrent neuroendocrine tumor. Eur J Nucl Med Mol Imaging 2020;47:2711-2712.
22. Ballal S, Yadav MP, Bal C, Sahoo RK, Tripathi M. Broadening horizons with ^{225}Ac-DOTATATE targeted alpha therapy for gastroenteropancreatic neuroendocrine tumour patients stable or refractory to ^{177}Lu-DOTATATE PRRT: first clinical experience on the efficacy and safety. Eur J Nucl Med Mol Imaging 2020;47:934-946.
23. Ballal S, Yadav MP, Tripathi M, Sahoo RK, Bal C. Survival Outcomes in Metastatic Gastroenteropancreatic Neuroendocrine Tumor Patients receiving Concomitant ^{225}Ac-DOTATATE Targeted Alpha Therapy and Capecitabine: A Real-world Scenario Management Based Long-term Outcome Study. J Nucl Med 2022:jnumed.122.264043.
24. Tafreshi NK, Pandya DN, Tichacek CJ, Budzevich MM, Wang Z, Reff JN, Engelman RW, Boulware DC, Chiappori AA, Strosberg JR, Ji H, Wadas TJ, El-Haddad G, Morse DL. (2021) Preclinical evaluation of [225Ac]Ac-DOTATATE for treatment of lung neuroendocrine neoplasms. European Journal of Nuclear Medicine and Molecular Imaging 48:3408-3421
25. Strosberg JR, Al-Toubah T, Pellè E, Smith J, Haider M, Hutchinson T, Fleming JB, El-Haddad G. Risk of Bowel Obstruction in Patients with Mesenteric or Peritoneal Disease Receiving Peptide Receptor Radionuclide Therapy. J Nucl Med 2021;62:69-72.
26. McDevitt MR, Ma D, Simon J, Frank RK, Scheinberg DA. Design and synthesis of 225Ac radioimmunopharmaceuticals. Appl Radiat Isot 2002;57:841-847.
27. Deal KA, Davis IA, Mirzadeh S, Kennel SJ, Brechbiel MW. Improved in vivo stability of actinium-225 macrocyclic complexes. J Med Chem 1999;42:2988-2992.

Interesting Image
Mol Imaging Radionucl Ther 2023;32:233-236 DOI:10.4274/mirt.galenos.2023.92499

Long-term Intense ^{18}F-FDG Uptake by the Homeostatic Matrix-associated Inflammatory Response May Mimic Malignancy Recurrence

Homeostatik Matriks ile İlişkili Enflamatuvar Yanıtta Gözlenen Uzun Dönem Yoğun ^{18}F-FDG Tutulumu, Malignite Nüksünü Taklit Edebilir

Fatih Tamer[1], Bülent Yazıcı[2], Aylin Oral[2], Ayşegül Akgün[2]

[1]Niğde Ömer Halisdemir University Training and Research Hospital, Department of Nuclear Medicine, Niğde, Türkiye
[2]Ege University Faculty of Medicine, Department of Nuclear Medicine, İzmir, Türkiye

Abstract

A 70-year-old man underwent right upper lobectomy for lung adenocarcinoma. During the operation, hemostatic matrix (as known Floseal®) was used to prevent pulmonary laceration-associated bleeding. When ^{18}F-fluorodeoxyglucose (FDG) positron emission tomography/computed tomography was performed for staging after surgery, intense ^{18}F-FDG uptake was observed in the cicatricial fibrotic tissue in the operation area, and no significant change was observed in that area during the 4-year follow-up. Because it remained stable for several years without treatment, this finding was thought to be due to a foreign body reaction caused by the homeostatic material.

Keywords: Homeostatic matrix, false positivity, positron emission tomography, lung cancer

Öz

Yetmiş yaşında bir erkek hastaya, akciğer adenokarsinomu nedeniyle sağ üst lobektomi uygulandı. Operasyon sırasında, pulmoner laserasyona bağlı kanamayı önlemek için hemostatik matriks (Floseal®) kullanıldı. Operasyon sonrasında evreleme amacıyla ^{18}F-florodeoksiglukoz (FDG) pozitron emisyon tomografisi/bilgisayarlı tomografi yapıldığında girişim bölgesindeki skatrisyel fibrotik dokuda yoğun ^{18}F-FDG tutulumu saptandı ve 4 yıllık takibinde bu bulguda anlamlı bir değişiklik gözlenmedi. Sürecin bir bölümünde tedavi uygulanmayan ve stabil olarak izlenen bulguların homeostatik materyalin neden olduğu yabancı cisim reaksiyonundan kaynaklandığı düşünüldü.

Anahtar kelimeler: Homeostatik matriks, yanlış pozitiflik, pozitron emisyon tomografisi, akciğer kanseri

Address for Correspondence: Fatih Tamer MD, Niğde Ömer Halisdemir University Training and Research Hospital, Department of Nuclear Medicine, Niğde, Türkiye
Phone: +90 388 232 22 20 **E-mail:** drfatihtamer@gmail.com ORCID ID: orcid.org/0000-0002-5656-9955
Received: 12.01.2023 **Accepted:** 04.02.2023

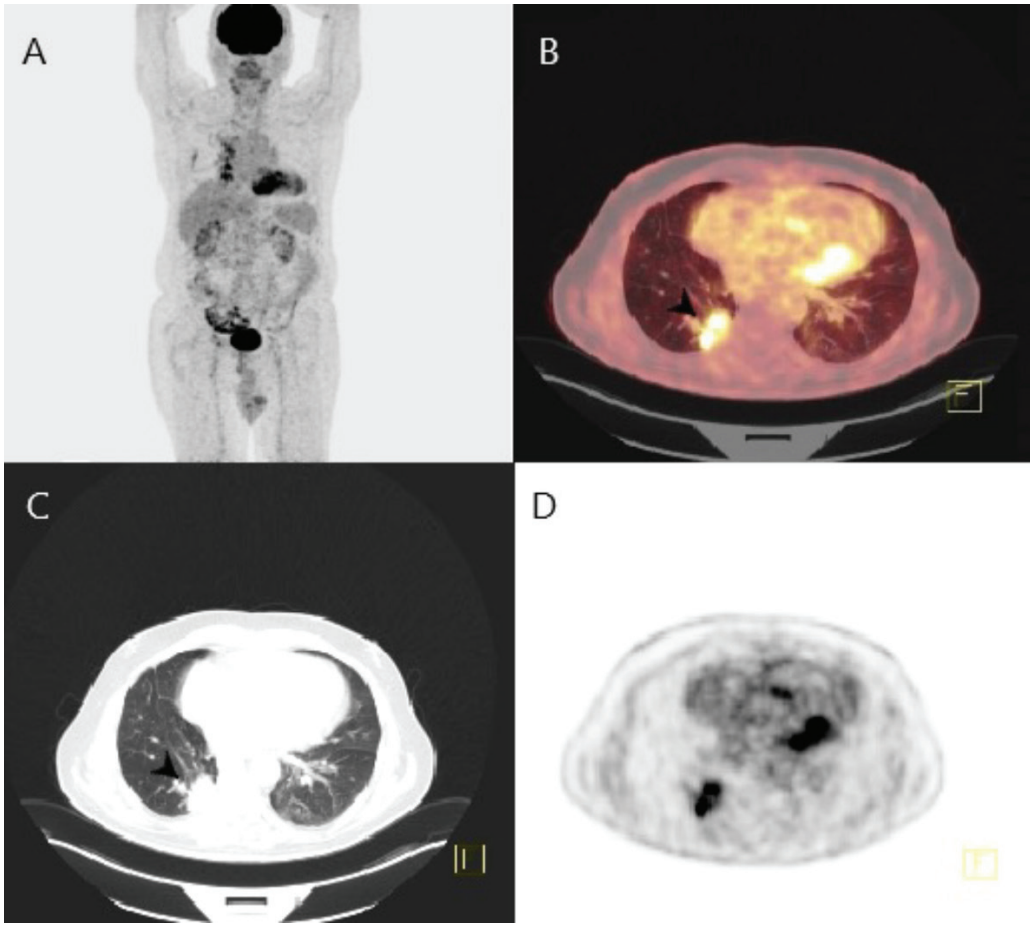

Figure 1. In lung cancer, ^{18}F-fluorodeoxyglucose positron emission tomography/computed tomography (^{18}F-FDG PET/CT) imaging plays an important role in the diagnosis, staging, treatment response, and detection of regional recurrence. In addition to malignancies, many infectious-inflammatory processes and benign neoplasms in the lungs can show increased ^{18}F-FDG uptake and mimic malignancies (1). Whole body ^{18}F-FDG PET/CT was performed for staging in a 70-year-old man with lung adenocarcinoma who had undergone right upper lobectomy. Images were acquired 60 min after intravenous administration of 8.7 mCi of ^{18}F-FDG. Axial PET, CT, fused PET/CT, and maximum intensity projection (MIP) images revealed intense ^{18}F-FDG uptake in nodular consolidations, as seen in cicatricial fibrotic tissue at the resection site (images A-D; black arrow). Because the patient did not receive radiotherapy and did not have clinical and laboratory signs of infection the findings were initially thought to be due to local recurrence, and the patient was followed up with a chemotherapy regimen.

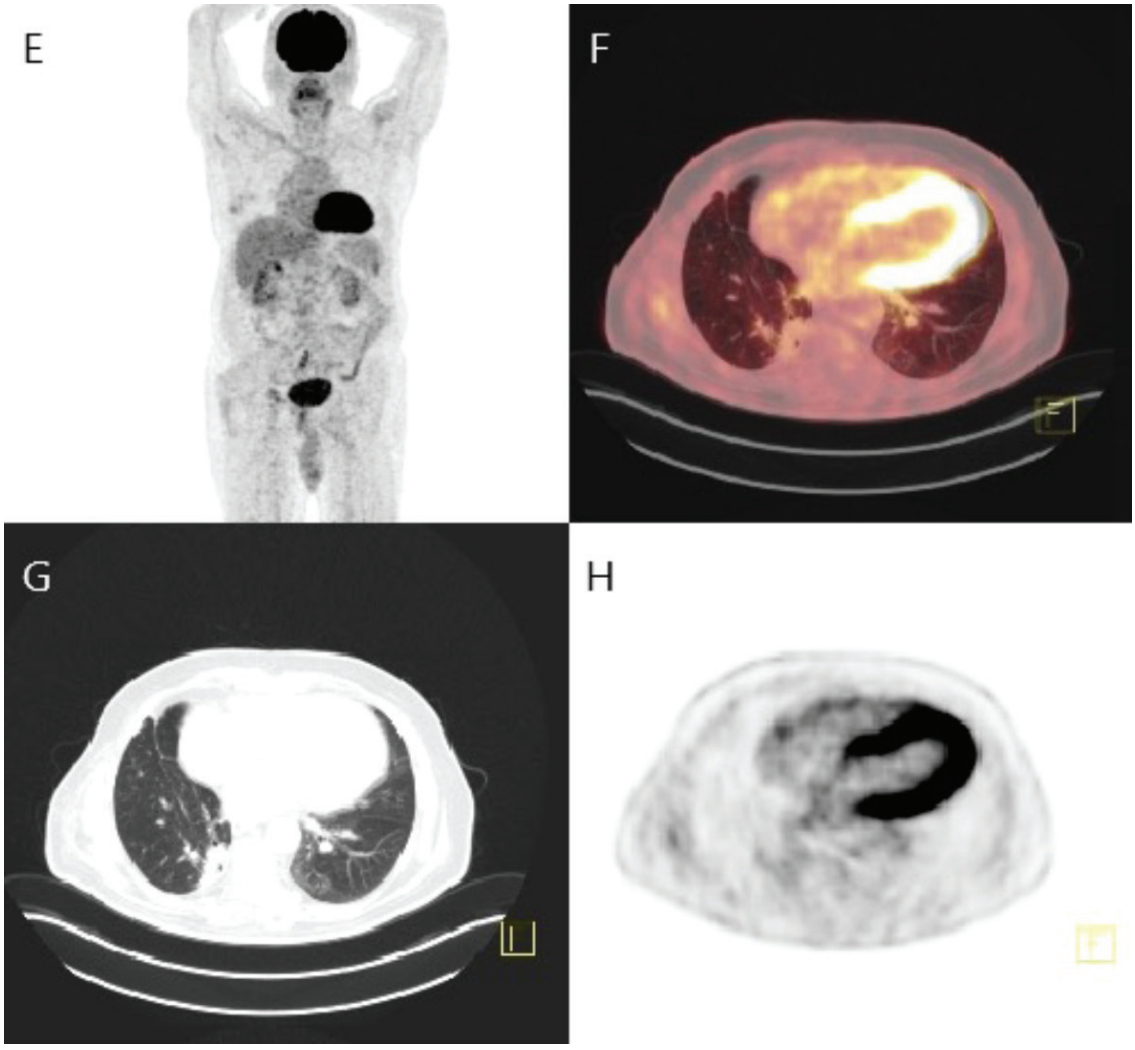

Figure 2. In serial follow-up ^{18}F-FDG PET/CT scans for 4 years, no significant morphological and metabolic changes were observed, although chemotherapy was not applied in the last 2 years of this period. In addition, on axial MIP, PET, CT, fuzed PET/CT, and MIP images taken after the 4-year period, ^{18}F-FDG uptake in this field had regressed (images E-H). When the surgical reports were examined in detail, it was observed that hemostatic material was used to prevent bleeding due to pulmonary laceration during the operation. Hemostatic agents are used in most surgical procedures to control bleeding complications and prevent secondary morbidity and mortality. The homeostatic matrix (as known Floseal®) is one of the agents used for this purpose and consists of the bovine gelatin matrix and human thrombin component (2). It is known that foreign body reaction and inflammatory response to materials used in surgery practice may cause increased ^{18}F-FDG uptake, which may continue for a long time in follow-up (3,4). In some publications related to thoracic surgery practice, false-positive ^{18}F-FDG avidity has been defined as mimicking malignancy such as suture granuloma (5,6,7). And another paper also demonstrated the development of false-positive ^{18}F-FDG-avid pulmonary nodules secondary to polysaccharide-based hemostatic agent use, mimicking metastasis (8). We considered that this increased ^{18}F-FDG uptake is associated with a chronic inflammatory response to the homeostatic material, which is used to control bleeding due to pulmonary laceration during pulmonary lobectomy surgery. Although not in this study, defining false positive findings using pathological sampling when necessary is important in preventing unnecessary treatments and additional investigations. We emphasize that in interpreting the pathological findings on PET/CT images, patients' information, including surgical reports, should be examined in detail, and the surgical materials used and the places where it was applied should be considered.

Ethics

Informed Consent: Informed consent was obtained from the patient.

Peer-review: Externally peer-reviewed.

Authorship Contributions

Surgical and Medical Practices: F.T., B.Y., A.O., A.A., Concept: F.T., B.Y., A.O., A.A., Design: F.T., B.Y., A.O., A.A., Data Collection or Processing: F.T., A.A., Analysis or Interpretation: F.T., B.Y., A.O., A.A., Literature Search: F.T., A.A., Writing: F.T., A.A.

Conflict of Interest: No conflicts of interest were declared by the authors.

Financial Disclosure: The authors declare that this study has received no financial support.

References

1. Shim SS, Lee KS, Kim BT, Choi JY, Chung MJ, Lee EJ. Focal parenchymal lung lesions showing a potential of false-positive and false-negative interpretations on integrated PET/CT. AJR Am J Roentgenol 2006;186:639-648.
2. Echave M, Oyagüez I, Casado MA. Use of Floseal®, a human gelatine-thrombin matrix sealant, in surgery: a systematic review. BMC Surg 2014;14:111.
3. Yilmaz M, Sevinc A, Aybasti N, Celen Z, Zincirkeser S. FDG uptake in abdominal mesh implant on FDG PET/CT. Clin Nucl Med 2008;33:351-352.
4. Chism CB, Somcio R, Chasen BA, Ravizzini GC. Increased 18F-FDG Uptake Associated With Gastric Banding Surgical Mesh on PET/CT. Clin Nucl Med 2016;41:410-411.
5. Ruiz-Zafra J, Rodríguez-Fernández A, Sánchez-Palencia A, Cueto A. Surgical adhesive may cause false positives in integrated positron emission tomography and computed tomography after lung cancer resection. Eur J Cardiothorac Surg 2013;43:1251-1253.
6. Keyzer C, Corbusier F, Kyratzi E, Sokolow Y, Gevenois PA, Goldman S. FDG uptake at the bronchial stump after curative lobectomy for non-small cell lung cancer. Eur J Nucl Med Mol Imaging 2016;43:832-838.
7. Okazaki M, Sano Y, Mori Y, Sakao N, Yukumi S, Shigematsu H, Izutani H. Two cases of granuloma mimicking local recurrence after pulmonary segmentectomy. J Cardiothorac Surg 2020;15:7.
8. Oksuzoglu K, Ones T, Bozkurtlar E, Bostanci K, Tureli D. FDG-Avid Lung Nodule Formation by the Use of Hemostatic Powder: A Potential Cause of False-Positive FDG PET/CT. Clin Nucl Med 2021;46:e94-e96.

Interesting Image
Mol Imaging Radionucl Ther 2023;32:237-238 DOI:10.4274/mirt.galenos.2023.07830

Pneumonia with Intense ^{68}Ga-FAPI Uptake Mimicking Metastasis on ^{68}Ga-FAPI PET/CT in a Patient with Rectal Cancer

Rektum Kanseri Tanılı Olguda Pnömonide ^{68}Ga-FAPI PET/BT'de Metastazı Taklit Eden Yoğun ^{68}Ga-FAPI Tutulumu

Özge Erol Fenercioğlu[1], Ediz Beyhan[1], Nilay Şengül Samancı[2], Tevfik Fikret Çermik[1], Nurhan Ergül[1]

[1]University of Health Sciences Türkiye, İstanbul Training and Research Hospital, Clinic of Nuclear Medicine, İstanbul, Türkiye
[2]University of Health Sciences Türkiye, İstanbul Training and Research Hospital, Clinic of Medical Oncology, İstanbul, Türkiye

Abstract

A 70-year-old man with newly diagnosed rectum adenocarcinoma was referred to ^{18}F-fluorodeoxyglucose positron emission tomography/computed tomography (^{18}F-FDG PET/CT) for staging, and ^{68}Ga-fibroblast activation protein inhibitor (FAPI)-04 PET/CT for ongoing trial. Both ^{18}F-FDG PET/CT and ^{68}Ga-FAPI-04 PET/CT showed intense uptake in the primary rectal tumor, and also in nodular areas in the right lung. Due to intense ^{68}Ga-FAPI-04 and ^{18}F-FDG uptake, the lung lesions were considered as metastases. However the lesions were reduced in size on CT after 20 days antibiotherapy and diagnosed as pneumonia.

Keywords: ^{68}Ga-FAPI, PET/CT, CT, pneumonia

Öz

Yeni rektum kanseri tanılı 70 yaşında erkek hasta evreleme amacıyla ^{18}F-florodeoksiglukoz pozitron emisyon tomografisi/bilgisayarlı tomografiye (^{18}F-FDG PET/BT) ve devam eden çalışma için ^{68}Ga-fibroblast aktivasyon proteini inhibitörü (FAPI)-04 PET/BT'ye gönderildi. Hem ^{18}F-FDG PET/BT hem de ^{68}Ga-FAPI-04 PET/BT'de primer rektal tümörde ve sağ akciğerde yer alan nodüler alanlarda yoğun radyofarmasötik tutulumu izlendi. Bu yüzden akciğer lezyonları metastaz olarak değerlendirildi. Antibiyoterapiden 20 gün sonra lezyonlar BT'de rezolüsyona uğradı ve tanı pnömoni olarak doğrulandı.

Anahtar kelimeler: ^{68}Ga-FAPI, PET/BT, BT, pnömoni

Address for Correspondence: Özge Erol Fenercioğlu MD, University of Health Sciences Türkiye, İstanbul Training and Research Hospital, Clinic of Nuclear Medicine, İstanbul, Türkiye
Phone: +90 212 459 60 00 **E-mail:** ozge.erol@yahoo.com ORCID ID: orcid.org/0000-0002-5359-9964
Received: 18.07.2022 **Accepted:** 04.02.2023

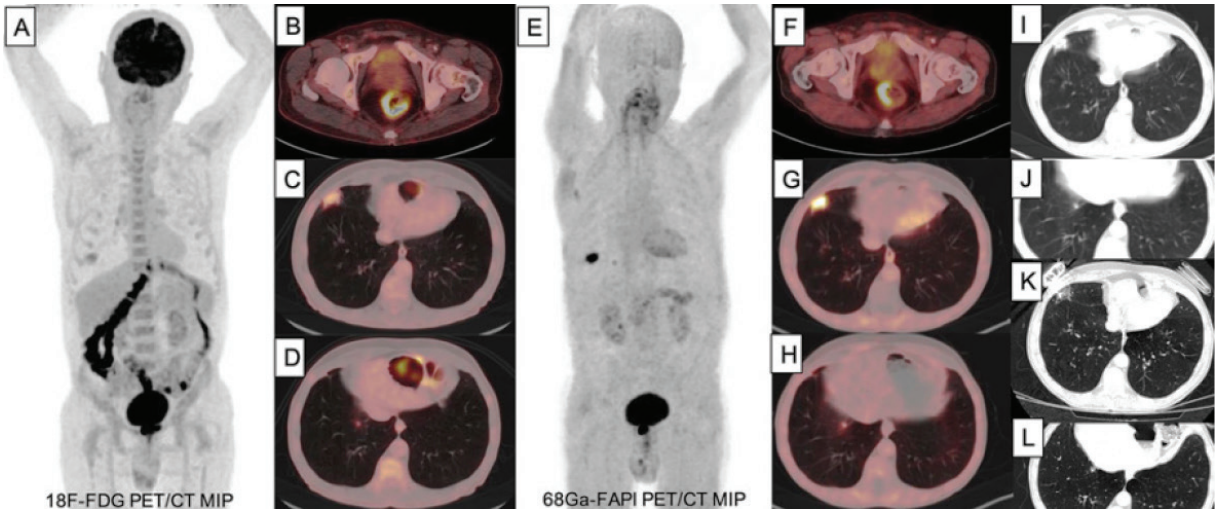

Figure 1. A 70 year-old man presented with changes in defecation habits and hematochezia. Colonoscopy showed tumor in the rectum and biopsy was confirmed as adenocarcinoma. Patient was referred to ^{18}F-fluorodeoxyglucose positron emission tomography/computed tomography (^{18}F-FDG PET/CT) for staging. After 6 hours of fasting 222 MBq ^{18}F-FDG was injected intravenously. PET/CT was performed after 1 hour of distribution time. The primary tumor in the rectum with intense ^{18}F-FDG uptake [maximum standardized uptake value (SUV_{max}): 17.9] along with diffuse colonic uptake (SUV_{max}: 28.9) was observed on PET/CT **(A, B)**. In addition, there was increased ^{18}F-FDG uptake at consolidation area and subsantimetric nodulary lesion in the anterior segment of the right upper lung (SUV_{max}: 4.5) **(C, D)**. ^{68}Ga-fibroblast activation protein inhibitor (FAPI)-04 PET/CT was performed after 155.4 MBq ^{68}Ga-FAPI-04 injection after 1 hour in the same week with ^{18}F-FDG PET/CT, for an ongoing clinical trial. ^{68}Ga-FAPI-04 PET/CT showed intense uptake at the rectal tumor (SUV_{max}: 14.8) without inflammatory colonic uptake and at lung lesions (SUV_{max}: 12.2) **(E, F, G, H, I, J)**. Lung lesions with both increased ^{18}F-FDG and ^{68}Ga-FAPI-04 uptake were suspected for lung metastases of rectum cancer. After antibiotherapy for 20 days, it was seen that the lesions were resolved and reduced in size on thorax CT and diagnosed as pneumonia **(K, L)**. ^{68}Ga-FAPI PET/CT has been the subject of increasing research in recent years with its success in tumor imaging (1). Fibroblast activation protein is over-expressed on cancer-associated fibroblasts and also in tissue remodeling sites associated with fibrosis, cirrhosis, atherosclerosis, cardiac injury, and pneumonia (2,3,4,5,6). Although ^{68}Ga-FAPI PET/CT is reported to be superior to ^{18}F-FDG PET/CT for detecting metastasis and primary tumor due to high tumor/background ratio and absence of inflammatory colonic ^{18}F-FDG uptake as in our case, the reasons for false positives should be also kept in mind (7,8).

Ethics

Informed Consent: Written informed consent was obtained from the participant.

Peer-review: Externally and internally peer-reviewed.

Authorship Contributions

Surgical and Medical Practices: Ö.E.F., E.B., N.Ş.S., T.F.Ç., N.E., Concept: Ö.E.F., E.B., N.Ş.S., T.F.Ç., N.E., Design: Ö.E.F., E.B., N.Ş.S., T.F.Ç., N.E., Data Collection or Processing: Ö.E.F., E.B., N.Ş.S., T.F.Ç., N.E., Analysis or Interpretation: Ö.E.F., E.B., N.Ş.S., T.F.Ç., N.E., Literature Search: Ö.E.F., E.B., N.Ş.S., T.F.Ç., N.E., Writing: Ö.E.F., E.B., N.Ş.S., T.F.Ç., N.E.

Conflict of Interest: No conflicts of interest were declared by the authors.

Financial Disclosure: The authors declare that this study has received no financial support.

References

1. Kratochwil C, Flechsig P, Lindner T, Abderrahim L, Altmann A, Mier W, Adeberg S, Rathke H, Röhrich M, Winter H, Plinkert PK, Marme F, Lang M, Kauczor HU, Jäger D, Debus J, Haberkorn U, Giesel FL. 68Ga-FAPI PET/CT: Tracer Uptake in 28 Different Kinds of Cancer. J Nucl Med 2019;60:801-805.
2. Dendl K, Koerber SA, Kratochwil C, Cardinale J, Finck R, Dabir M, Novruzov E, Watabe T, Kramer V, Choyke PL, Haberkorn U, Giesel FL. FAP and FAPI-PET/CT in Malignant and Non-Malignant Diseases: A Perfect Symbiosis? Cancers (Basel) 2021;13:4946.
3. Erol Fenercioğlu Ö, Beyhan E, Ergül N, Arslan E, Çermik TF. 18F-FDG PET/CT and 68Ga-FAPI-4 PET/CT Findings of Bilateral Knee Osteoarthritis in a Patient With Uveal Malignant Melanoma. Clin Nucl Med 2022;47:e144-e146.
4. Tang W, Wu J, Yang S, Wang Q, Chen Y. Organizing Pneumonia With Intense 68Ga-FAPI Uptake Mimicking Lung Cancer on 68Ga-FAPI PET/CT. Clin Nucl Med 2022;47:223-225.
5. Liu H, Wang Y, Zhang W, Cai L, Chen Y. Elevated 68Ga-FAPI Activity in Splenic Hemangioma and Pneumonia. Clin Nucl Med 2021;46:694-696.
6. Zheng S, Lin R, Chen S, Zheng J, Lin Z, Zhang Y, Xue Q, Chen Y, Zhang J, Lin K, You X, Yao S, Miao W. Characterization of the benign lesions with increased 68Ga-FAPI-04 uptake in PET/CT. Ann Nucl Med 2021;35:1312-1320.
7. Pang Y, Zhao L, Luo Z, Hao B, Wu H, Lin Q, Sun L, Chen H. Comparison of 68Ga-FAPI and 18F-FDG Uptake in Gastric, Duodenal, and Colorectal Cancers. Radiology 2021;298:393-402.
8. Çermik TF, Ergül N, Yılmaz B, Mercanoğlu G. Tumor Imaging With 68Ga-DOTA-FAPI-04 PET/CT: Comparison With 18F-FDG PET/CT in 22 Different Cancer Types. Clin Nucl Med 2022;47:e333-e339.

Interesting Image
Mol Imaging Radionucl Ther 2023;32:239-243 DOI:10.4274/mirt.galenos.2023.55798

PET/CT Imaging of Inflammatory Myofibroblastic Tumor of the Thigh

Uylukta Enflamatuvar Miyofibroblastik Tümörün PET/BT ile Görüntülenmesi

Refia Yükseltürk, Aslıhan Yıldırım, Nedim C.M. Gülaldı

University of Health Sciences Türkiye, Ankara City Hospital, Clinic of Nuclear Medicine, Ankara, Türkiye

Abstract

A 13-year-old male patient presented with right leg pain and walking difficulty. Contrast-enhanced magnetic resonance imaging showed a soft-tissue lesion between muscle groups in the anterior half of the right thigh. The excisional biopsy result ended in an inflammatory myofibroblastic tumor (IMT). The ^{18}F-fluorodeoxyglucose positron emission tomography/computed tomography (PET/CT) scan showed hypermetabolism in the multifocal soft tissue lesion and also confirmed that no other distant foci were present. A three-phase Tc-99m-methylene diphosphonate study of the region showed heterogeneously increased vascularity within the region. We described an unusual case of IMT in a pediatric patient and the importance of PET/CT scanning to delineate the lesion.

Keywords: Inflammatory myofibroblastic tumor, bone scan, magnetic resonance imaging, ^{18}F-FDG PET/CT

Öz

On üç yaşında erkek hasta sağ bacakta ağrı ve yürümede zorluk ile başvurdu. Kontrastlı manyetik rezonans görüntülemede sağ uyluk ön grup kasları arasında yumuşak doku lezyonu saptandı. Yapılan eksizyonel biyopsi sonucu enflamatuvar miyofibroblastik tümör (İMT) olarak sonuçlandı. ^{18}F-florodeoksiglukoz (^{18}F-FDG) pozitron emisyon tomografisi/bilgisayarlı tomografi (PET/BT) çalışmasında uzak metastaz olmaksızın yumuşak doku lezyonunda multifokal hipermetabolizma izlendi. Üç fazlı Tc-99m-metilendifosfonat çalışmasında, bölgede heterojen artmış vaskülarite izlendi. Biz pediyatrik bir hastada sıra dışı bir İMT olgusu ve lezyonu tanımlamada ^{18}F-FDG PET/BT'nin önemini anlattık.

Anahtar kelimeler: Enflamatuvar miyofibroblastik tümör, kemik sintigrafisi, manyetik rezonans görüntüleme, ^{18}F-FDG PET/BT

Address for Correspondence: Refia Yükseltürk MD, University of Health Sciences Türkiye, Ankara City Hospital, Clinic of Nuclear Medicine, Ankara, Türkiye
Phone: +90 552 868 64 45 **E-mail:** refiaturk@gmail.com ORCID ID: orcid.org/0000-0002-4515-9707
Received: 14.10.2022 **Accepted:** 04.02.2023

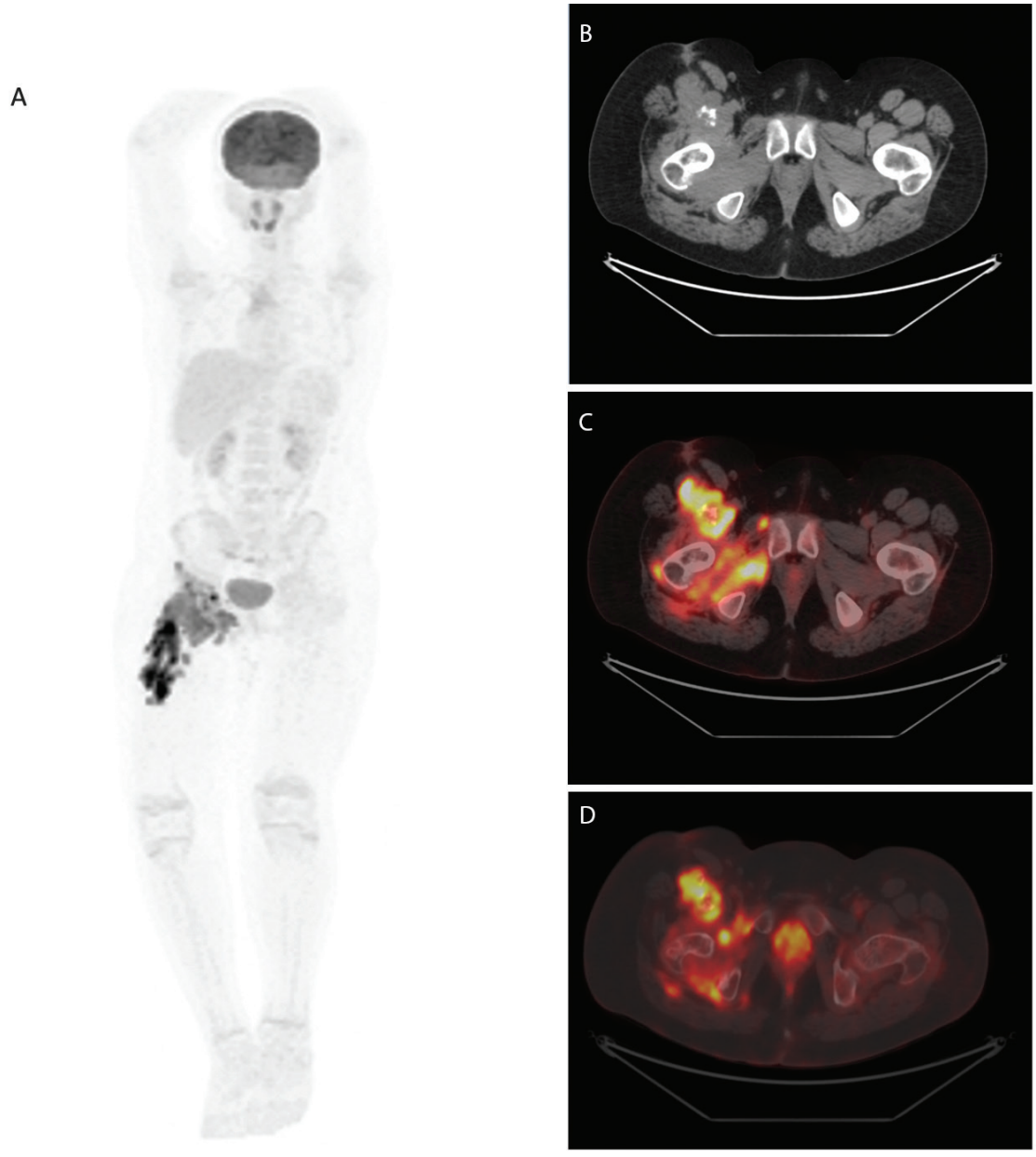

Figure 1. A 13-year-old male patient with an inflammatory myofibroblastic tumor of the right thigh. Maximum intensity projection ^{18}F-fluorodeoxyglucose (^{18}F-FDG) positron emission tomography (PET) image **(A)**, axial computed tomography (CT) **(B)**, and axially fused ^{18}F-FDG PET image **(C)** showed increased ^{18}F-FDG uptake [maximum standardized uptake value (SUV_{max}): 28.60] in the multifocal mass with heterogeneous calcifications through the anterior part of the femur. Bone structure findings in the axial CT bone window **(D)** are within normal limits.

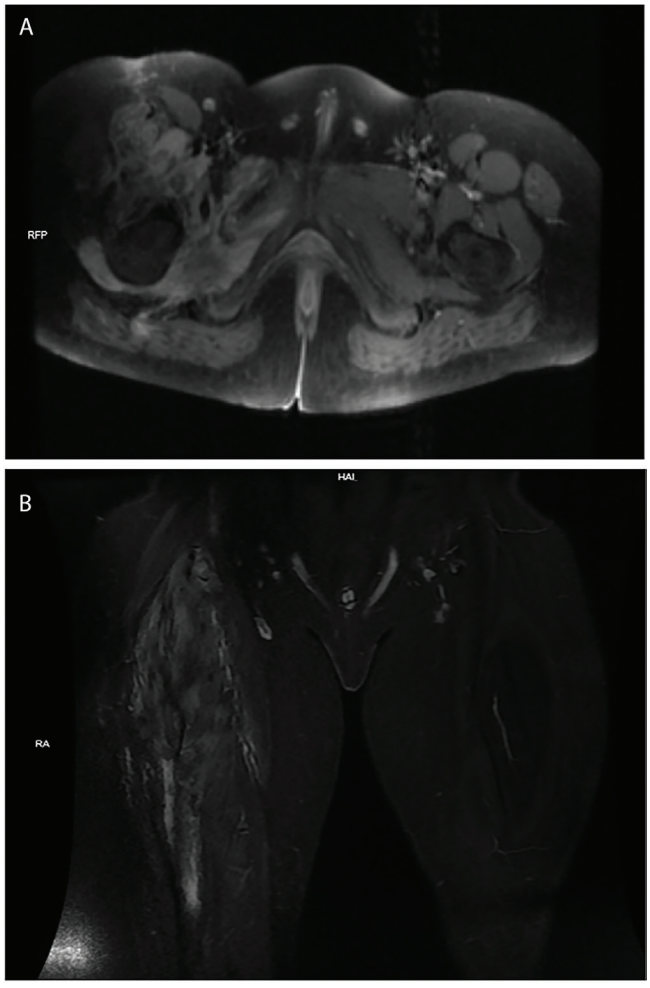

Figure 2. Axial T1-weighted magnetic resonance imaging (MRI) image **(A)** shows an inhomogeneous hypointense mass in the anterior right thigh. The lesion shows an inhomogeneous hyperintense signal on MRI coronal STIR images **(B)**.

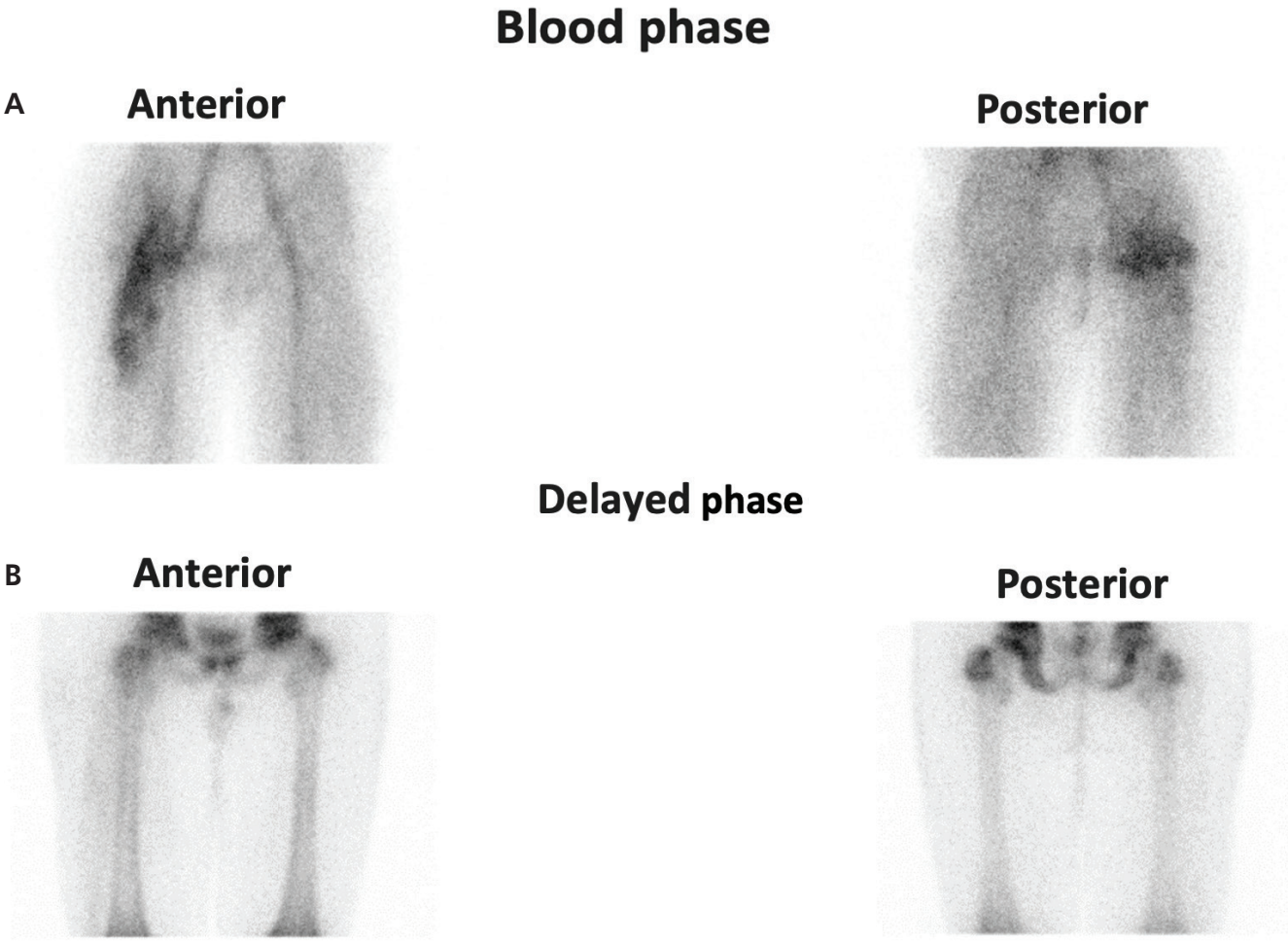

Figure 3. Triphasic Tc-99m-methylene diphosphonate bone scan of the upper part of lower extremities demonstrated heterogeneously increased vascularity and perfusion of the right proximal half of the femur and the right acetabular region **(A)**. A minimal reduction in activity accumulation was observed in the right hip epiphyseal line compared to the contralateral side. However, there was no increased activity accumulation at nearby pelvic bones and the right femur on delayed images **(B)**. An excisional biopsy was performed for the mass measuring 35x25x10 mm with a soft consistency, creamy white and brown in places. The diagnosis of inflammatory myofibroblastic tumors (IMT) was confirmed histopathologically with a large number of lymphoplasmacytic cells, destroying muscle structure. No significant mitotic activity and necrosis were observed. Ki-67 positive tumor cells accounted for approximately 5-6%. IMT is a neoplasm of intermediate biological potential with partial local invasion and recurrence, but they rarely metastasize (1). IMTs can occur in various systems including central nervous system, internal organs, and extremities (2,3). Older children can sometimes be affected by this disease, and it has also been reported as a very rare condition (4). The specific pathogenesis of IMT is unknown, while various infections, inflammatory and autoimmune diseases, and trauma are among the most commonly suspected etiologies of the disease. The clinical presentation of IMT varies depending on the anatomical location and it sometimes mimics lymphoma (5). Patients generally present with general inflammatory symptoms such as fever, weight loss, pain, and malaise which may also raise suspicion of lymphoproliferative malignancies. CT and MR are the most commonly used imaging modalities when evaluating of IMTs. In most cases, a histological examination must be carried out for a reliable diagnosis. ^{18}F-FDG PET/CT scan is useful for detection of primary tumor, local recurrence, treatment response, and distant metastasis (6,7). Histopathologically our case showed low mitotic activity and indicates the uptake of ^{18}F-FDG, mainly related to high glucose utilization of the inflammatory cells contained in the tumor. PET/CT helps in delineating the tumor burden to guide surgery and thus prevents the damage to normal anatomical structures. The best treatment strategy for this type of tumor is complete resection if achieved surgically. Due to the high ^{18}F-FDG avidity of the tumor, the PET/CT scan is also useful to identify local recurrence after resection of the primary tumor.

Ethics

Informed Consent: The patient consent was obtained.

Peer-review: Externally peer-reviewed.

Authorship Contributions

Concept: N.C.M.G., Design: N.C.M.G., Data Collection or Processing: R.Y., A.Y., Analysis or Interpretation: R.Y., N.C.M.G., Literature Search: R.Y., A.Y., Writing: R.Y., N.C.M.G.

Conflict of Interest: No conflicts of interest were declared by the authors.

Financial Disclosure: The authors declare that this study has received no financial support.

References

1. Savvidou OD, Sakellariou VI, Papakonstantinou O, Skarpidi E, Papagelopoulos PJ. Inflammatory myofibroblastic tumor of the thigh: presentation of a rare case and review of the literature. Case Rep Orthop 2015;2015:814241.
2. Raad RA, Haddad L, Jabbour T, El-Rassi Z. Inflammatory Myofibroblastic Tumor of the Liver Mimicking Metastasis on 18F-FDG PET/CT. Clin Nucl Med 2021;46:47-48.
3. Liu H, Yang X, Fan D, Lv T, Chen Y. Mesenteric Inflammatory Myofibroblastic Tumor on 68Ga-FAPI PET/CT. Clin Nucl Med 2021;46:1026-1027.
4. Dalton BG, Thomas PG, Sharp NE, Manalang MA, Fisher JE, Moir CR, St Peter SD, Iqbal CW. Inflammatory myofibroblastic tumors in children. J Pediatr Surg 2016;51:541-544.
5. Ma C, Lu J, Chen G, Wang W, Su F, Su X. Inflammatory myofibroblastic tumor mimicking lymphoma on 18F-FDG PET/CT. Report of a case and review of the literature. Hell J Nucl Med 2018;21:77-80.
6. Dong A, Wang Y, Dong H, Gong J, Cheng C, Zuo C, Lu J. Inflammatory myofibroblastic tumor: FDG PET/CT findings with pathologic correlation. Clin Nucl Med 2014;39:113-121.
7. Jiang JY, Comsa M, Wong VCK, Mansberg R. Steroid responsive inflammatory myofibroblastic tumor of the lung evaluated by FDG PET/CT imaging. Radiol Case Rep 2022;17:907-910.

Interesting Image
Mol Imaging Radionucl Ther 2023;32:244-246 DOI:10.4274/mirt.galenos.2023.03780

Isolated Castrate-resistant Prostate Cancer Metastasis to Both Adrenal Glands Detected on ^{68}Ga PSMA PET/CT

^{68}Ga PSMA PET/BT'de Her İki Adrenal Bezde Saptanan İzole Kastrasyon Dirençli Prostat Kanseri Metastazı

Osman Kanatsız[1], Filiz Özülker[1], Tamer Aydın[2], Tamer Özülker[1]

[1]University of Health Sciences Türkiye, İstanbul Prof. Dr. Cemil Taşcıoğlu City Hospital, Clinic of Nuclear Medicine, İstanbul, Türkiye
[2]University of Health Sciences Türkiye, İstanbul Prof. Dr. Cemil Taşcıoğlu City Hospital, Clinic of Pathology, İstanbul, Türkiye

Abstract

A 61-year-old male patient, who had undergone radical prostatectomy, underwent ^{68}Ga labeled prostate-specific membrane antigen (PSMA) positron emission tomography/computerized tomography (PET/CT) for evaluation of suspected biochemical recurrence of prostate cancer (PCa). PET/CT scan showed increased ^{68}Ga PSMA expressions in hypodense mass lesions in both adrenal gland localizations. An adrenal gland tru-cut biopsy was performed for the right side, which showed poor-differentiated carcinoma metastases associated with the patient's high-grade PCa. As far as we could determine based on an extensive literature search, this is the second case in which isolated adrenal metastasis was detected by ^{68}Ga PSMA PET/CT study in a patient with PCa.

Keywords: Prostate cancer, ^{68}Ga PSMA PET/CT, adrenal metastasis

Öz

Radikal prostatektomi geçirmiş 61 yaşındaki erkek hastaya, şüpheli biyokimyasal prostat kanseri (PCa) nüksünün değerlendirilmesi için ^{68}Ga etiketli prostat spesifik membran antijeni (PSMA) pozitron emisyon tomografisi/bilgisayarlı tomografi (PET/BT) yapıldı. PET/BT taraması, her iki adrenal bez lokalizasyonunda hipodens kitle lezyonlarında ^{68}Ga PSMA ekspresyonlarında artış gösterdi. Sağ taraf için, hastanın yüksek dereceli PCa'sı ile ilişkili kötü diferansiye karsinom metastazları gösteren bir adrenal bez tru-cut biyopsisi yapıldı. Geniş bir literatür taraması ile tespit edebildiğimiz kadarıyla bu, PCa'lı bir hastada ^{68}Ga PSMA PET/BT çalışması ile izole adrenal metastaz saptanan ikinci olgudur.

Anahtar kelimeler: Prostat kanseri, ^{68}Ga PSMA PET/BT, adrenal metastazı

Address for Correspondence: Filiz Özülker Assoc. Prof., University of Health Sciences Türkiye, İstanbul Prof. Dr. Cemil Taşcıoğlu City Hospital, Clinic of Nuclear Medicine, İstanbul, Türkiye
Phone: +90 554 693 78 80 **E-mail:** fozulker@gmail.com ORCID ID: orcid.org/0000-0003-2075-1429
Received: 01.05.2022 **Accepted:** 15.02.2023

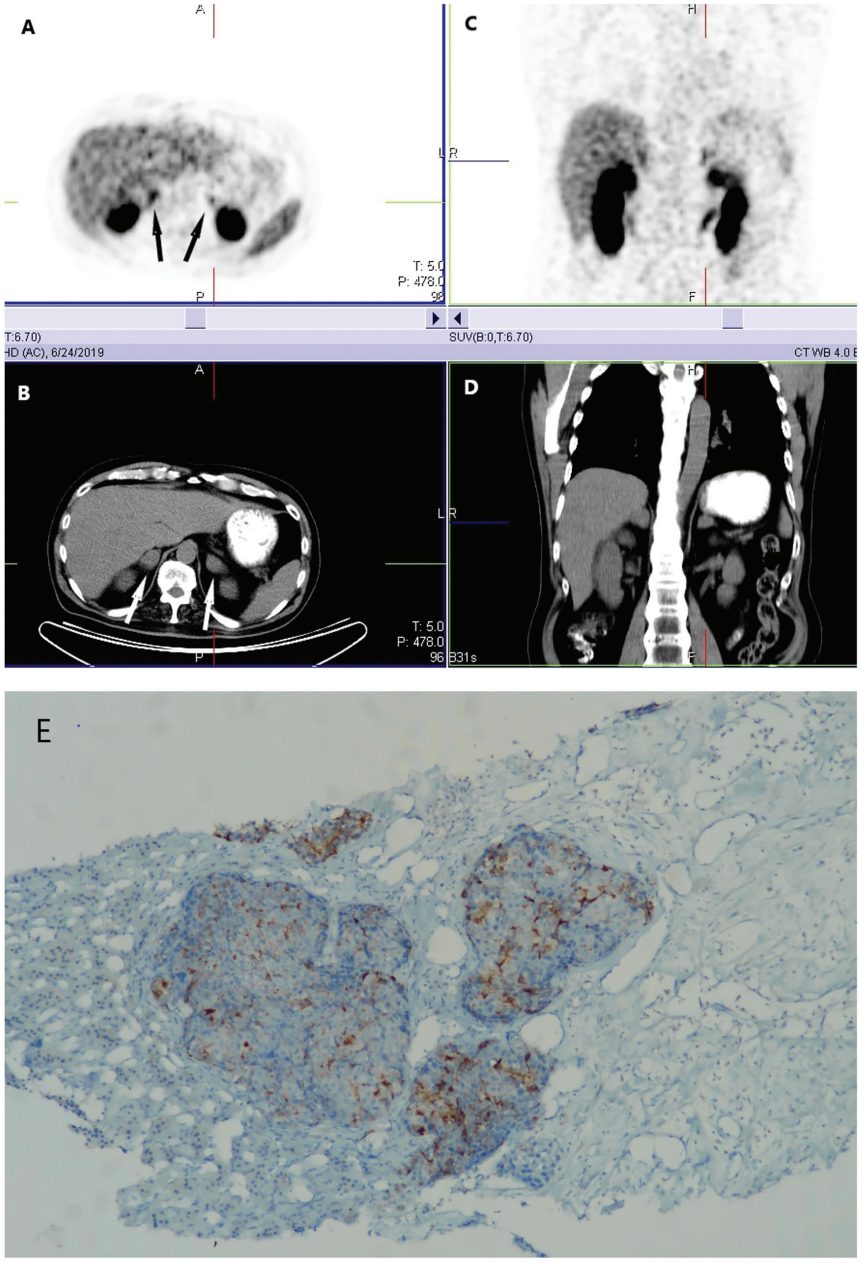

Figure 1. A 61-year-old male patient was admitted to our positron emission tomography/computerized tomography (PET/CT) unit for evaluation of suspected biochemical recurrence of prostate cancer (PCa) in June 2019. The patient had undergone radical prostatectomy in February 2017 and had been treated with adjuvant chemotherapy and external radiotherapy for Gleason 4+5 grade and T3BN1M0 stage prostate adenocarcinoma. He has been followed by androgen deprivation therapy. After a recent elevation in his prostate specific antigen (PSA) levels, the patient was scanned with ^{68}Ga labeled prostate-specific membrane antigen (PSMA) PET/CT. Axial **(A, B)** (arrows) and coronal **(C, D)** slices of PET and CT showed increased ^{68}Ga PSMA expressions in hypodense mass lesions in both adrenal gland localizations [maximum standardized uptake value (SUV_{max}) for right adrenal gland: 7.3, SUV_{max} for left adrenal gland: 4,6]. Other than those, there were not any other pathological findings. The results were found suspicious for metastatic involvement, hence magnetic resonance imaging scan was performed. It identified metastatic mass lesions in the adrenal glands; 40x18 mm. on the right and 32x20 mm on the left side. An adrenal gland tru-cut biopsy was performed for the right side, which showed poor-differentiated carcinoma metastases associated with the patient's high-grade PCa. A tumoral infiltration containing solid groups of prominent macronuclei is seen in the fibrous desmoplastic stroma (E; 100x high-power field). While immunohistochemical staining in tumoral cells was positive for PSA, it was negative for inhibin, Melan A, and Pax 8. The tumor is surrounded by adrenal cortical tissue. Adrenal metastasis of PCa is relatively rare when compared to

the other visceral metastatic sites and is detected in 13-15% of metastatic cases (1,2). In an analysis of 74,826 patients with metastatic PCa, kidney, and adrenal were involved in 0.3% of patients with a single-site metastasis (3). Detection of single-site metastasis of the adrenal gland is crucial, since metastasectomy may provide a durable biochemical response, and improve progression-free survival in men with oligometastatic PCa (4).

PET/CT scan with ^{68}Ga PSMA, owing to its exquisite sensitivity in the detection of PCa metastases, has gained widespread use for the evaluation of PCa in recent years. ^{68}Ga PSMA uptake can exhibit physiologic uptake in adrenal glands (5,6) and benign adrenal adenomas (7) causing misleading false-positive interpretations very rarely. Depending on the preliminary reports describing PSMA expression in adrenocortical carcinoma, this type of malignancy should also be taken into account while evaluating ^{68}Ga PSMA uptake in adrenal glands in PET/CT studies (8,9). As far as we could determine based on an extensive literature search, we found that there is only one report of single-lesion adrenal metastasis of PCa detected by ^{68}Ga PSMA PET/CT (10).

Ethics

Informed Consent: Patient consent for the diagnostic study was obtained.

Peer-review: Internally peer-reviewed.

Authorship Contributions

Concept: O.K., F.Ö., Design: O.K., F.Ö., Data Collection or Processing: O.K., F.Ö., T.A., Analysis or Interpretation: O.K., F.Ö., T.A., T.Ö., Literature Search: O.K., F.Ö., T.Ö., Writing: O.K., F.Ö., T.Ö.

Conflict of Interest: No conflicts of interest were declared by the authors.

Financial Disclosure: The authors declare that this study has received no financial support.

References

1. Bubendorf L, Schöpfer A, Wagner U, Sauter G, Moch H, Willi N, Gasser TC, Mihatsch MJ. Metastatic patterns of prostate cancer: an autopsy study of 1,589 patients. Hum Pathol 2000;31:578-583.
2. Vinjamoori AH, Jagannathan JP, Shinagare AB, Taplin ME, Oh WK, Van den Abbeele AD, Ramaiya NH. Atypical metastases from prostate cancer: 10-year experience at a single institution. AJR Am J Roentgenol 2012;199:367-72.
3. Gandaglia G, Abdollah F, Schiffmann J, Trudeau V, Shariat SF, Kim SP, Perrotte P, Montorsi F, Briganti A, Trinh QD, Karakiewicz PI, Sun M. Distribution of metastatic sites in patients with prostate cancer: A population-based analysis. Prostate 2014;74:210-216.
4. Ashrafi AN, Fay C, Yip W, de Freitas DM, Nabhani J, Aron M. Durable biochemical response following adrenal metastasectomy for oligometastatic castrate-resistant prostate cancer. Urol Case Rep 2020;32:101229.
5. Strele-Trieb P, Dunzinger A, Sonnberger M, Wolfsgruber J, Pichler R. Uptake of 68Ga-Prostate-Specific Membrane Antigen PET in Adrenal Gland: A Potential Pitfall. Clin Nucl Med 2018;43:50-51.
6. Demirci E, Sahin OE, Ocak M, Akovali B, Nematyazar J, Kabasakal L. Normal distribution pattern and physiological variants of 68Ga-PSMA-11 PET/CT imaging. Nucl Med Commun 2016;37:1169-1179.
7. Law WP, Fiumara F, Fong W, Miles KA. Gallium-68 PSMA uptake in adrenal adenoma. J Med Imaging Radiat Oncol 2016;60:514-517.
8. Crowley MJ, Scognamiglio T, Liu YF, Kleiman DA, Beninato T, Aronova A, Liu H, Jhanwar YS, Molina A, Tagawa ST, Bander NH, Zarnegar R, Elemento O, Fahey TJ 3rd. Prostate-Specific Membrane Antigen Is a Potential Antiangiogenic Target in Adrenocortical Carcinoma. J Clin Endocrinol Metab 2016;101:981-987.
9. Arora S, Damle NA, Aggarwal S, Passah A, Behera A, Arora G, Bal C, Tripathi M. Prostate-Specific Membrane Antigen Expression in Adrenocortical Carcinoma on 68Ga-Prostate-Specific Membrane Antigen PET/CT. Clin Nucl Med 2018;43:449-451.
10. Ribeiro AMB, Lima ENP, Garcia D, Bezerra SM. Single Adrenal Metastasis From Prostate Cancer Detected by 68Ga-PSMA PET/CT and Confirmed by Biopsy: A Case Report. Clin Nucl Med 2022;47:61-62.

Interesting Image
Mol Imaging Radionucl Ther 2023;32:247-249 DOI:10.4274/mirt.galenos.2023.98216

Alterations in ^{18}F-FDG Uptake Patterns may Limit Cross-sectional Evaluation of Adrenal Adenomas Using Single ^{18}F-FDG PET/CT Imaging

^{18}F-FDG Tutulum Paternlerinde Gözlenen Değişiklikler, Adrenal Adenomların ^{18}F-FDG PET/BT ile Kesitsel Olarak Değerlendirilmesini Sınırlayabilir

Fatih Tamer[1], *Ülkem Yararbaş*[2]

[1]*Niğde Ömer Halisdemir University Training and Research Hospital, Clinic of Nuclear Medicine, Niğde, Türkiye*
[2]*Ege University Faculty of Medicine, Department of Nuclear Medicine, İzmir, Türkiye*

Abstract

Adrenal adenomas are observed in up to 7% of the population and are predominantly non-functional, increased ^{18}F-fluorodeoxyglucose (FDG) uptake is seen in only a small portion of them on ^{18}F-FDG positron emission tomography/computed tomography (PET/CT) imaging. In this report, we present the sequential ^{18}F-FDG PET/CT imaging findings of 2 patients with radiologically or pathologically confirmed adrenal adenomas who had severely altered ^{18}F-FDG uptake patterns in adrenal lesions in different imaging studies of the same patient. In light of these findings, we wanted to highlight that evaluating adrenal adenomas as cross-sectional with semi-quantitative PET/CT parameters obtained from single imaging may cause misinterpretation.

Keywords: Adrenal adenoma, ^{18}F-FDG, positron emission tomography

Öz

Adrenal adenomlar popülasyonun yaklaşık %7'sine kadar gözlenir ve ağırlıklı olarak fonksiyon göstermemektedir. ^{18}F-florodeoksiglukoz (FDG) pozitron emisyon tomografisi/bilgisayarlı tomografi (PET/BT) görüntülemede bunların sadece küçük bir bölümünde artmış ^{18}F-FDG tutulumu gözlenmektedir. Bu raporda, adrenal lezyonlarda ^{18}F-FDG tutulum paternlerini belirgin şekilde değiştiren radyolojik veya patolojik olarak doğrulanmış adrenal adenomu olan 2 hastanın ardışık ^{18}F-FDG PET/BT görüntüleme bulgularını sunuyoruz. Bu bulgular ışığında adrenal adenomların tek görüntülemeden elde edilen semi-kantitatif PET/BT parametreleri ile kesitsel olarak değerlendirilmesinin yanlış yorumlamalara yol açabileceğini vurgulamak istedik.

Anahtar kelimeler: Adrenal adenom, ^{18}F-FDG, pozitron emisyon tomografi

Address for Correspondence: Fatih Tamer MD, Niğde Ömer Halisdemir University Training and Research Hospital, Clinic of Nuclear Medicine, Niğde, Türkiye
Phone: +90 388 232 22 20 **E-mail:** drfatihtamer@gmail.com ORCID ID: orcid.org/0000-0002-5656-9955
Received: 11.01.2023 **Accepted:** 01.03.2023

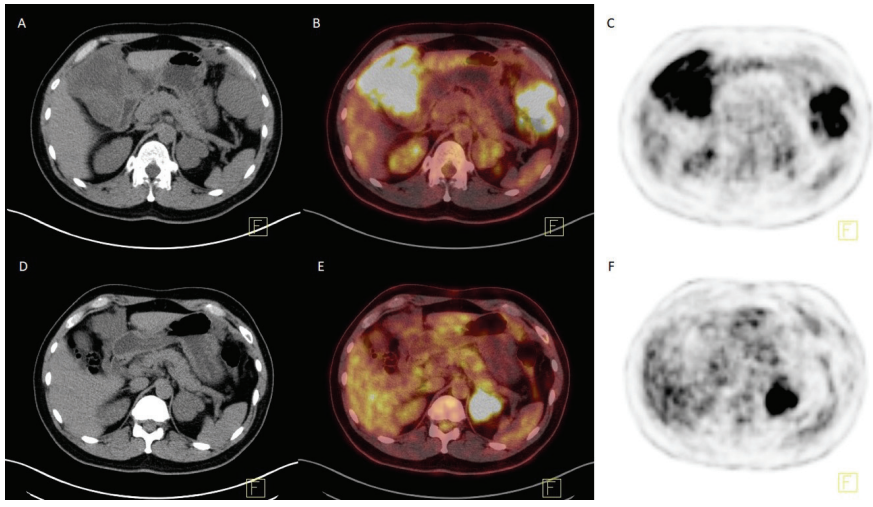

Figure 1. A 40-year-old patient presented with abdominal pain and was diagnosed with metastatic gastrointestinal stromal tumor (GIST). Staging ^{18}F-fluorodeoxyglucose (FDG) positron emission tomography/computed tomography (PET/CT) images **(A, B, C)** revealed intra-abdominal hypermetabolic gross mass lesions as well as a well-defined nodular lesion with moderate ^{18}F-FDG uptake in the left adrenal gland [maximum standardized uptake value (SUV_{max}): 4.6 g/mL]. On the subsequent ^{18}F-FDG PET/CT images **(D, E, F)** taken after 4 months of imatinib treatment, metabolic regression as well as significant necrotic hypometabolic findings were observed in the abdominopelvic mass lesions. However, it was noted that intense ^{18}F-FDG uptake developed in the left adrenal nodular lesion without significant morphological changes (SUV_{max}: 12.8 g/mL). Left adrenal tru-cut biopsy was performed because of the relatively rare occurrence of adrenal metastasis in GIST cases and suspicious findings observed during the course of the disease, and it was reported to be consistent with adrenal cortical adenoma without any further features.

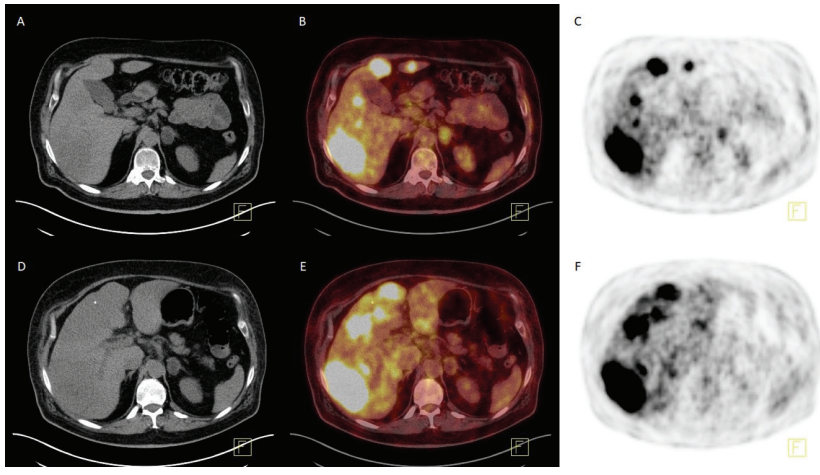

Figure 2. ^{18}F-FDG PET/CT scan was performed on a 51-year-old patient who was diagnosed with anaplastic thyroid cancer from a nodule found in the left lobe of the thyroid gland. On the axial PET, CT, and fused PET/CT images obtained **(A, B, C)**, a nodular lesion with increased ^{18}F-FDG uptake was observed in the left adrenal gland, except for lung, liver, and bone metastases (SUV_{max}: 5.8 g/mL). Although progression was detected in metastatic foci in ^{18}F-FDG PET/CT images **(D, E, F)** taken after chemotherapy (carboplatin and paclitaxel) regimen, it was noted that the metabolic activity of the morphologically stable left adrenal nodular lesion regressed (SUV_{max}: 3.7 g/mL). On magnetic resonance imaging, the lesion was reported to be compatible with adrenal adenoma. Increased ^{18}F-FDG uptake is observed in only 5% of adrenal adenomas, which is common in oncologic imaging practice (1). In the literature, the effectiveness of semi-quantitative ^{18}F-FDG PET/CT parameters, primarily SUV_{max}, in differentiating adrenal lesions as benign or malignant at different threshold values has been evaluated with various reports (2,3,4,5). Although there are several descriptions regarding the alterations in ^{18}F-FDG uptake patterns observed in adrenal adenomas, especially possible circadian rhythm of the hormone-secreting tissues, as well as the differences in the cell content of the lesions (especially cell content with increased GLUT1 expression), information on this issue is still limited (6,7,8). Considering the variability of ^{18}F-FDG uptake of adrenal adenomas as we presented in our cases and possible differences in clinical-technical characteristics between scans (serum glucose level, fasting period, injection time, and time between imaging and injection), we wanted to highlight the limitations in cross-sectional evaluation of adrenal lesions with a single PET/CT imaging.

Ethics

Informed Consent: Patient consent was obtained.

Peer-review: Externally and internally peer-reviewed.

Authorship Contributions

Surgical and Medical Practices: F.T., Ü.Y., Concept: F.T., Ü.Y., Design: F.T., Ü.Y., Data Collection or Processing: F.T., Ü.Y., Analysis or Interpretation: F.T., Ü.Y., Literature Search: F.T., Ü.Y., Writing: F.T., Ü.Y.

Conflict of Interest: No conflict of interest was declare by the authors.

Financial Disclosure: The authors declared that this study received no financial support.

References

1. Chong S, Lee KS, Kim HY, Kim YK, Kim BT, Chung MJ, Yi CA, Kwon GY. Integrated PET-CT for the characterization of adrenal gland lesions in cancer patients: diagnostic efficacy and interpretation pitfalls. Radiographics 2006;26:1811-1824.
2. Ansquer C, Scigliano S, Mirallié E, Taïeb D, Brunaud L, Sebag F, Leux C, Drui D, Dupas B, Renaudin K, Kraeber-Bodéré F. 18F-FDG PET/CT in the characterization and surgical decision concerning adrenal masses: a prospective multicentre evaluation. Eur J Nucl Med Mol Imaging 2010;37:1669-1678.
3. Boland GW, Dwamena BA, Jagtiani Sangwaiya M, Goehler AG, Blake MA, Hahn PF, Scott JA, Kalra MK. Characterization of adrenal masses by using FDG PET: a systematic review and meta-analysis of diagnostic test performance. Radiology 2011;259:117-126.
4. Kim SJ, Lee SW, Pak K, Kim IJ, Kim K. Diagnostic accuracy of 18F-FDG PET or PET/CT for the characterization of adrenal masses: a systematic review and meta-analysis. Br J Radiol 2018;91:20170520.
5. He X, Caoili EM, Avram AM, Miller BS, Else T. 18F-FDG-PET/CT Evaluation of Indeterminate Adrenal Masses in Noncancer Patients. J Clin Endocrinol Metab 2021;106:1448-1459.
6. Takanami K, Kaneta T, Morimoto R, Satoh F, Nakamura Y, Takase K, Takahashi S. Characterization of lipid-rich adrenal tumors by FDG PET/CT: Are they hormone-secreting or not? Ann Nucl Med 2014;28:145-153.
7. Lang BH, Cowling BJ, Li JY, Wong KP, Wan KY. High False Positivity in Positron Emission Tomography is a Potential Diagnostic Pitfall in Patients with Suspected Adrenal Metastasis. World J Surg 2015;39:1902-1908.
8. Murayama R, Nishie A, Hida T, Baba S, Inokuchi J, Oda Y, Honda H. Uptake of 18F-FDG in Adrenal Adenomas Is Associated With Unenhanced CT Value and Constituent Cells. Clin Nucl Med 2019;44:943-948.

Interesting Image
Mol Imaging Radionucl Ther 2023;32:250-251 DOI:10.4274/mirt.galenos.2023.81594

Incidental Detection of Sarcomatoid Lung Cancer by [^{18}F] Choline Positron Emission Tomography/Computed Tomography

Sarkomatoid Akciğer Kanserinin [^{18}F] Kolin Pozitron Emisyon Tomografisi/Bilgisayarlı Tomografi ile Rastlantısal Tespiti

Rensi Marco[1], *Decio Capobianco*[1], *Di Gregorio Fernando*[1], *Laura Evangelista*[2]

[1]*Azienda Sanitaria Universitaria Integrata, Nuclear Medicine Unit, Udine, Italy*
[2]*University of Padua, Department of Medicine DIMED, Nuclear Medicine and Molecular Imaging Unit, Padua, Italy*

Abstract

A 79-year-old man treated for prostate cancer (PCa) in 2018 with concurrent hormone therapy and radical radiotherapy (RT) was given metastasis-directed RT because of skeletal progression of PCa in 2021. On [^{18}F]-choline positron emission tomography/computed tomography (CT) for biochemical recurrence (prostate-specific antigen level: 4.96 ng/mL), he showed significant uptake in multiple skeletal lesions and focal uptake in a left lung nodule. CT-guided biopsy revealed a sarcomatoid lung carcinoma. This case confirms that histopathological evaluation is mandatory in the event of significant radiolabeled choline uptake in a single lung nodule.

Keywords: Fluorocholine, cancer, interpretation

Öz

2018 yılında prostat kanseri (PCa) nedeniyle eşzamanlı hormon tedavisi ve radikal radyoterapi (RT) ile tedavi edilen 79 yaşındaki erkek hastaya, 2021 yılında PCa'nın kemik tutulumu nedeniyle metastaz odaklı RT uygulandı. Biyokimyasal nüks (prostat spesifik antijen düzeyi: 4,96 ng/mL) açısından [^{18}F]-kolin pozitron emisyon tomografisi/bilgisayarlı tomografide (BT), çoklu kemik lezyonlarında belirgin tutulum ve sol akciğer nodülünde fokal bir tutulum gösterildi. BT eşliğinde yapılan biyopside sarkomatoid akciğer karsinomu saptandı. Bu olgu, tek bir akciğer nodülünde anlamlı radyoaktif işaretli kolin tutulumunun olması durumunda histopatolojik değerlendirmenin zorunlu olduğunu doğrulamaktadır.

Anahtar kelimeler: Florokolin, kanser, yorum

Address for Correspondence: Prof. Laura Evangelista MD, University of Padua, Department of Medicine DIMED, Nuclear Medicine and Molecular Imaging Unit, Padua, Italy
Phone: +39 0498211310 **E-mail:** laura.evangelista@unipd.it ORCID ID: orcid.org/0000-0002-5955-9488
Received: 06.02.2023 **Accepted:** 05.03.2023

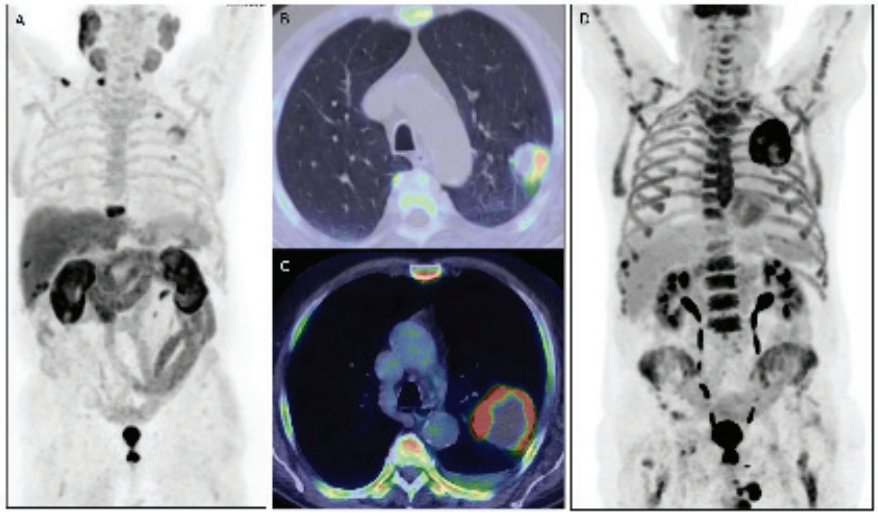

Figure 1. A 79-year-old man with a history of confined bladder cancer treated with transurethral resection of bladder (TURB) tumor in 2003 and prostate cancer (PCa). The patient was administered concurrent hormone therapy and radical radiotherapy (RT) in 2018 (cT2N0M0, Gleason score: 10, ISUP grade: V). Three years later, the patient underwent metastasis-directed RT for disease progression in the skeleton (vertebra D9). In April 2022, increased prostate-specific antigen levels (PSA: 4.96 ng/mL) prompted an [^{18}F]-choline positron emission tomography/computed tomography (PET/CT) scan, which revealed high radiopharmaceutical uptake in multiple skeletal lesions [maximum intensity projection (MIP); **A**] and in a solitary left lung nodule (continuous arrow; **B**). The maximum standardized uptake value (SUV_{max}) of the solitary left lung nodule was 8.2. Three months later, a CT-guided biopsy was performed, and histological examination revealed sarcomatoid lung carcinoma. For disease staging purposes, ^{18}F-fluorodeoxyglucose (^{18}F-FDG) PET/CT was performed three weeks after the biopsy. The results showed an increase in the dimensions of the left lung lesion (continuous arrow; **C**) and diffuse bone marrow activation (MIP; **D**). Radiolabeled choline PET/CT has been used extensively in patients with recurrent PCa (1,2) and can also incidentally detect malignant or benign lung lesions, such as bronchioloalveolar cancer (3) or pulmonary tuberculosis (4). However, this is the first report of ^{18}F-choline uptake revealing sarcomatoid lung cancer. Geraldo et al. (5) described a case of sarcomatoid metastases from PCa detected by ^{68}Ga-prostate-specific membrane antigen PET/CT. Some published studies have discussed the role of ^{18}F-FDG PET/CT in assessing primary and secondary sarcomatoid lung lesions (6,7,8). Histopathological examination should be mandatory in cases of single lung lesions and choline uptake on PET/CT to distinguish between recurrence of PCa and other etiologies.

Ethics

Informed Consent: Patient consent was obtained.

Peer-review: Externally peer-reviewed.

Authorship Contributions

Surgical and Medical Practices: R.M., D.C., Concept: R.M., L.E., Data Collection or Processing: R.M., D.C., Analysis or Interpretation: D.G.F., Literature Search: L.E., Writing: L.E., R.M., D.G.F.

Conflict of Interest: No conflict of interest was declared by the authors.

Financial Disclosure: The authors declared that this study has received no financial support.

References

1. Ferrari M, Renard J, Pereira Mestre R, Bosetti DG, Stoffel F, Treglia G. Change of management by using hybrid imaging with radiolabeled choline in biochemical recurrent prostate cancer: a systematic review and a meta-analysis. Clin Transl Imaging 2021;9:57-71.
2. Gillebert Q, Huchet V, Rousseau C, Cochet A, Olivier P, Courbon F, Gontier E, Nataf V, Balogova S, Talbot JN; other ICHOROPRO investigators. 18F-fluorocholine PET/CT in patients with occult biochemical recurrence of prostate cancer: Detection rate, impact on management and adequacy of impact. A prospective multicentre study. PLoS One 2018;13:e0191487.
3. Balogova S, Huchet V, Kerrou K, Nataf V, Gutman F, Antoine M, Ruppert AM, Prignon A, Lavolée A, Montravers F, Mayaud C, Cadranel J, Talbot JN. Detection of bronchioloalveolar cancer by means of PET/CT and 18F-fluorocholine, and comparison with 18F-fluorodeoxyglucose. Nucl Med Commun 2010;31:389-397.
4. Hara T, Kosaka N, Suzuki T, Kudo K, Niino H. Uptake rates of 18F-fluorodeoxyglucose and 11C-choline in lung cancer and pulmonary tuberculosis: a positron emission tomography study. Chest 2003;124:893-901.
5. Geraldo L, Ceci F, Uprimny C, Kendler D, Virgolini I. Detection of Sarcomatoid Lung Metastasis With 68GA-PSMA PET/CT in a Patient With Prostate Cancer. Clin Nucl Med 2016;41:421-422.
6. Wu X, Huang Y, Li Y, Wang Q, Wang H, Jiang L. 18F-FDG PET/CT imaging in pulmonary sarcomatoid carcinoma and correlation with clinical and genetic findings. Ann Nucl Med 2019;33:647-656.
7. Rapicetta C, Lococo F, Stefani A, Rossi G, Ricchetti T, Filice A, Franceschetto A, Treglia G, Paci M. Primary Sarcomatoid Carcinoma of the Lung: Radiometabolic ((18)F-FDG PET/CT) Findings and Correlation with Clinico-Pathological and Survival Results. Lung 2016;194:653-657.
8. Fuser D, Hedberg ML, Dehner LP, Dehdashti F, Siegel BA. Extensive Metastatic Sarcomatoid Renal Cell Carcinoma Evaluated by 18F-FDG PET/CT: a Case Report and Review of Literature. J Kidney Cancer VHL 2018;5:1-6.

Interesting Image
Mol Imaging Radionucl Ther 2023;32:252-254 DOI:10.4274/mirt.galenos.2023.53254

A Rare Case of "Periportal Cuffing" as an Incidental Finding on ^{18}F-FDG PET/CT

^{18}F-FDG PET/BT'de İnsidental Olarak Saptanan Nadir Bir "Periportal Cuffing" Olgusu

Burak Demir[1], Elgin Özkan[1], Seda Kaynak Şahap[2], Gizem Sütçü[1], Ceyda Tuna Kırsaçlıoğlu[3], Çiğdem Soydal[1], Ömer Suat Fitoz[2], Aydan Kansu Tanca[3], Emel Ünal[4]

[1]*Ankara University Faculty of Medicine, Department of Nuclear Medicine, Ankara, Türkiye*
[2]*Ankara University Faculty of Medicine, Department of Radiology, Ankara, Türkiye*
[3]*Ankara University Faculty of Medicine, Department of Pediatrics, Division of Pediatric Gastroenterology, Ankara, Türkiye*
[4]*Ankara University Faculty of Medicine, Department of Pediatrics, Division of Pediatric Oncology, Ankara, Türkiye*

Abstract

A 7-year-old boy with known diagnosis of hereditary spherocytosis and ulcerative colitis was referred for ^{18}F-fluorodeoxyglucose (^{18}F-FDG) positron emission tomography/computed tomography after detection of a 28 mm lesion suspicious for malignancy in spleen on upper abdomen magnetic resonance imaging (MRI). As an incidental finding, a moderately increased uptake of ^{18}F-FDG was observed in periportal region with no definable mass. MRI revealed compatible findings with "periportal cuffing" as described on ultrasonography.

Keywords: Periportal cuffing, fluorodeoxyglucose, positron emission tomography, magnetic resonance imaging

Öz

Bilinen herediter sferositoz ve ülseratif kolit tanısı olan 7 yaşında erkek hastaya dalakta 28 mm boyutlu malignite şüpheli lezyon görülmesi sebebiyle ^{18}F-florodeoksiglukoz (^{18}F-FDG) pozitron emisyon tomografisi/bilgisayarlı tomografi uygulanmıştır. İnsidental bir bulgu olarak periportal bölgede karşılığında tanımlanabilen bir lezyon olmayan artmış ^{18}F-FDG tutulumu izlenmiştir. Manyetik rezonans görüntülemede ise aynı bölgede daha önce ultrasonografide tanımlanan "periportal cuffing" ile uyumlu bulgular saptanmıştır.

Anahtar kelimeler: Periportal cuffing, florodeoksiglukoz, pozitron emisyon tomografi, manyetik rezonans görüntüleme

Address for Correspondence: Burak Demir MD, Ankara University Faculty of Medicine, Department of Nuclear Medicine, Ankara, Türkiye
Phone: +90 555 817 07 10 **E-mail:** 4burakfe@gmail.com ORCID ID: orcid.org/0000-0002-0966-9988
Received: 18.01.2023 **Accepted:** 13.03.2023

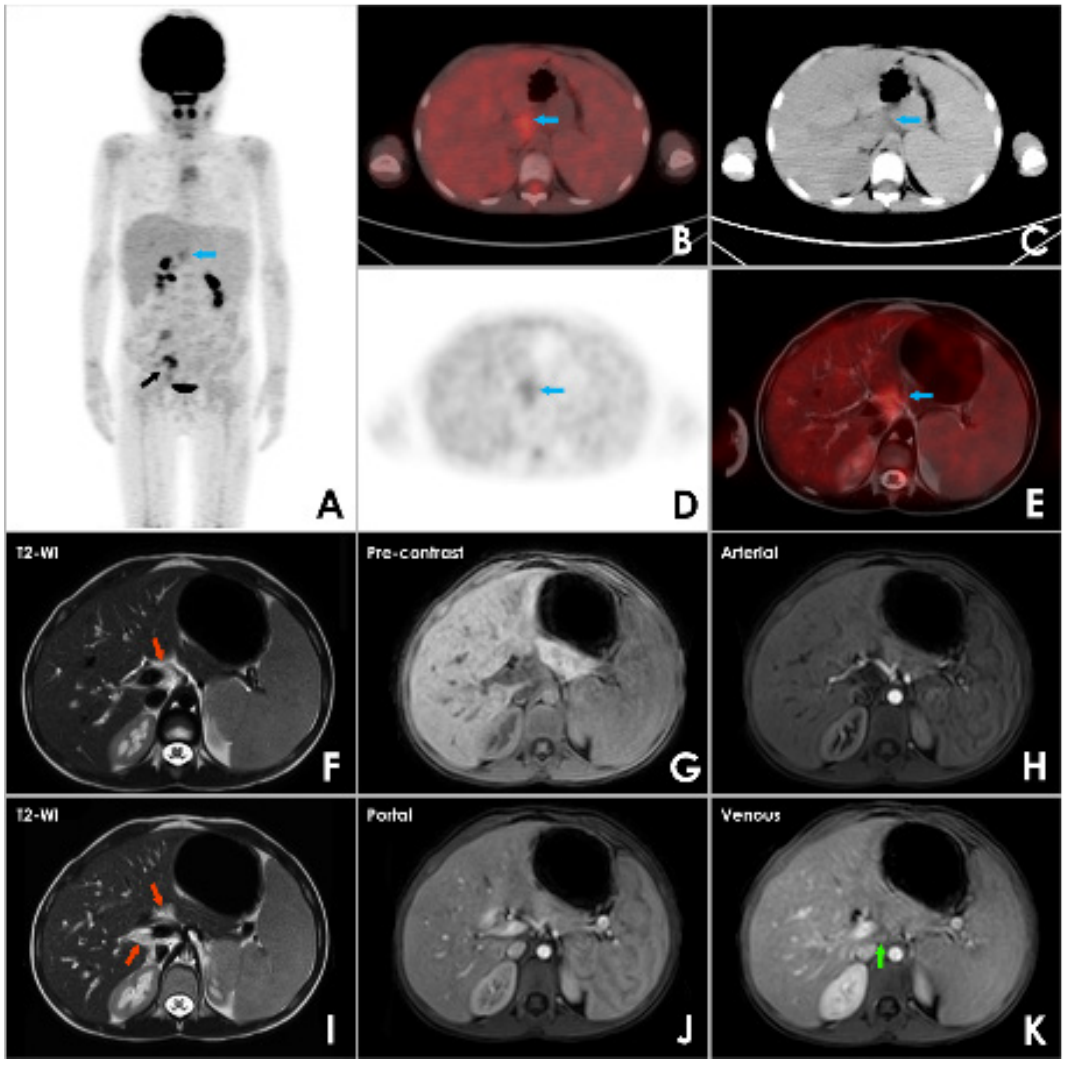

Figure 1. A 7-year-old boy with known diagnosis of hereditary spherocytosis and ulcerative colitis was referred for ^{18}F-fluorodeoxyglucose (^{18}F-FDG) positron emission tomography/computed tomography (PET/CT) after detection of a 28 mm lesion in spleen on upper abdomen magnetic resonance imaging (MRI). The lesion was hypointense on all MRI sequences and no pathological ^{18}F-FDG uptake was detected in PET/CT. Also, there was increased uptake localized to the right colon segment can be observed on MIP **(A)** in the right lower quadrant of abdomen (black arrow) which could be associated with ulcerative colitis. However, as an incidental finding, a moderately increased uptake (blue arrows) of ^{18}F-FDG was observed in periportal region on MIP **(A)** and transaxial **(B, C, D)** images with no definable mass. On the light of the ^{18}F-FDG PET/CT, retrospective evaluation of previous MRI revealed periportal hyperintensity (red arrows) on T2-weighted images **(F, I)** compatible with "periportal cuffing" as described on ultrasonography. Dynamic contrast-enhanced imaging **(G, H, J, K)** showed a progressive contrast enhancement (green arrow) in periportal area. Extrahepatic biliary system was normal and magnetic resonance cholangiopancreatography findings were negative for the primary sclerosing cholangitis. On fusion images of PET/CT and T2-weighted images **(E)** it can be clearly seen that increased ^{18}F-FDG uptake on periportal region corresponds to periportal hyperintensity on MRI.

Ulcerative colitis is a chronic inflammatory disease of bowel and is characterized by mucosal inflammation of colon and rectum (1). Also, it is known that ulcerative colitis is associated with primary sclerosing cholangitis and pericholangitis (2,3,4). Echo-rich periportal cuffing (ErPC) is a rare ultrasonographic finding which can be seen in patients with hepatitis, inflammatory bowel diseases (IBD) and liver transplants. It is theorized that ErPC is caused by lymphatic fluid obstructing periportal tissue but also can be a result of inflammation of periportal zones in patients with IBD (5,6). IBD can also cause aberrant cell migration from the intestinal mucosa into the portal system via enterohepatic circulation, which can result in hyperechogenic periportal cuffing (5,6). It is known that inflammatory and infectious pathologies can be imaged with ^{18}F-FDG PET/CT. Also, in literature there are studies that suggest ^{18}F-FDG PET/CT can be used for assessing disease activity in IBD (7,8,9,10). Even though there are multiple reports of ^{18}F-FDG PET/CT in IBD, to the best of our knowledge, there is no report of periportal cuffing associated with increased ^{18}F-FDG uptake in literature and it is not defined in benign conditions that exhibits increased ^{18}F-FDG uptake (11).

Ethics

Informed Consent: Patient consent was obtained.

Peer-review: Internally peer-reviewed.

Authorship Contributions

Surgical and Medical Practices: B.D., E.Ö., S.K.Ş., G.S., C.T.K., Ö.S.F., A.K.T., E.Ü., Concept: B.D., E.Ö., C.T.K., Ç.S., Ö.S.F., A.K.T., E.Ü., Design: B.D., A.K.T., E.Ü., Data Collection or Processing: B.D., S.K.Ş., G.S., Ç.S., Ö.S.F., Analysis or Interpretation: B.D., E.Ö., S.K.Ş., G.S., C.T.K., Ç.S., Ö.S.F., Literature Search: B.D., E.Ö., C.T.K., Writing: B.D., E.Ö.

Conflict of Interest: No conflict of interest was declared by the authors.

Financial Disclosure: The authors declared that this study has received no financial support.

References

1. Ordás I, Eckmann L, Talamini M, Baumgart DC, Sandborn WJ. Ulcerative colitis. Lancet 2012;380:1606-1619.
2. Van Der Have M, Oldenburg B. Is Ulcerative Colitis Associated With Primary Sclerosing Cholangitis an Undertreated Condition? Inflamm Bowel Dis 2020;26:780-781.
3. de Vries AB, Janse M, Blokzijl H, Weersma RK. Distinctive inflammatory bowel disease phenotype in primary sclerosing cholangitis. World J Gastroenterol 2015;21:1956-1971.
4. Palmela C, Peerani F, Castaneda D, Torres J, Itzkowitz SH. Inflammatory Bowel Disease and Primary Sclerosing Cholangitis: A Review of the Phenotype and Associated Specific Features. Gut Liver 2018 12:17-29.
5. Neesse A, Huth J, Heumann T, Michl P, Steinkamp M, Gress TM, Görg C, Kunsch S. Echo-rich and echo-poor periportal cuffing: pole position for inflammatory bowel diseases. Ultraschall Med 2008;29:633-638.
6. Neesse A, Heumann T, Görg C, Kiessling A, Klose KJ, Gress TM, Steinkamp M. Periportal cuffing in inflammatory bowel diseases: mystery of stars and stripes. Inflamm Bowel Dis 2010;16:1275-1276.
7. Ahmadi A, Li Q, Muller K, Collins D, Valentine JF, Drane W, Polyak S. Diagnostic value of noninvasive combined fluorine-18 labeled fluoro-2-deoxy-D-glucose positron emission tomography and computed tomography enterography in active Crohn's disease. Inflamm Bowel Dis 2010;16:974-981.
8. Meisner RS, Spier BJ, Einarsson S, Roberson EN, Perlman SB, Bianco JA, Taylor AJ, Einstein M, Jaskowiak CJ, Massoth KM, Reichelderfer M. Pilot study using PET/CT as a novel, noninvasive assessment of disease activity in inflammatory bowel disease. Inflamm Bowel Dis 2007;13:993-1000.
9. Lemberg DA, Issenman RM, Cawdron R, Green T, Mernagh J, Skehan SJ, Nahmias C, Jacobson K. Positron emission tomography in the investigation of pediatric inflammatory bowel disease. Inflamm Bowel Dis 2005;11:733-738.
10. Brodersen JB, Hess S. FDG-PET/CT in Inflammatory Bowel Disease: Is There a Future? PET Clin 2020;15:153-162.
11. Altini C, Lavelli V, Ruta R, Ferrari C, Nappi AG, Pisani A, Sardaro A, Rubini G. Typical and atypical PET/CT findings in non-cancerous conditions. Hell J Nucl Med 2020;23:48-59.

Letter to the Editor
Mol Imaging Radionucl Ther 2023;32:255-256 DOI:10.4274/mirt.galenos.2023.06641

Use of Oxidized Regenerated Cellulose in Patients with Lung Cancer: A Biomaterial to Handle with Caution!

Akciğer Kanserli Hastalarda Okside Rejenere Selülozun Kullanımı: Dikkatle Kullanılması Gereken Bir Biyomateryal!

Gianluca Franceschini

Fondazione Policlinico Universitario Agostino Gemelli IRCCS, Department of Women, Children and Public Health Sciences, Rome, Italy

Keywords: Oxidized regenerated cellulose, lung cancer, surgery, imaging

Anahtar kelimeler: Okside rejenere selüloz, akciğer kanseri, cerrahi, görüntüleme

Dear Editor,

I read with interest the article of Sayan et al. (1) and would like to make some appraisals about using oxidized regenerated cellulose (ORC).

ORC is a bioabsorbable, sterile material prepared by the controlled oxidation of regenerated cellulose. It is used in surgery for its hemostatic properties; once the ORC has been left in the surgical bed and saturated with blood, it forms a black or brownish lump with a gel-like consistency that allows the clot formation, so acting as an adjuvant in the process of local hemostasis (2,3); in addition to its hemostatic properties, ORC has bactericidal activity thanks to its ability to reduce pH levels below 4.0, blocking bacterial survival (2).

However, as ORC is increasingly used in thoracic surgery, it is imperative to underline not only the benefits but also the possible problems.

I agree with Sayan et al. (1) that ORC used as a hemostatic agent in lung cancer surgery, can cause false tumor recurrence in imaging modalities in postsurgical follow-up (1).

ORC-induced fibrogenetic reaction can determine a granulomatous reaction that may simulate an abscess, hematoma, fat necrosis, or cancer recurrence, creating a difficult challenge in differential diagnosis and sometimes diagnostic mistakes during follow-up (2,3).

A study on rats showed that ORC absorption is not always complete, resulting in biomaterial retention (4); when the ORC is used, the tissues present chronic inflammation, central liponecrosis and diffuse fibrosis; an excessive and improper fibrogenesis due to ORC can culminate in the creation of a three-dimensional fibrotic structure with a peculiar imaging and enhance the risk of diagnostic mistake during follow-up (2,3,5).

In addition, ORC can cause allergic reactions, seromas, and foreign-body reactions with a risk of extrusion due to its inadequate and suboptimal absorption (2,3); high rates of red syndrome, postoperative seromas, and cases

Address for Correspondence: Prof. Gianluca Franceschini MD, Fondazione Policlinico Universitario Agostino Gemelli IRCCS, Department of Women, Children and Public Health Sciences, Rome, Italy
Phone: +390630156327 **E-mail:** gianlucafranceschini70@gmail.com ORCID ID: orcid.org/0000-0002-2950-3395
Received: 26.03.2023 **Accepted:** 03.07.2023

of foreign-body reaction, requiring surgical removal, were reported in literature (2,3); these complications can compromise clinical outcomes and lead to delayed oncological treatments with a negative impact on patient survival, quality of life and overall hospital costs.

Compliance with standardized recommendations is essential to prevent the aforementioned problems and minimize surgical issues: appropriate selection of candidates to surgery with ORC (patients with specific medical comorbidities, immune diseases or non-controlled diabetes mellitus should not be considered for the use of ORC due to higher risk of postoperative infections); calibrated use of ORC to prevent overdose and avoid excessive fibrosis and foreign-body reaction (ORC pieces must properly fill the surgical bed but should not bulge excessively); prophylactic administration of antibiotic therapy in the postoperative time to prevent infections; detailed description in the surgical report about use of ORC to ensure a correct interpretation of the imaging by radiologists.

In conclusion, ORC is an optimal hemostatic agent that may be left in the surgical site to control bleeding thanks to ease-of-use and favorable biocompatibility; however, a trained and aware thoracic surgeon should use this biomaterial with due caution and correctly report its application to avoid unnecessary re-surgical interventions.

Ethics

Peer-review: Internally peer-reviewed.

Financial Disclosure: The author declared that this study received no financial support.

References

1. Sayan M, Çelik A, Şatır Türk M, Özkan D, Akarsu I, Yazıcı O, Aydos U, Yılmaz Demirci N, Akyol G, Kurul İC, Taştepe Aİ. Oxidized regenerated cellulose can be a cause of false tumor recurrence on pet/ct in patients with lung cancer treated surgically. Mol Imaging Radionucl Ther 2023;32:8-12.
2. Franceschini G. Internal surgical use of biodegradable carbohydrate polymers. Warning for a conscious and proper use of oxidized regenerated cellulose. Carbohydr Polym 2019;216:213-216.
3. Piozzi GN, Reitano E, Panizzo V, Rubino B, Bona D, Tringali D, Micheletto G. Practical Suggestions for prevention of complications arising from oxidized cellulose retention: a case report and review of the literature. Am J Case Rep 2018;19:812-819.
4. Franceschini G, Visconti G, Sanchez AM, Di Leone A, Salgarello M, Masetti R. Oxidized regenerated cellulose in breast surgery: experimental model. J Surg Res 2015;198:237-244.
5. Giuliani M, Fubelli R, Patrolecco F, Rella R, Borelli C, Buccheri C, Di Giovanni SE, Belli P, Romani M, Rinaldi P, Bufi E, Franceschini G, Bonomo L. Mammographic and ultrasonographic findings of oxidized regenerated cellulose in breast cancer surgery: a 5-year experience. Clin Breast Cancer 2015;15:e249-256.

DOI:10.4274/mirt.galenos.2022.97658

Kupik O, Tuncel M, Özgen Kıratlı P, Gülsün Akpınar M, Altundağ K, Başaran Demirkazık F, Erbaş B. Value of Dynamic ^{18}F-FDG PET/CT in Predicting the Success of Neoadjuvant Chemotherapy in Patients with Locally Advanced Breast Cancer: A Prospective Study. Mol Imaging Radionucl Ther 2023;32:94-102.

The mistake have been made inadvertently by the author.

*The sentence on page 95 of the relevant article has been changed.

- Incorrect sentence; Dynamic phase images were recorded for 32 min, including ten frames of **30 min**, five frames of 1 min, five frames of 2 min each, and four frames of 3 min (12).

- Corrected sentence; Dynamic phase images were recorded for 32 min, including ten frames of **30 seconds**, five frames of 1 min, five frames of 2 min each, and four frames of 3 min (12).

2023 Referee Index - 2023 Hakem Dizini

Ayşe Mavi
Ayşegül Akgün
Berna Okudan Tekin
Billur Çalışkan
Bircan Sönmez
Bülent Turgut
Cengiz Taşçı
Corinna Altini
Cüneyt Türkmen
Dragana Sobic Saranovic
Elgin Özkan
Emre Entok
Fatma Suna Kıraç
Feyza Çağlıyan
Fikriye Gül Gümüşer
Filiz Özülker
Funda Üstün
Gamze Çapa Kaya
Gonca G. Bural
Gözde Dağlıöz Görür
Hakan Demir
Mahmut Yüksel
Meliha Korkmaz
Meryem Kaya
Mine Araz
Mustafa Demir
Nedim C. M. Gülaldı
Nilüfer Yıldırım
Nosheen Fatimn
Olga Yaylalı
Rabia Lebriz Uslu Beşli
Serkan İşgören
Seyhan Karaçavuş
Tansel Ansal Balcı
Tarık Şengöz
Yakup Yürekli

2023 Author Index - 2023 Yazar Dizini

2023 Author Index - 2023 Yazar Dizini

2023 Author Index - 2023 Yazar Dizini

2023 Subject Index / 2023 Konu Dizini

2023 Subject Index / 2023 Konu Dizini

2023 Subject Index / 2023 Konu Dizini